

DNA hybridisation detection on chemically modified electrodes with bioelectrocatalytic amplification of signal

Submitted by:

Joanna Hajdukiewicz, M.Sc.

**Thesis Submitted for
the Ph.D Degree by Research
of The National University of Ireland**



Research was Conducted in: School of Chemistry,
College of Science,
The National University of Ireland,
Galway.

Month and Year of Submission: December, 2011

Supervisor of the Research: Dr. Dónal Leech.

Title page	I
Table of contents	II
Acknowledgements	V
Declaration of authorship	VI
Abstract	VII

1. Introduction

1.1. Chemically modified electrodes	2
1.2. Characterisation of the redox hydrogels on electrodes	8
1.3. Electrochemistry of nucleic acids	11
1.3.1. Structure and properties of DNA	11
1.3.2. Electrochemical activity of DNA bases	15
1.3.3. Immobilisation chemistry of DNA for sensor development	16
1.3.4. Electrochemical detection of DNA hybridization	19
1.4. Thesis outline	21
1.5. References	23

2. DNA sensor based upon bioelectrocatalytic amplification using osmium redox polymer modified gold microelectrodes

2.1. Introduction	28
2.2. Experimental	33
2.2.1. Materials and reagents	33
2.2.2. Instrumentation and techniques	33
2.2.3. Preparation and characterization of electrodes	34
2.2.4. Detection of DNA hybridization	39
2.3. Results and Discussion	40
2.3.1. Voltammetry of redox polymer films on gold microelectrodes	40
2.3.2. Amperometric detection of DNA hybridization	53
2.4. Conclusions	58

2.5.	References.....	59
3.	<u>DNA detection at hydrogels prepared via attachment of carboxymethylated dextran to electrodes</u>	
3.1.	Introduction.....	62
3.2.	Experimental.....	66
3.2.1.	Materials.....	66
3.2.2.	Methods.....	66
3.2.3.	Deposition of the sensing layer.....	66
3.2.4.	Assay procedure.....	67
3.2.5.	Optical characterization of DNA-modified surfaces.....	68
3.3.	Results and discussion.....	69
3.3.1.	Development of the sensing layer.....	69
3.3.2.	Redox probe studies of modified surfaces.....	77
3.3.3.	Optical characterization of DNA-modified surfaces.....	82
3.3.4.	Amperometric detection of DNA hybridization with ssDNA grafted onto CM Dextran with ferrocenemethanol as diffusional mediator.....	83
3.3.5.	Amperometric detection of DNA hybridization with ssDNA grafted onto CM Dextran with osmium redox complex co-immobilised at the electrode surface.....	91
3.4.	Conclusions.....	97
3.5.	References.....	99
	Appendix.....	102
4.	<u>Electrochemistry of screen-printed electrodes and their application to DNA hybridization sensor.</u>	
4.1.	Introduction.....	111
4.2.	Experimental.....	113
4.2.1.	Materials and reagents.....	113
4.2.2.	Instrumentation and techniques.....	114
4.2.3.	Estimation of electrochemically active area.....	115
4.2.4.	Preparation and characterization of electrodes.....	116

4.2.5. Detection of DNA hybridisation	117
4.3. Results and discussion	118
4.3.1. Basic electrochemistry of screen-printed electrodes	118
4.3.2. Formation of redox films on screen-printed electrodes	129
4.3.3. Amperometric detection of DNA hybridization with ssDNA grafted onto CM Dextran with ferrocenemethanol as diffusional mediator on screen-printed electrodes	135
4.4. Conclusions	141
4.5. References	142
5. Conclusions and future directions	144
5.1. References	152
List of abbreviations	153
Papers, presentations, awards	155

Acknowledgements

I offer my gratitude to my PhD supervisor, Dr Dónal Leech for allowing me the opportunity to study in his group and for all the help, guidance and advice he has given me during my studies.

I would like to thank all the members of my research group over the time I have been in Galway for providing a friendly atmosphere and for useful discussions on my work. Especially I would to thank Dr Susan Boland and Dr Paul Kavanagh for their contribution to my research.

I am grateful to Dr Anna Nowicka and Dr Zbigniew Stojek from Warsaw University for the effective collaboration on microelectrode sensors.

Thanks must also go to many of the members of the academic and technical staff of the University for all of the help, which was given me; in particular Dr Alan Ryder for providing access to the fluorescence microscope, Gerry Reilly, Dermot McGrath, John Muldoon, Jim Cotter, Seamus Kellehan and Owen Doherty.

Thanks go to the technical staff from Department of Microbiology and Physics.

I would like to also thank to my family and friends for the support they have given me during this study.

I also thank David, for his love, support and patience.

EPA Ireland is gratefully acknowledged for financial support for this project.

Also, I would to thank Professor David Schiffrin and ELCAT Initial Training Network for additional financial support and training during my studies.

I hereby declare this submission is my own work and that, to my best knowledge and belief, it contains no materials previously published or written by another person nor material which to a substantial extent has been accepted for the award of any other degree or diploma of a university or other institution of higher education, except where due acknowledgement is made in the text.

Data presented in Chapter 2 was obtained in partnership with Dr Anna Maria Nowicka from University of Warsaw.

Joanna Hajdukiewicz

Abstract

Electrochemical detection of DNA hybridization is a viable alternative to optical and radio-labelled techniques. The benefits of using biosensors based on electrochemical systems are: high sensitivity, possible development of miniature systems interfaced to electronic devices as well as low cost of operation and small sample requirements.

In detail in this thesis development of an electrochemical DNA hybridization assay, based on deposition of films consisting of single-strand DNA cross-linked with an osmium-based redox polymer on gold microelectrodes modified with self assembled monolayer of cysteamine. A signal, corresponding to hybridization between the immobilized probe ssDNA and a biotin-conjugated target DNA is amplified by addition of glucose oxidase-avidin conjugate and glucose substrate. The interaction between target DNA, glucose oxidase-avidin and osmium redox polymer layer generates a bioelectrocatalytic current in the presence of glucose. Catalytic currents corresponding to oxidation of glucose scale with complementary DNA concentration. A sensitivity improvement is gained when replacing gold macroelectrode ($\phi = 2 \text{ mm}$) with microelectrode ($\phi = 40 \text{ }\mu\text{m}$).

In a further study, modification of carbon electrodes via aryl diazonium electroreduction was investigated to provide a more robust sensing platform. The electrografted layer, consisting of aromatic amine, can be then used to anchor carboxymethylated dextran, allowing further attachment of single stranded DNA within the anchored film. Hybridisation of biotinylated complementary DNA sequence followed by reaction between biotin and glucose oxidase-avidin results in bioelectrocatalytic current in the presence of glucose and ferrocenemethanol in solution as electron transfer mediator. As was observed for the microelectrode sensor, the signals scale with the concentration of target DNA yielding a sigmoidal curve, when plotting current versus logarithm of concentration. The more robust sensing platform allows for use of blocking agents with this assay. Presence of milk powder and detergent (sodium dodecyl sulphate) in hybridisation solution improved the specificity of the sensor.

DNA sensing requires analysis of an enormous number of samples. A high through-put approach using the sensing platform developed can be achieved using disposable electrodes. The same approach to sensing platform development was thus applied to screen-printed carbon electrodes. Such screen-printed sensors, as in the previous cases, allowed distinguishing between complementary and non-complementary sequences of target DNA. The standard deviation of the signals was, however, higher for screen-printed electrodes than that observed for graphite disc electrodes.

Future work should focus on improving the precision of the assay. This would involve seeking well-defined and reproducible electrodes and also investigating the use of reagents which have minimum effect on background currents of carbon electrodes.

Chapter 1

Introduction

1.1. Chemically modified electrodes

Chemically modified electrodes (CMEs) have received considerable attention since first described by Murray and co-workers in 1975. (1) They represent the class of electrodes where molecules participating in the electrochemical reaction are concentrated within an electrode surface. They find application in vast areas of science, such as sensors, (2) energy conversion, (3) molecular electronics, (4) electrochromic displays (5) and electro-organic synthesis. (6) Most of CMEs fall into four main categories: chemisorbed and covalently bound monolayers, polymer films and composite systems, as described by Murray et al. (7) The brief overview of types of chemically modified electrodes is shown in **Table 1.1 A and B**.

Use of chemically modified electrodes enables electrocatalysis at the electrode/solution interface by immobilised molecular catalysts. In the case of many electrochemical reactions a bare electrode provides too high an overpotential for a process to occur at high efficiency. Changing the chemical nature of the electrode surface allows the reaction to occur closer to that which is predicted thermodynamically. It might be worth mentioning, that tuning of the catalytic properties of the electrode can be achieved not only by immobilising catalysts on the electrode surface, but also by controlling geometry of the electrode surface, for instance by attaching nanoparticles (8) or nanotubes (9) or forming different crystalline form of the electrode material, e.g. stepped surfaces.(10)

Table 1.1 A An overview of types of chemically modified electrodes

Method	Description	Examples	Ref.
Chemisorption	Chemical film strongly and irreversibly adsorbed on the electrode.	Chemisorption of Lewis acids - carboxylic acids, aliphatic and aromatic amines, and phosphonic acids on metal oxide surfaces	(11)
		Adsorption of alkenes on platinum	(12)
		Self-assembled monolayers – formed on the substrate via adsorption from homogenous solution	(13)
		Langmuir-Blodgett formed via adsorption of existing organized layer from water-air interface. The monolayer is organized prior to deposition due to presence of head hydrophilic and tail hydrophobic group	(14)
Covalent coupling	Formation of a stable covalent bond between the modifier and the electrode material.	Coupling to functional groups –OH, -COOH or NH ₂ formed on the surface of carbon	(15)
		Reduction of aryl diazonium salts	(16)
		Oxidation of amines on glassy carbon	(17)
		Covalent bonding of alkenes and alkynes to graphite	(18)
		Coupling of organosilanes to carbon surfaces	(19)

Table 1.1 B An overview of types of chemically modified electrodes – cont.

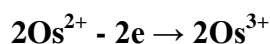
Method	Description	Examples	Ref.
Polymer film coating	A polymer film layer is formed either via physisorption, electropolymerisation at the electrode surface, electrostatic interaction or covalent bonding.	Layered polyelectrolyte films – “layer-by-layer” - polymer deposited on the charged surface via electrostatic interactions, multilayers formed due to interactions between polycations and polyanions	(20)
		Conducting polymers- polypyrrole, polythiophene, polyaniline, and their analogues prepared by oxidative polymerization of the corresponding monomers, either chemically in the presence of the catalyst or electrochemically on the electrode surface	(21)
		Redox polymers - polymers possessing isolated electrochemically active sites, the electron hopping occurs in between the sites; examples include polyvinylferrocene, osmium and ruthenium bipyridyl complexes	(22)
Composite electrodes	Consists of two or more phases, frequently an inorganic oxide and other organic or inorganic components incorporated into the structure. Could be encapsulated with biomolecules.	Gold nanoparticle - DNA composite immobilised on gold electrode – sensor for detection of paraquat	(23)
		Carbon nanotube/ Teflon composite – it possesses electrocatalytic activity towards hydrogen peroxide and NADH	(24)
		Composite films made of polyaniline and cadmium sulfide – a material for electrochromic devices	(25)
		A hybrid material containing Zr-O-Si covalent bonds – used to build semiconductors	(26)

A range of electrochemical sensors operate on the basis of oxidation/reduction of the analyte catalysed by immobilised molecules. The interactions between the electrode surface and the analyte are translated into a measurable signal, such as potential, current, conductivity, resistance, charge density or electric permittivity. (27) For majority of sensors the recognition occurs between the solution and the electrode as in the case of the reduction of oxygen by chemically-bound metal porphyrines (28) or substrate recognition by immobilised enzyme. (29) A more complex mechanism applies to bioaffinity sensors. Many of protein and DNA sensors and immunoassays require incubation with the analyte prior to the detection. (30) Furthermore, not all of bio-interactions result in sufficient change in electrical properties of the electrode surface. Electroactive labels, e.g. nanoparticles, (31-34) metal complexes, (35) and enzymes (36) are introduced for the electrochemical reaction to occur generating a signal.

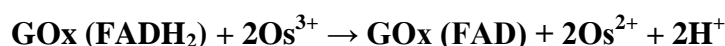
The mediated electrocatalysis of enzymes is of special interest in biological sensing; the main role of the enzyme is to act as the catalyst specific for the analyte. Activation of the enzyme often requires the presence of an electron transfer mediator; the electron is passed between an electrode, the mediator, the enzyme and the substrate. (**Scheme 1.1**)

Mediated oxidation of glucose by glucose oxidase using osmium redox complexes could be used as a specific example:

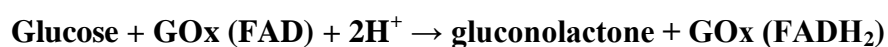
First, oxidation of the mediator occurs:

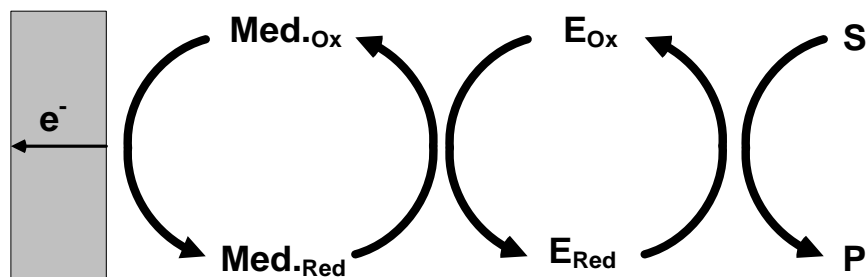


Then the redox cofactor flavin adenine dinucleotide (FADH₂ in its reduced form) in glucose oxidase is oxidised to FAD (oxidised form of flavin adenine dinucleotide):



GOx (FAD) catalyses oxidation of glucose to gluconolactone:





Scheme 1.1 Electron transfer path in redox mediated systems. In the anodic process oxidation of the mediator (**Med.Ox**, **Med.Red**) by the electrode withdraws electrons from the enzyme. Enzyme in its oxidised form (**E_{Ox}**) catalyses oxidation of the substrate (**S**) and beside the products (**P**) a reduced form of the enzyme is formed (**E_{Red}**), enzyme is oxidised back and releases the electrons, which are then used to recycle the mediator. The opposite is the case of catalytic reduction; mediator is reduced and passes electrons onto the enzyme. Reduced form of the enzyme is capable of reducing the substrate and then as in the previous case, the enzyme and the mediator are recycled.

The chemical structures of **FAD** and **FADH** redox cofactors are presented in **Figure 1.1**

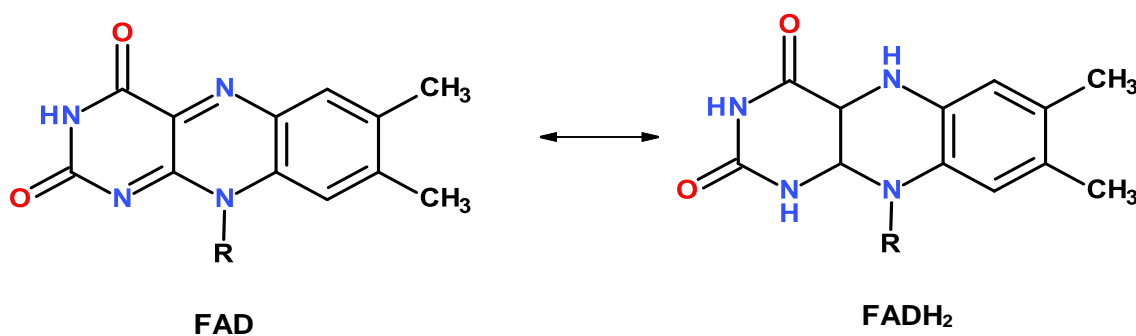


Figure 1.1 Chemical structures of flavin groups of FAD and FADH₂ cofactors showing quinone/hydroquinone redox transition, R represents adenosine diphosphate linked to flavin via ribitol bridge.

Chemical structures of selected redox mediators are presented in **Figure 1.2**.

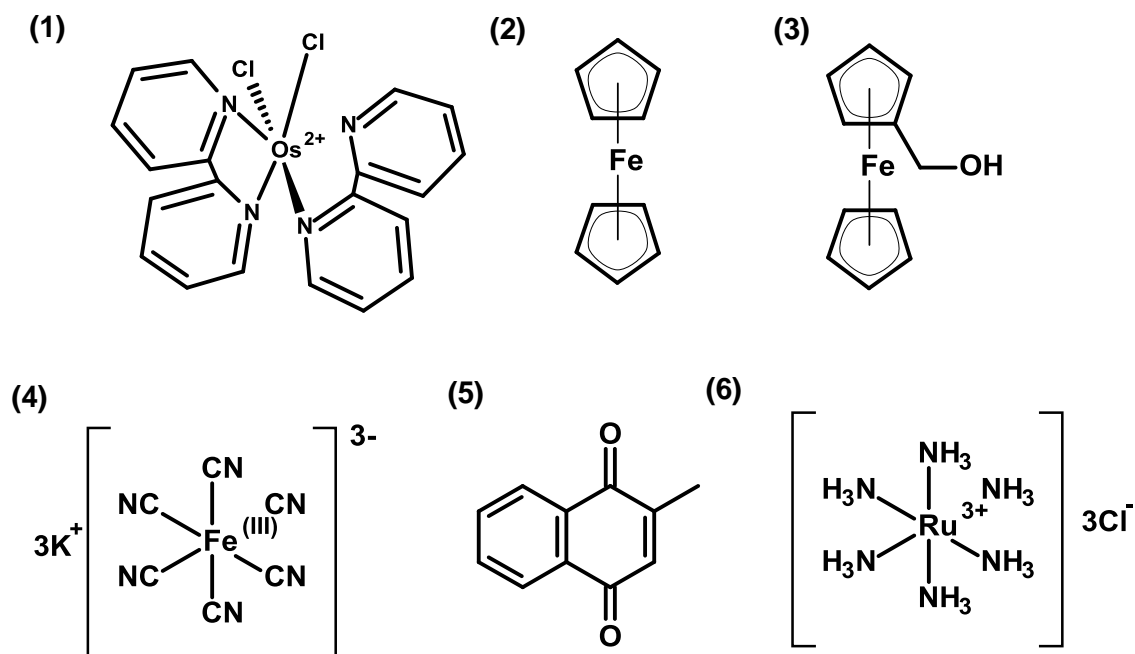


Figure 1.2 Structures of selected redox mediators, (1) $\text{Os}(2,2'\text{-bipyridine})_2\text{Cl}_2$, (2) ferrocene, (3) ferrocenemethanol, (4) potassium ferricyanide, (5) 2-methyl-1,4-naphthoquinone, (6) hexaammineruthenium (III) chloride.

Bioelectrocatalysis by glucose oxidase forms the principle of detection in most amperometric glucose sensors. A range of methodologies for preparation of electrodes modified with glucose oxidase and the redox mediator is reported in the literature. (37) One of the first reports in the field was published by Foulds and Lowe, who described a glucose sensing electrode containing a polymeric layer of ferrocene-conjugated polypyrrole and GOx. (38) A distinct contribution to the glucose sensing technology was made by Adam Heller's group. (37, 39-42) A glucose detection platform, where glucose oxidase is 'wired' to osmium 2,2'-bipyridine based redox polymer was developed and successfully tested in 'in-vivo' applications. (41) Besides recognition of specific analytes, enzymes are widely used for indirect detection of binding events, such as antibody/antigen coupling, (43) protein binding (44) and DNA hybridisation. (45, 46)

1.2. Characterisation of the redox hydrogels on electrodes

Cyclic voltammetry is one of the most convenient methods for studying the redox processes of chemically bound species. The voltammetric peak current for an immobilised redox monolayer is modelled mathematically by **Equation 1.1**. The voltammetric peak currents are proportional to the scan rate. (47)

$$I_p = \frac{n^2 F^2 A \Gamma_T v}{4RT} \quad (1.1)$$

Where:

I_p – peak current

n - number of electrons exchanged in the redox process

F - Faraday constant

A – electrode area

Γ_T - surface coverage of electroactive sites

R - gas constant

v - scan rate

T - temperature

Integration of the charge under the voltammetric peak allows quantifying of the electroactive sites of the immobilised layer. Surface coverage of surface-bound redox-active centres is described by the **Equation 1.2**.

$$\Gamma = \frac{Q}{nFA} \quad (1.2)$$

Figure 1.3 illustrates a cyclic voltammogram of an electrode modified with an electroactive film. Examination of the parameters of the voltammetric curve allows probing of the nature of electrochemical reaction, kinetics of electron transfer and interactions with the electrolyte.

For example proportionality of peak currents versus scan rate and near-zero peak-to-peak splitting indicate a reversible electrochemical reaction and a fast electron

transfer within the film. Also E_{FWHM} (FWHM – full width at half peak maximum) for an ideally reversible process should not exceed $90.6/n$ mV. (48)

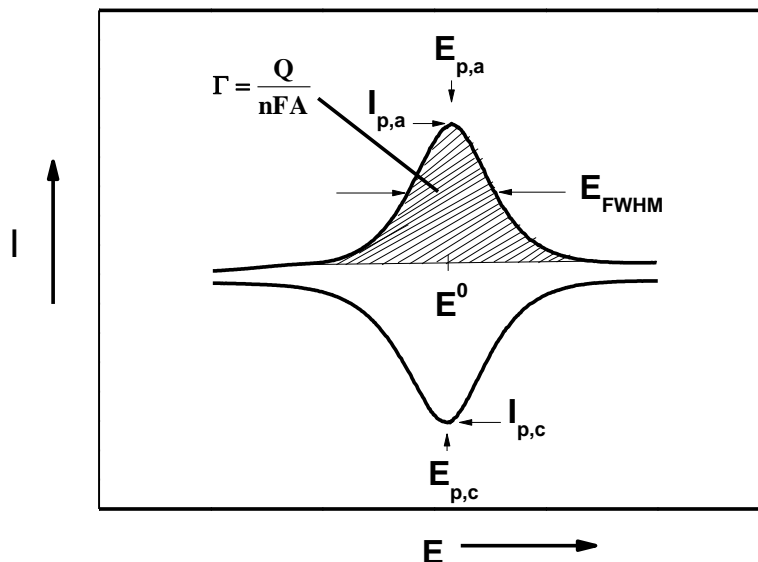


Figure 1.3 Cyclic voltammogram of immobilised redox species, basic parameters, which allow to characterise the layer are depicted in the figure; $I_{p,a}$ – anodic current, $I_{p,c}$ – cathodic current, $E_{p,a}$ – oxidation potential, $E_{p,c}$ – reduction potential, E^0 – formal potential of electrochemical reaction, E_{FWHM} (FWHM) – full width at half peak maximum, Γ – surface coverage. Adapted from reference (48)

Characterisation of the multilayered films, commonly formed from redox active polymers is more complex and the mechanism of charge transport in redox polymer films is the subject of intense debate among researchers. The elementary theory of this phenomenon states that the electrons are transferred between neighbouring redox sites, followed by the motion of counter ions and solvent through the film. In analogy to solution phase redox reactions, the laws of diffusion apply to charge transport in redox polymer films. Voltammetric peak currents scale linearly with the square root of the scan rate at high polarization rates. For low scan rates finite diffusion model applies and the peak currents scale linearly with the scan rate. (48)

At relatively rapid scan rates, where semi-infinite diffusion is operational, an estimate of rates of charge transfer can be evaluated from the parameter $D_{CT}^{1/2}C_0$ (D_{CT} – charge transfer diffusion coefficient, C_0 – concentration of electroactive sites)

using the Randles-Sevcik equation, usually expressed at a temperature of 25°C (Equation 1.3):

$$I_p = 2.69 \times 10^5 n^{\frac{3}{2}} A D_{CT}^{\frac{1}{2}} C_o v^{\frac{1}{2}} \quad (1.3)$$

The electron hopping between sites is influenced by properties of the polymeric layer, such as redox site loading, type of polymer backbone and presence of a cross-linker. Increasing distance between the electroactive sites should lead to slower electron transfer, but in case when large void space between redox polymer chains exists, movement of counter ions through the film adds more significant contribution to the charge transport. Forster and Vos (49) examined the effect of chemical structure of the polymer on charge transport. They found that intermediate loadings of osmium redox sites yield maximum charge transport rates. As found by Inzelt (50) diffusion coefficient determined from cyclic voltammetry response of surface-bound redox polymer scales linearly with the number of electroactive sites.

Also, the experimental conditions, such as the choice of solvent, type and concentration of the supporting electrolyte, pH, and temperature have a severe impact on electrochemical behaviour of redox polymer films. Polymer network swells, when exposed to solvent increasing distances between the redox sites and subsequently affecting electron hopping rate. (50) Several researchers including Ju et al., (51) Forster and Vos, (52) Inzelt and Szabo (53) have examined the dependence of charge transport on supporting electrolyte type and concentration. Cyclic voltammetry studies by Forster et al. (54) showed a linear relationship between ionic strength and diffusion coefficient except for perchlorate ions for which $D_{CT}^{1/2}C$ values decrease with ionic strength. Influence of counter ion is related to solubility of the salt of the redox polymer. Low degree of solubility would restrict the solvent penetration and results in diminished response, when concentration of counter ion increases. Dependence on pH was also reported, (51) (55) however it does not seem to appear in highly-crosslinked films. (56)

1.3. Electrochemistry of nucleic acids

1.3.1. Structure and properties of DNA

DNA testing has become a widely adopted technique in laboratory screening, including for diagnosis of diseases, pathogen identification and determination of inheritance patterns. As genetic testing has become a viable part of routine laboratory analysis, there is a demand for fast, sensitive and selective methods of identification and quantification of DNA sequences.

Since its discovery in 1869 DNA (57) has been proven to play a vital role in carrying biological information needed to form and maintain, with an exception of some viruses, most of the living organisms.

DNA is a polymeric molecule consisting of monomeric subunits – nucleotides. Each nucleotide is a combination of a nitrogen-containing base, 5-carbon sugar-deoxyribose and a phosphate backbone. There are four major bases present within DNA structure: single ring pyrimidines: cytosine (C) and thymine (T) and double ring purines: adenine (A) and guanine (G) with the structure presented in **Figures 1.4 and 1.5**. The sugar units are linked between 5' position and 3' by phosphodiester bonds. Two strands of DNA (or one of DNA and one of RNA) form a double helix where bases adenine and thymine, guanine and cytosine form pairs via hydrogen bonds. (**Figures 1.4 and 1.5**) Pairing of single DNA strands of different origin is known as DNA hybridisation.

From crystallographic data it is known today that approximately 8000 conformations of DNA and DNA/protein complexes exist. The most basic conformations are the variations of the helical structure: B-DNA, A-DNA and left-handed Z form. (**Figure 1.6**)

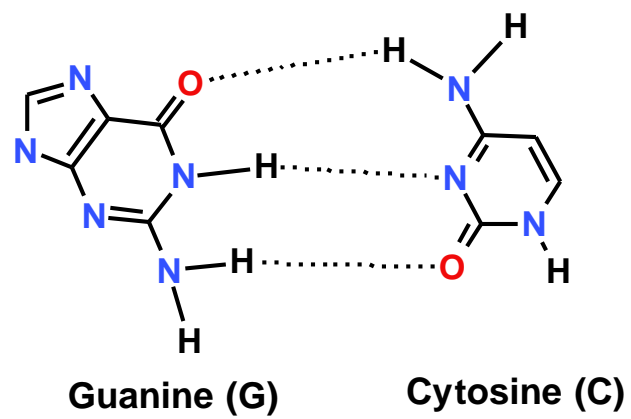
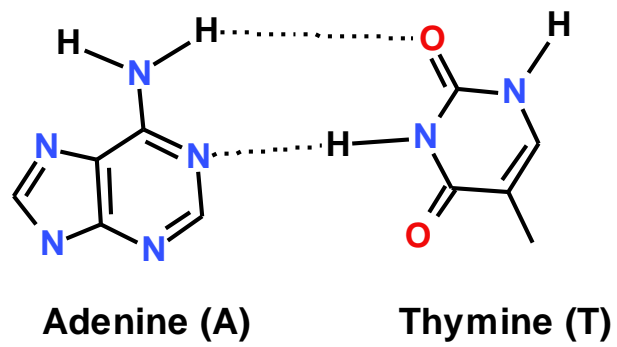


Figure 1.4 Base pairs of Adenine (A) and Thymine (T), Guanine (G) and Cytosine (C)

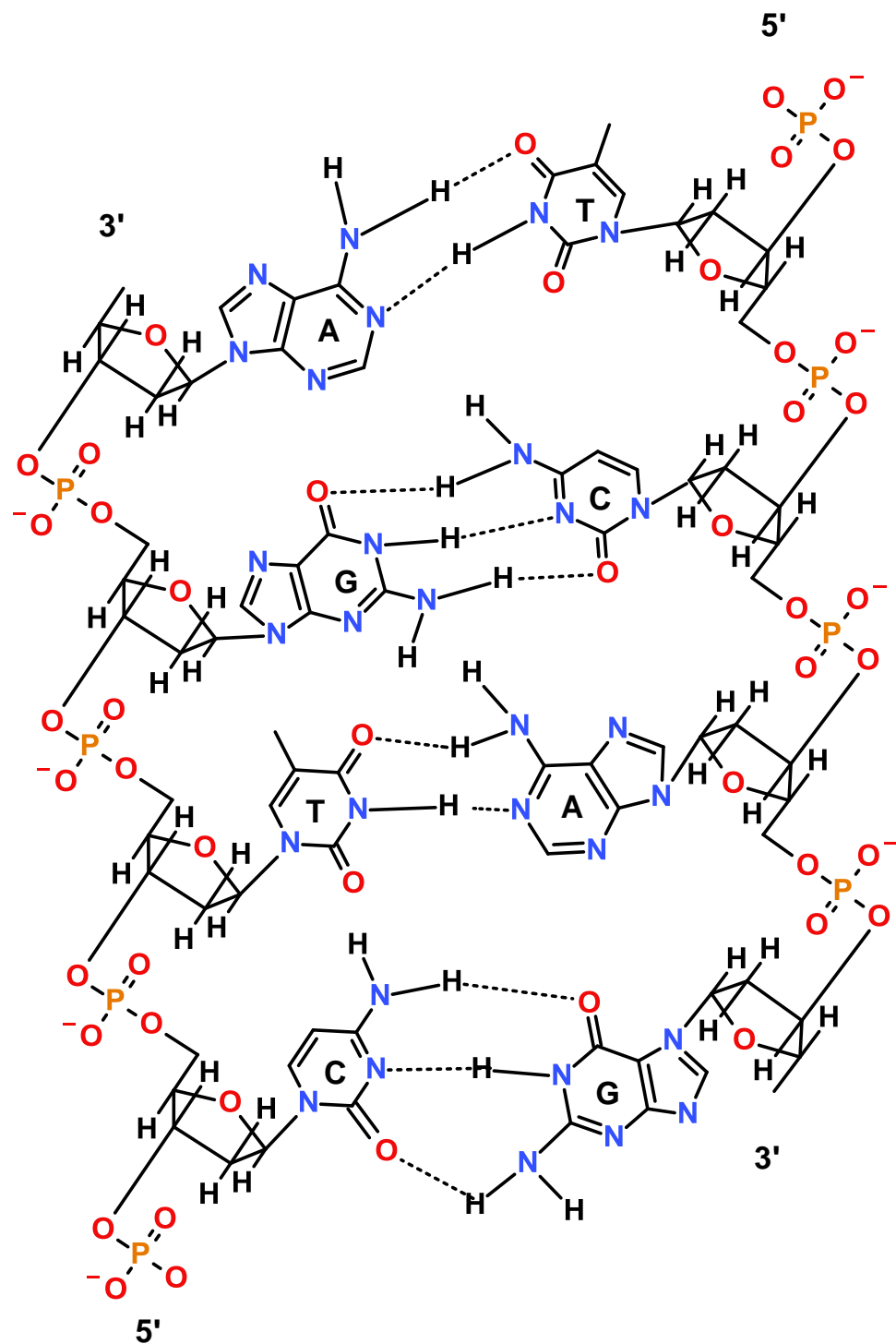


Figure 1.5 Basic structures of DNA strand showing hydrogen bonding between base pairs. Symbols for DNA bases are as follows: A- adenine, T- thymine, C- cytosine, G- guanine

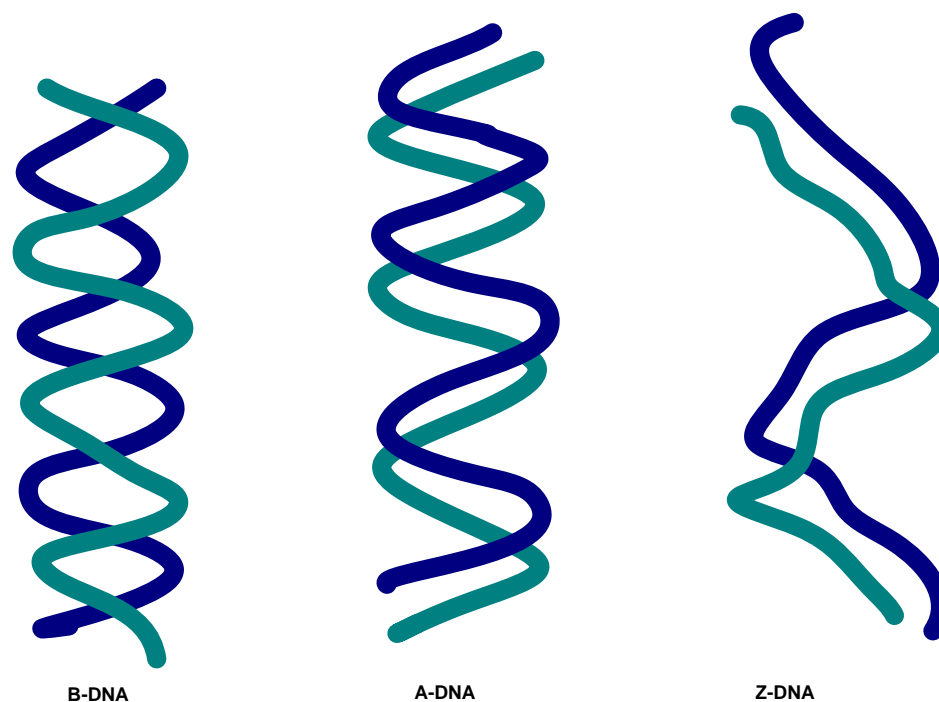


Figure 1.6 Basic conformations of the double helix.

The analysis of nucleic acids is complex and an enormous number of protocols adapted for specific samples exist. A general procedure for *in vitro* analysis of DNA involves DNA extraction, target amplification, cleavage by restriction enzymes and denaturation. This is followed by hybridisation with a known probe and determination of the signals generated by labelling of the double strand with isotopes, optically active molecules or redox enzymes. (58)

Electrochemical DNA sensors are an attractive alternative to traditional DNA screening methods. Although the optical detection methods were proven to meet analytical laboratory requirements, the high cost and large size of the instrumentation compare poorly with electronic components. Electrochemical sensors can be produced at relatively low cost and also could be easily miniaturised and integrated into electronic circuits. (59)

1.3.2. Electrochemical activity of DNA bases

The idea that DNA can be electrochemically active emerged in 1950s and the most significant contribution was made by E. Paleček who studied polarography of DNA and RNA. (60-64) From all the nucleic acid components only the DNA bases are electrochemically active. They are reducible at mercury electrodes, this reaction occurs at negative potentials that cannot be achieved on carbon electrodes in aqueous media. (A lower potential limit for carbon electrode is in the region of -1.4 V versus saturated calomel electrode, when using KCl as an electrolyte (47))

Reduction of adenine, guanine and cytosine in aqueous media was reported. (65) Later in 1970s, carbon was found suitable to study oxidation of guanine and adenine. (66) Oxidation of other pyrimidines was thought to be impossible until 1997, when Brett and Matysik (67) demonstrated electroactivity of cytosine and thymine at glassy carbon electrodes nearly thirty years after first reports on DNA oxidation appeared. Mercury electrodes and DNA are both hydrophobic and the DNA bases are strongly absorbed on the electrode surface preventing the formation of the double helix, making the study of hybridisation at such electrodes difficult. (68)

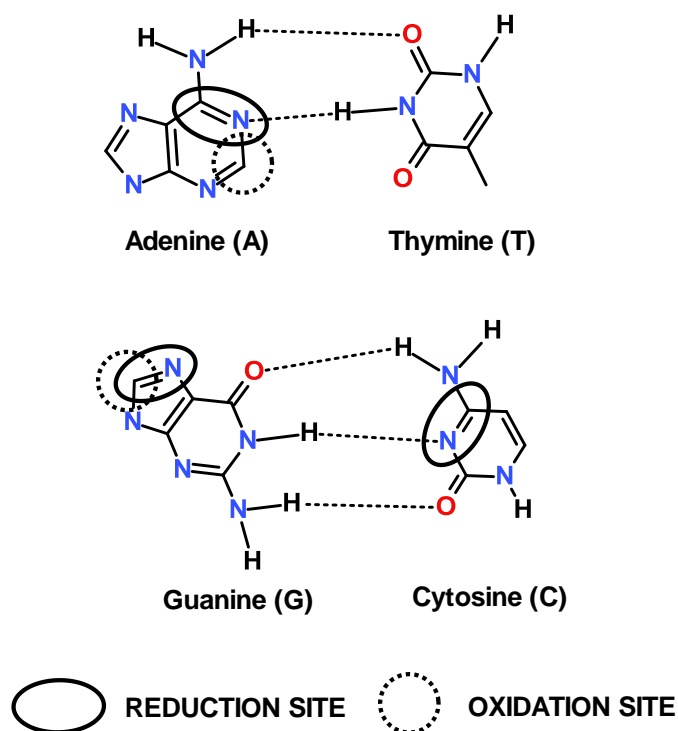


Figure 1.7 Reduction and oxidation sites of the DNA bases. Adapted from reference (63)

1.3.3. Immobilisation chemistry of DNA for sensor development

In 1986 E. Paleček proposed cumulative pre-adsorption of DNA and proteins on the hanging mercury drop electrode. This technique has allowed extending the range of electrolytes available for electrochemical experiment and also reducing the sample size to the level of few microliters. (69) Another step forward was to study interactions between immobilised DNA and the sample. As mentioned in the previous section, DNA hybridisation is not very likely to occur at mercury electrodes. In addition, toxicity of mercury as well as technical difficulties with immobilising the probe for repetitive analysis must contribute to the fact that, when selecting the substrate for a DNA biosensor, solid electrodes, such as gold and carbon, are preferred.

Many different approaches have been adopted for entrapment of ssDNA onto electrodes. Brett and Chiorcea described the formation of adsorbed DNA film on highly oriented pyrolytic graphite electrode. Well ordered DNA lattices are formed in the pH controlled conditions and also with the potential applied to the electrode. (70) DNA can be easily adsorbed on cationic polymers, such as polyallylamine, poly-L-lysine and polyethylenimine. (71)

One of the most common methods involves immobilisation of DNA using biotin-avidin, or biotin- streptavidin conjugate formation, (72-74) because of the high binding constant of avidin-biotin complex formation, estimated to be 10^{15}M^{-1} . (73) Williams et al. published on a genosensor based on streptavidin/graphite/epoxy composite. (72) Streptavidin was used to capture a biotinylated ssDNA probe. Popularity of the method is undoubtedly related to the fact that biotin-modified DNA sequences are readily available from commercial sources. The structure of a biotin modification is presented in **Figure 1.8**.

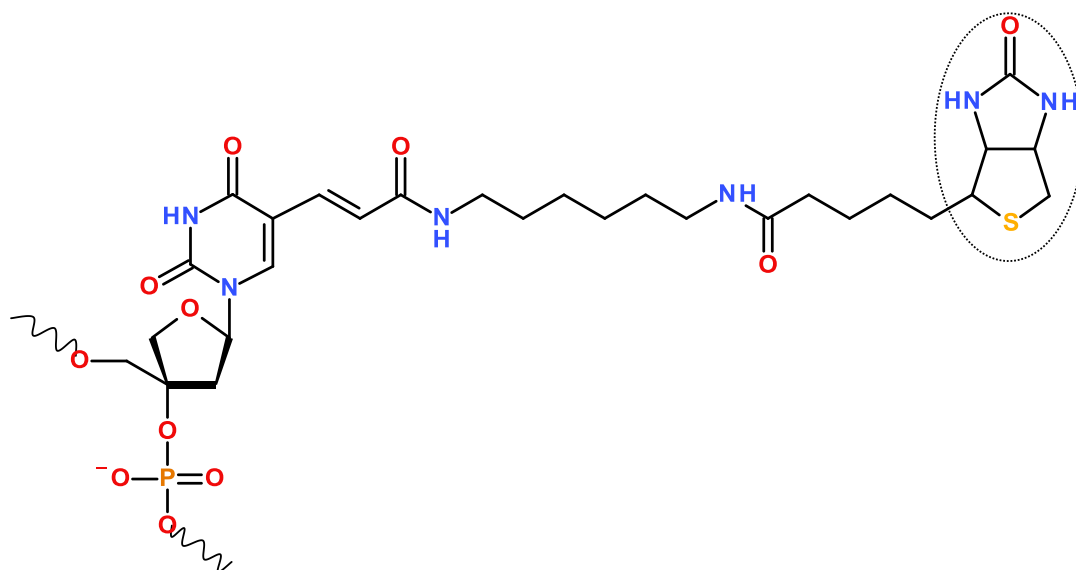


Figure 1.8 Biotin modification to the 5' end of the DNA chain. A dotted contour line indicates biotin molecule

Probe DNA can be also chemisorbed on gold electrodes via self assembly. This could be achieved by incubation of the electrode in the solution containing thiolated DNA sequences (HSssDNA). (75-77) Due to large size and hydrophilic nature of DNA these monolayers are not densely packed and they exhibit poor thermal stability. (78) Herne and Tarlov (75) underline the importance of forming mixed monolayers of HSssDNA and mercaptohexanol. If the electrode is treated with mercaptohexanol subsequent to HSssDNA immobilisation, non-specific adsorption of the DNA probe can be reduced and, as the result, accessibility of the probe for the hybridisation is improved. In another approach DNA is crosslinked to a self-assembled monolayer of alkanethiols bearing amino-, carboxyl- or hydroxyl- functionality. Silva et al. report on the genosensor, where the probe is attached to cysteamine monolayer via crosslinking of amino- groups with glutaraldehyde. (79) An example of self-assembled monolayer of alkanethiol on electrode surface is presented in **Figure 1.9**.

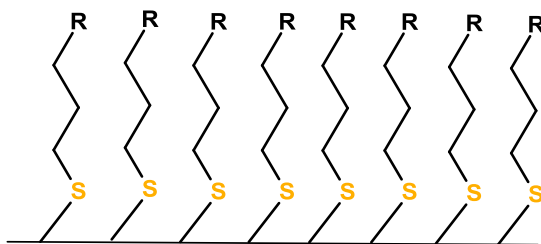


Figure 1.9 Schematic representation of self-assembled monolayer of thiol on the electrode surface. Alkanethiols used for monolayer formation vary by the alkane chain length and functional groups. R could equal to $-\text{NH}_2$, $-\text{OH}$, $-\text{COOH}$, $-\text{SH}$. The stability and the degree of order of the monolayer increases with longer alkane chains (80)

Figure 1.10 presents a structure of amino-modification to the sugar-phosphate backbone. Amino- group could be used to link DNA to another functional group on the electrode. Reacting of the amine to carboxylic group on the electrode forms an amide bridge. The formation of the amide could be catalyzed by carbodiimide/N-hydroxysuccinimide by the mechanism shown on **Figure 1.11**.

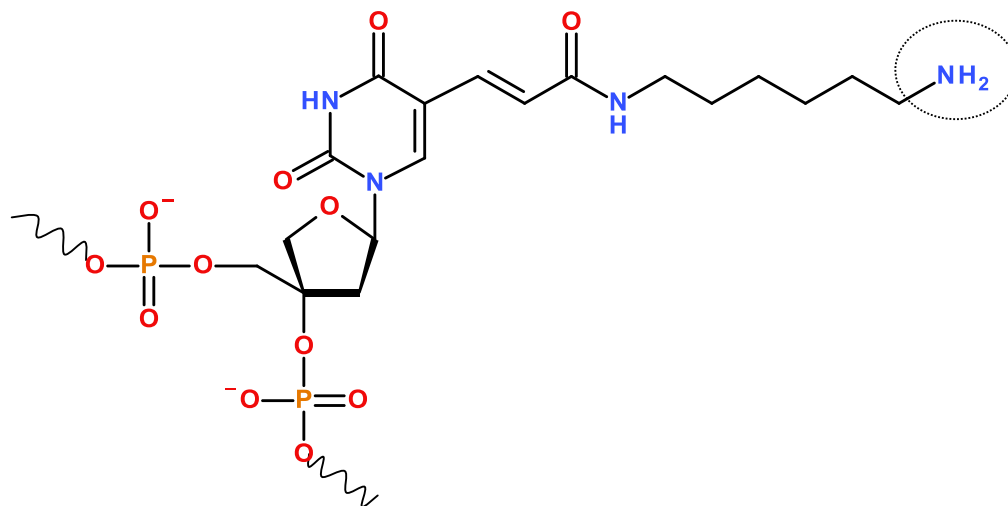


Figure 1.10 Amino- modification to the 5' end of the DNA chain

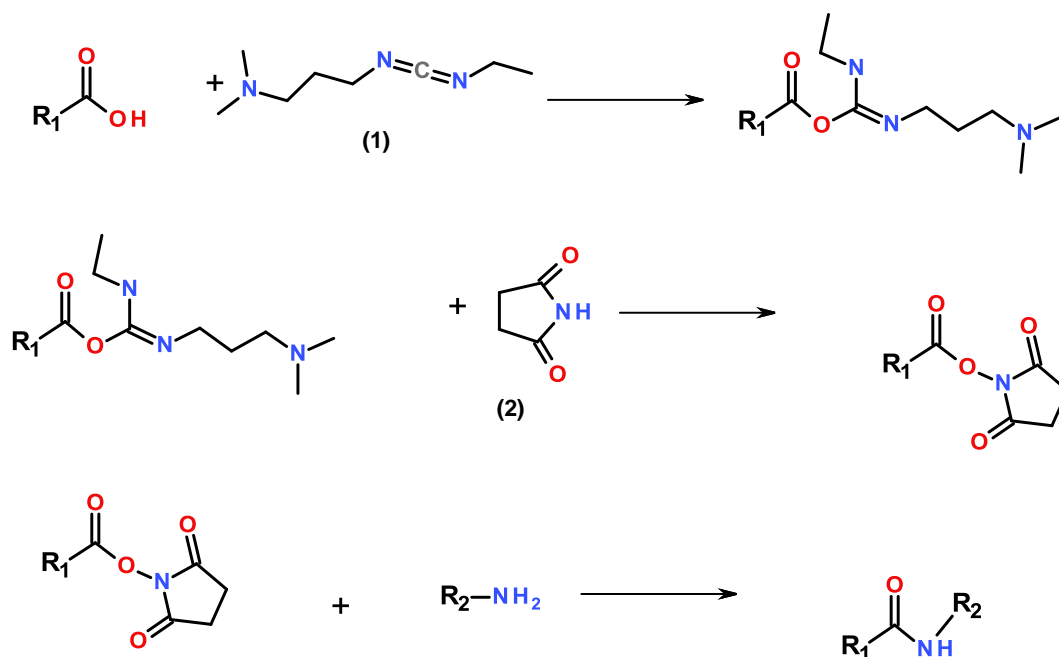


Figure 1.11 Mechanism of **EDC/NHS** coupling (EDC - 1-ethyl-3-(3-dimethylaminopropyl)carbodiimide (1), NHS - N-hydroxysuccinimide (2))

DNA can be covalently linked to a polymer deposited on the electrode. The carbodiimide coupling between phosphate backbone of the DNA to Os-PAA-PVI (osmium complex bound to a polyallylamine-polyvinylimidazole co-polymer) towards formation of hydrazides was described by Heller's group. (81) Also, a reaction with a functionalised polypyrrole backbone is possible. (82) The covalent immobilization on carbon surfaces was also reported. Fang Teh at al. coupled a capture probe to glassy carbon electrode derivatised with 4-aminobenzoic acid. (83) A method based on covalent coupling to carboxylated carbon nanotubes/ carbon ink composite was published by Erdem et al. (84)

1.3.4. Electrochemical detection of DNA hybridisation

Direct detection of DNA hybridisation is a progressing field of research, but the methodology is still far from achieving high-throughput and sensitivity. (85) Signal

amplification can overcome problems with detection of low quantities of target and with matrix interferences.

Redox-active metal complexes, (86) organic and metal complex intercalators, (87) nanoparticles (88) and enzymes (89) are commonly used as tags to indicate helix formation.

Enzyme labelling is particularly attractive for sensor applications due to commercial availability of enzymes and large signal amplifications as a result of substrate turnover. (90) Generally, hybridization is indicated by the enzyme-catalyzed electro-oxidation/reduction of a substrate to an electrochemically detectable product. During the catalytic process a large number of electrons are transferred between the enzyme and the electrode (**Scheme 1.1**) as the result of hybridization event, thereby generating an amplified electrochemical signal. Commonly used enzymes include alkaline phosphatase (91), horseradish peroxidase (HRP), (92-100) glucose oxidase, (101) glucose dehydrogenase, (102) soybean peroxidase (103) and bilirubin oxidase. (104) Enzymes are usually coupled to the target or reporter DNA strand via avidin (or streptavidin, neutravidin) - biotin binding technology, (101) or by chemical coupling. (81)

Heller and coworkers have reported a number of highly sensitive sandwich-type assays for enzyme-amplified amperometric DNA detection using a horseradish peroxidase (HRP) labelled target sequence with an electron mediating osmium redox polymer film. (92, 96-98) Upon hybridization with the probe sequence, the HRP redox enzyme is 'wired' to the electrode via mediating redox polymer. This contact enables the bioelectrocatalytic reduction of H_2O_2 to water, generating a current proportional to the amount of hybridized target sequences. Caruana and Heller (103) subsequently used this approach to detect a single base mismatch in an 18-base oligonucleotide at elevated temperatures, using the redox-enzyme soybean peroxidase (SBP), recording the signal corresponding to reduction of H_2O_2 to water.

1.4. Thesis outline

The aim of this thesis is to investigate the performance of DNA- modified electrodes for enzyme-amplified detection of short sequences of DNA. The sensors are developed with a view to be used for screening of short sequences extracted from pathogenic bacteria. The present study focuses on the use of microelectrodes and mass-produced carbon electrodes to provide a base for DNA sensing platform.

Chapter 2 addresses the preparation and electrochemical characterisation of DNA sensing films using osmium redox polymers on gold microelectrodes. A probe DNA confined to the electrode surface is hybridised to a biotinylated target DNA, which is further labelled with glucose oxidase:avidin conjugate resulting in an electrocatalytic surface capable of oxidising glucose. Bioelectrocatalytic current corresponding to oxidation of glucose is an indication of DNA hybridisation. The electrochemical parameters and stability of the redox hydrogel are discussed in detail. Chapter 2 is also concerned with the effect of miniaturisation on the detection limits: performance of microelectrodes is compared to that of macroelectrodes.

In Chapter 3, another surface preparation methodology is introduced. The development of sensors for DNA hybridisation within carboxymethylated dextran matrix on electrodes is probed. To this end, different functionalised electrode materials are examined as the substrates for dextran hydrogel immobilisation: thiol modified gold; and glassy carbon and graphite derivatised via reduction of aryl diazonium salts. A model study, where an osmium complex $[\text{Os}(2,2'\text{-bipyridine})_2(4\text{-aminoethylpyridine})\text{Cl}]\text{PF}_6$ is attached to carboxymethylated dextran on the electrode via carbodiimide coupling was undertaken to estimate the density of the carboxylic groups of the polymer available for attachment of probe DNA. Hybridisation events were detected at the electrode surface using the same glucose oxidase labelling approach as in Chapter 2, but a solution phase mediator was employed instead of co-immobilised osmium complex. The hybridisation protocol was altered and a more rigorous washing and surface blocking was introduced in order to reduce non-specific binding of the DNA strands and enzyme avidin conjugate. Bioelectrocatalytic detection of DNA mediated by $[\text{Os}(2,2'\text{-bipyridine})_2(4\text{-aminomethylpyridine})\text{Cl}]\text{PF}_6$, co-immobilised to the dextran was investigated, in a preliminary study aimed at providing reagentless DNA hybridisation sensors.

In Chapter 4, a range of screen-printed carbon electrodes is electrochemically characterised towards their response to basic electrolyte solution and redox probes. Then the electrodes are derivatised with carboxymethylated dextran and ssDNA in a similar manner as in Chapter 3, to assess their suitability as surfaces for mass-produced DNA hybridisation sensors.

The main findings of the research are summarised in Chapter 5 and proposals for future studies discussed.

1.5. References

1. P. R. Moses, L. Wier, R. W. Murray, *Anal. Chem.* **47**, 1882 (1975).
2. J. Janata, *Principles of Chemical Sensors*. (Springer, 2009).
3. M. T. S. Nair, P. K. Nair, R. A. Zingaro, E. A. Meyers, *J. Appl. Phys.* **75**, 1557 (1994).
4. C. A. Mirkin, M. A. Ratner, *Annu. Rev. Phys. Chem.* **43**, 719 (1992).
5. F. B. Kaufman, A. H. Schroeder, E. M. Engler, V. V. Patel, *Appl. Phys. Lett.* **36**, 422 (1980).
6. J.-I. Yoshida, K. Kataoka, R. Horcajada, A. Nagaki, *Chem. Rev.* **108**, 2265 (2008).
7. R. W. Murray, A. G. Ewing, R. A. Durst, *Anal. Chem.* **59**, 379A (1987).
8. S. G. Ramos, M. S. Moreno, G. A. Andreasen, W. E. Triaca, *Int. J. Hydrogen Energy* **35**, 5925 (2010).
9. K. Matsubara, K. Waki, *Electrochim. Acta* **55**, 9166 (2010).
10. N. P. Lebedeva, M. T. M. Koper, J. M. Feliu, R. A. van Santen, *J. Phys. Chem. B* **106**, 12938 (2002).
11. Y. Gushikem, S. S. Rosatto, *J. Braz. Chem. Soc.* **12**, 695 (2001).
12. R. F. Lane, A. T. Hubbard, *J. Phys. Chem.* **77**, 1401 (1973).
13. H. O. Finklea, in *Electroanalytical chemistry. A series of advances. Organized monolayers on electrodes*, A. J. Bard, I. Rubinstein, Eds. (Marcel Dekker, New York, 1996), vol. 19, pp. 109-335.
14. L. M. Goldenberg, *Russ. Chem. Rev.* **66**, 1033 (1997).
15. V. J. Razumas, J. J. Jasaitis, J. J. Kulys, *Bioelectrochemistry and Bioenergetics* **12**, 297 (1984).
16. M. Delamar, G. Désarmot, O. Fagebaume, R. Hitmi, J. Pinson, J. Saveant, *Carbon* **35**, 801 (1997).
17. R. S. Deinhammer, M. Ho, J. W. Anderegg, M. D. Porter, *Langmuir* **10**, 1306 (1994).
18. S. Ssenyange, F. Anariba, D. F. Bocian, R. L. McCreery, *Langmuir* **21**, 11105 (2005).
19. C. M. Elliott, R. W. Murray, *Anal. Chem.* **48**, 1247 (1976).
20. J. Rusling, *Progr. Colloid. Polym. Sci.* **103**, 170-180 (1997)
21. U. Lange, N. V. Roznyatovskaya, V. M. Mirsky, *Anal. Chim. Acta* **614**, 1 (2008).
22. A. Heller, *Curr. Opin. Chem. Biol.* **10**, 664 (2006).
23. J. A. Ribeiro, C.A. Carreira, H.J. Lee, F. Silva, A. Martins, C.M. Pereira *Electrochim. Acta* **55**, 7892 (2010).
24. J. Wang, M. Musameh, *Anal. Chem.* **75**, 2075 (2003).
25. H. Yoneyama, M. Tokuda, S. Kuwabata, *Electrochim. Acta* **39**, 1315 (1994).
26. S. K. Dey, C.-G. Wang, D. Tang, M. J. Kim, R. W. Carpenter, C. Werkhoven, E. Shero, *J. Appl. Phys.* **93**, 4144 (2003).
27. A. Hulanicki, S. Glab, F. Ingman, *Pure & Appl. Chem.* **63**, 1247 (1991).
28. J. Zagal, M. Páez, A. A. Tanaka, J. R. dos Santos Jr, C. A. Linkous, *J. Electroanal. Chem.* **339**, 13 (1992).
29. I. Karube, Y. Nomura, *J. Mol. Catal. B: Enzym.* **10**, 177 (2000).
30. O. A. Sadik, A. O. Aluoch, A. Zhou, *Biosens. Bioelectron.* **24**, 2749 (2009).

31. P. Fortina, J. Wang, S. Surrey, J. Y. Park, L. J. Kricka, in *Integrated Biochips for DNA Analysis*, R. H. Liu, A. P. Lee, Eds. (Springer New York, 2007), pp. 187-197.
32. J. Wang, in *Biosensing for the 21st Century*, R. Renneberg, F. Lisdat, Eds. (Springer Berlin / Heidelberg, 2008), vol. 109, pp. 239-254.
33. J. Wang, in *Microarrays*, K. Dill, R. H. Liu, P. Grodzinski, Eds. (Springer New York, 2009), pp. 339-353.
34. Z. Wang, B. Yang, in *MicroRNA Expression Detection Methods*. (Springer Berlin Heidelberg, 2010), pp. 191-198.
35. K.-W. K. Lo, S.-Y. L. Lau, in *Coordination Chemistry Research Progress*, T. W. Cartere, K. S. Verley, Eds. (Nova Science Publishers, 2008).
36. X.-M. Li, X.-Y. Yang, S.-S. Zhang, *TrAC Trends Anal. Chem.* **27**, 543 (2008).
37. B. A. Gregg, A. Heller, *Anal. Chem.* **62**, 258 (1990).
38. N. C. Foulds, C. R. Lowe, *Anal. Chem.* **60**, 2473 (1988).
39. M. V. Pishko, A. C. Michael, A. Heller, *Anal. Chem.* **63**, 2268 (1991).
40. B. Linke, W. Kerner, M. Kiwit, M. Pishko, A. Heller, *Biosens. Bioelectron.* **9**, 151 (1994).
41. E. Csoeregi, D. W. Schmidtke, A. Heller, *Anal. Chem.* **67**, 1240 (1995).
42. D. W. Schmidtke, A. Heller, *Anal. Chem.* **70**, 2149 (1998).
43. A. Warsinke, A. Benkert, F. W. Scheller, *Fresenius J. Anal. Chem.* **366**, 622 (2000).
44. K. A. Mahmoud, H.-B. Kraatz, *Chem. –Eur. J.* **13**, 5885 (2007).
45. G. Carpini, F. Lucarelli, G. Marrazza, M. Mascini, *Biosens. Bioelectron.* **20**, 167 (2004).
46. P. Kavanagh, D. Leech, *Anal. Chem.* **78**, 2710 (2006).
47. A. J. Bard, L. R. Faulkner, *Electrochemical Methods, Fundamentals and Applications*. (John Wiley & Sons, Inc., New York, Chichester, Weinheim, Brisbane, Singapore, Toronto, ed. 2nd, 2001).
48. R. W. Murray, in *Electroanalytical Chemistry*, A. J. Bard, Ed. (Marcel Dekker Inc., New York, 1984), vol. 13.
49. R. J. Forster, J. G. Vos, *Electrochim. Acta* **37**, 159 (1992).
50. G. Inzelt, *Electrochim. Acta* **34**, 83 (1989).
51. H. Ju, Y. Gong, H. Zhu, *Anal. Sci.* **17**, 59 (2001).
52. R. J. Forster, J. G. Vos, *Langmuir* **10**, 4330 (1994).
53. G. Inzelt, L. Szabo, *Electrochim. Acta* **31**, 1381 (1986).
54. R. J. Forster, A. J. Kelly, J. G. Vos, *J. Electroanal. Chem.* **270**, 365 (1989).
55. R. J. Forster, T. E. Keyes, A. M. Bond, *J. Phys. Chem. B* **104**, 6389 (2000).
56. A. Aoki, A. Heller, *J. Phys. Chem.* **97**, 11014 (1993/10/01, 1993).
57. R. Dahm, *Dev. Biol.* **278**, 274 (2005).
58. P. Tijssen, *Probe labeling and hybridization techniques*. P. C. van der Vliet, S. Pillai, Eds., *Laboratory Techniques in Biochemistry and Molecular Biology* (Elsevier, 1993).
59. A. Sassolas, B. Leca-Bouvier, L. Blum, *Chem. Rev.* **108**, 109 (2008).
60. E. Palecek, *Die Naturwissenschaften* **45**, 186 (1958).
61. E. Palecek, *Biochim. Biophys. Acta* **51**, 1 (1961).
62. E. Palecek, *J. Mol. Biol.* **20**, 263 (1966).
63. E. Palecek, *Electroanalysis* **8**, 7 (1996).
64. E. Palecek, *Electroanalysis* **21**, 239 (2009).
65. E. Palecek, *J. Electroanal. Chem.* **22**, 347 (1969).

66. V. Brabec, *J. Electroanal. Chem.* **128**, 437 (1981).
67. A. M. Oliveira Brett, F.-M. Matysik, *J. Electroanal. Chem.* **429**, 95 (1997).
68. X. Cai, G. Rivas, H. Shirashi, P. Farias, J. Wang, M. Tomschik, F. Jelen, E. Palecek, *Anal. Chim. Acta* **344**, 65 (1997).
69. E. Palecek, I. Postbieglová, *J. Electroanal. Chem.* **214**, 359 (1986).
70. A. M. Oliveira Brett, A.-M. Chiorcea, *Electrochem. Commun.* **5**, 178 (2003).
71. G. B. Sukhorukov, M. M. Montrel, A. I. Petrov, L. I. Shabarchina, B. I. Sukhorukov, *Biosens. Bioelectron.* **11**, 913 (1996).
72. E. Williams, M. I. Pividori, A. Merkoçi, R. J. Forster, S. Alegret, *Biosens. Bioelectron.* **19**, 165 (2003).
73. A. Dupont-Filliard, M. Billon, T. Livache, S. Guillerez, *Anal. Chim. Acta* **515**, 271 (2004).
74. G. Liu, Y. Wan, V. Gau, L. Wang, S. Song, C. Fan, *J. Am. Chem. Soc.* **130**, 6820 (2008).
75. T. M. Herne, M. J. Tarlov, *J. Am. Chem. Soc.* **119**, 8916 (1997).
76. A. W. Peterson, R. J. Heaton, R. Georgiadis, *J. Am. Chem. Soc.* **122**, 7837 (2000).
77. E. Pavlovic, R. Lai, T.T. Wu, B.S. Fergusson, R. Sun, K.W. Plaxco, H.T. Soh *Langmuir* **24**, 1102 (2008).
78. M. Yang, M. E. McGovern, M. Thompson, *Anal. Chim. Acta* **346**, 259 (1997).
79. M. Silva, I. Cavalcanti, M. Fatima Barroso, M. Goreti F. Sales, R. Fireman Dutra, *J. Chem. Sci.* **122**, 911-917 (2010)
80. G. Poirier, *Chem. Rev.* **97**, 1117 (1997).
81. T. De Lumley-Woodyear, D. Caruana, C. Campbell, A. Heller, *Anal. Chem.* **71**, 394 (1999).
82. H. Peng, C. Soeller, N. Vigar, P.A. Kilmartin, M.B. Cannell, G.A. Bowmaker, R.P. Cooney, J. Travas-Sejdic, *Biosens. Bioelectron.* **20**, 1821 (2005).
83. H. Teh, H. Gong, X. Dong, X. Zeng, A. Lai Kuan Tan, X. Yang, S. Ngim Tan, *Anal. Chim. Acta* **551**, 23 (2005).
84. A. Erdem, P. Papakonstantinou, H. Murphy, *Anal. Chem.* **78**, 6656 (2006).
85. A. Poghossian, A. Cherstvy, S. Ingebrandt, A. Offenhäusser, M. J. Schöning, *Sens. Actuators B* **111-112**, 470 (2005).
86. M. Fojta, L. Havran, S. Billova, P. Kostecka, M. Masarik, R. Kizek, *Electroanalysis* **15**, 431 (2003).
87. M. Gebala, L. Stoica, S. Neugebauer, W. Schuhmann, *Electroanalysis* **21**, 325 (2009).
88. M. Castañeda, S. Alegret, A. Merkoçi, *Electroanalysis* **19**, 743 (2007).
89. K. Dill, A. Ghindilis, in *Microarrays. Preparation, Microfluidics, Detection Methods, and Biological Applications*, K. Dill, H. L. Liu, P. Grodzinski, Eds. (Springer, New York, 2009), pp. 263-270.
90. M. J. Doyle, H. B. Halsall, W. R. Heineman, *Anal. Chem.* **56**, 2355 (1984).
91. P. Kara, A. Erdem, S. Girousi, M. Ozsoz, *J. Pharm. Biomed. Anal.* **38**, 191 (2005).
92. T. De Lumley-Woodyear, C. Campbell, A. Heller, *J. Am. Chem. Soc.* **118**, 5504 (1996).
93. T. De Lumley-Woodyear, C. Campbell, E. Freeman, A. Freeman, G. Georgiou, A. Heller, *Anal. Chem.* **71**, 535 (1999).

94. F. Azek, C. Grossiord, M. Joannes, B. Limoges, P. Brossier, *Anal. Biochem.* **284**, 107 (2000).
95. M. Pividori, A. Merkoçi, S. Alegret, *Biosens. Bioelectron.* **16**, 1133 (2001).
96. C. N. G. Campbell, D., N. Cristler, C. Banditrat, A. Heller, *Anal. Chem.* **74**, 158 (2002).
97. Y. Zhang, H. H. Kim, N. Mano, M. Dequaire, A. Heller, *Anal. Bioanal. Chem.* **374**, 1050 (2002).
98. Y. Zhang, H. Kim, A. Heller, *Anal. Chem.* **75**, 3267 (2003).
99. G. Marchand, C. Delattre, R. Campagnolo, P. Pouteau, F. Ginot, *Anal. Chem.* **77**, 5189 (2005).
100. N. Djellouli, M. Rochelet-Dequaire, B. Limoges, M. Druet, P. Brossier, *Biosens. Bioelectron.* **22**, 2906 (2007).
101. H. Xie, Y. Yu, F. Xie, Y. Lao, Z. Gao, *Clin. Chem.* **50**, 1231 (2004).
102. S. Suye, T. Matsuura, T. Kimura, H. Zheng, T. Hori, Y. Amano, H. Katayama, *Microelectron. Eng.* **81**, 441 (2005).
103. D. Caruana, A. Heller, *J. Am. Chem. Soc.* **121**, 769 (1999).
104. Y. Zhang, A. Pothukuchy, W. Shin, H. H. Kim, A. Heller, *Anal. Chem.* **75**, 4093 (2004).

Chapter 2

**DNA sensor based upon
bioelectrocatalytic amplification using
osmium redox polymer modified gold
microelectrodes**

2.1. Introduction

Microelectrodes are powerful tools for the study of electrochemical processes with a vast number of potential applications. Small dimensions, generally from dozens of micrometers to nanometers result in different qualities in comparison with macroelectrodes. These include reduced IR drop of potential, fast establishment of a steady-state signal, and increased signal-to-noise ratio. (1) Because of these properties microelectrodes have become invaluable in applications like kinetic studies, (2) measurements without supporting electrolyte, (3, 4) electrochemistry in the gas phase, (5) electrochemical detection in flowing liquids, (6) in-vivo measurements (7) and scanning electrochemical microscopy.(8) Also, microelectrodes are applied as detectors in chromatographic (5, 9) and electrophoretic instruments. (10)

Microelectrodes allow more sensitive analyte detection in comparison with conventional size electrodes. (11) Microelectrodes can replace macroelectrodes in gas-sensing systems, such as oxygen, (12) hydrogen sulphide, (13) nitric oxide. (14) Numerous works focus on use of microelectrodes in trace analysis, in particular on detecting low concentrations of metal ions in environmental samples. (15-20) Miniaturisation allowed pH sensors and ion-selective electrodes to be used directly in biological tissue samples. (21)

Some of the distinct properties of microelectrodes could be explained by the different mass transport effects in dynamic electrochemistry. (22) For example, the diffusion field at microelectrodes is of radial shape, in contrast with macroelectrodes, which consist of predominantly a planar diffusion of species towards the electrode surface. **(Figure 2.1)**

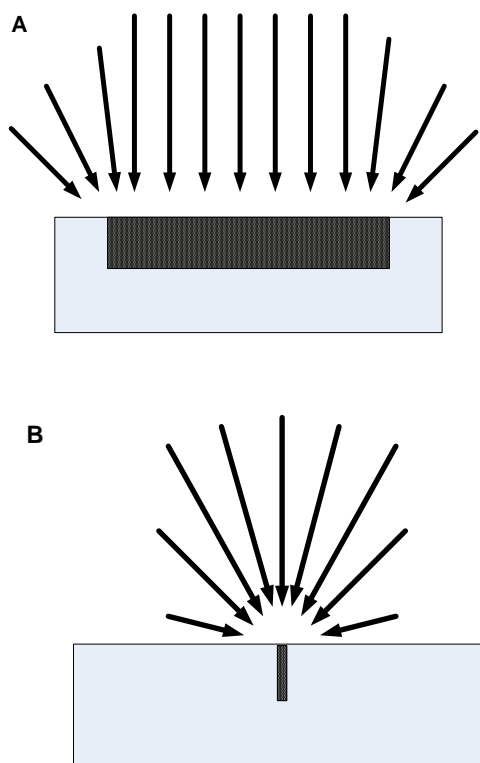


Figure 2.1 Example of diffusion field at macroelectrode (A) and at disc microelectrode (B). At microelectrodes, radial diffusion, negligible at macroelectrodes, becomes a dominating process. Adapted from reference (22)

Research data presented in this chapter is focused on the analytical response of microelectrodes, when applied to a DNA sensing platform. The work is a continuation of research presented in a report published by Kavanagh and Leech. (23) They developed a DNA sensor constructed via deposition of single-stranded DNA (ssDNA) probe sequences with an osmium-based redox polymer mediator on gold electrodes. An amino-terminated 20-base sequence probe DNA is cross-linked with $[\text{Os}(2,2'\text{-bipyridine})_2(\text{polyvinylimidazole})_{10}\text{Cl}]^{+/2+}$ using a poly-(ethylene glycol)bisglycidyl ether (PEGDGE) reagent that also crosslinks these films to the electrode via reaction with an anchoring self-assembled monolayer (SAM) of cysteamine. Structures of the redox polymer and the crosslinker are presented in **Figure 2.2**.

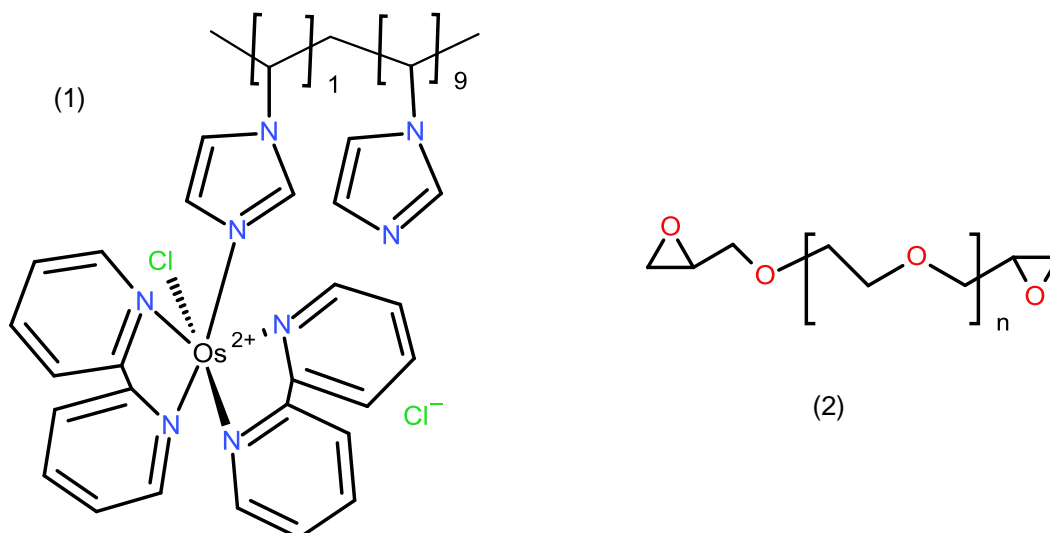


Figure 2.2 Structures of $[Os(2,2'-bipyridine)_2(polyvinylimidazole)_{10}Cl]Cl$ (OsPVI) redox polymer and the crosslinker poly-(ethylene glycol)bisglycidyl ether (PEGDGE)

Hybridization between the immobilized probe DNA at the electrode surface and a biotin-conjugated target DNA sequence, and further coupling of glucose oxidase-avidin establishes an electrical contact between the enzyme and the mediating redox polymer. In the presence of glucose, the current generated due to the catalytic oxidation of glucose to gluconolactone is measured, and a binding-dependent response, scaling from 10^{-9} M to 10^{-6} M of target ssDNA, obtained for films immobilised at gold macroelectrodes (2 mm diameter). (23) The design and the principles of operation are demonstrated in **Figure 2.3**.

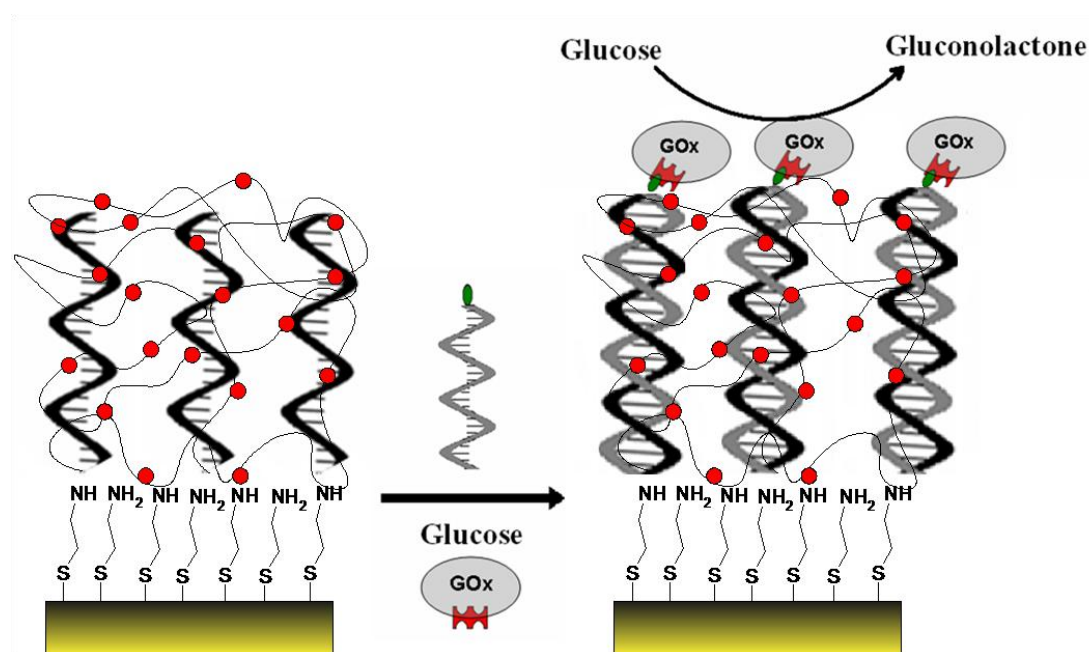


Figure 2.3 Schematic representation of the DNA sensor based upon ssDNA and OsPVI tethered to gold electrode via SAM of cysteamine (red dots indicate osmium redox centres, lines symbolise the polymer chain and the crosslinker). Reaction with biotinylated target ssDNA (biotin is presented as green dot) and glucose oxidase-avidin conjugate results in generation of bioelectrocatalytic current in the presence of glucose. (23)

In order to detect lower levels of DNA, it would be advantageous to reduce the detection limit to femtomolar (10^{-15} M) concentrations or below. Heller and co-workers previously achieved a $\sim 10^4$ fold improvement in detection limits, when they replaced a glassy carbon macroelectrode with a 10 μm diameter microelectrode in a DNA assay using a peroxidase-labelled reporter DNA sequence, allowing detection of 3000 copies of 38-base DNA in 10 μL droplet. (24)

Also, Djellouli et al. (25) observed a detection limit of 30 pM for ssDNA using a solution osmium redox complex to mediate the bioelectrochemistry of an anti-digoxigenin antibody conjugated to HRP following binding to digoxigenin1-labelled complementary nucleic acid sequences that had previously hybridized to ssDNA immobilized on screen-printed carbon macroelectrodes. In a related system, Aguilar reports a decrease in detection limit, from 146 nM (26) to 46 pM, at gold microwell cavity electrodes compared to gold macroelectrodes, using a DNA assay based on hybridization of alkaline phosphatase (AP)-labelled DNA to immobilized ssDNA on gold, followed by monitoring of the electroactive product, p-aminophenol, after

addition of p-aminophenylphosphate substrate. The same group report a detection limit of 56 fM for the AP-labelled immunoassay of IgG. (27) Xie et al. (28) has reported detection of DNA at fM levels using a thiolated-ssDNA modified gold electrode coupled with a GOx-labeled reporter sequence. Other enzyme-amplified amperometric assays at macro-electrodes, can detect down to 340 pM of target DNA sequence coding for *Legionella pneumophila* using alkaline phosphatase-labeled DNA. (29) Ghindilis et al. (30) report on an electrochemical microelectrode array system that can detect 0.75 pM of DNA or RNA, based on binding of streptavidin-labelled HRP to biotinylated hybridized DNA.

The strong literature evidence on sensitivity improvement upon miniaturisation of a DNA sensor supported replacement of gold macroelectrodes with microelectrodes.

2.2. Experimental

2.2.1. Materials and reagents

Redox polymer [Os(2,2'-bipyridine)₂(polyvinylimidazole)₁₀Cl]Cl was synthesised according to the literature procedures (abbreviation: OsPVI). (31) The cross-linker polyoxyethylene bis(glycidyl ether) (abbreviation: PEG) was purchased from Sigma-Aldrich. The probe oligonucleotide sequence (5'⇒3'): NH₂-C6-ATTTCGACAGGGATAGTTCGA was custom prepared by MWG-Biotech. The target oligonucleotide sequence (5'⇒3'): biotin-TCGAACTATCCCTGTTCGAAT (designed from the *ssrA* gene of *Listeria monocytogenes*, a common food pathogen) and control oligonucleotide sequence (5'⇒3'): biotin-ATTTCGACAGGGATAGTTCGA were also purchased from MWG-Biotech. Cysteamine was purchased from Sigma-Aldrich. Glucose oxidase-avidin D conjugate was purchased from Vector Laboratories. Glucose and all other used chemicals were purchased from Sigma-Aldrich

2.2.2. Instrumentation and techniques

The electrochemical measurements were performed using an Autolab, EcoChemie, PGSTAT12 potentiostat equipped with an ECD amplifier module (RC time settings: 0 s for scan rates > 10 mV/s, 0.1 s for scan rates < 10 mV/s. The module uses Savitzky-Golay algorithm to filter the noise). All experiments were carried out with a three-electrode system at room temperature. Gold disc microelectrodes of 25 μm, 40 μm and 100 μm in diameter were used as the working electrodes (manufactured by nLab, Warsaw). An Ag/AgCl electrode (CH Instruments) was used as a reference electrode and a platinum wire was used as a counter electrode. In all experiments, the electrochemical cell was kept in a home-built stainless steel Faraday cage to minimize the electrical noise.

2.2.3. Preparation and characterization of electrodes

Using microelectrodes is quite challenging, when considering the fact that polycrystalline solid surfaces are never perfectly flat on the atomic scale. (32) Minor surface defects, pits or scratches few microns in size have negligible effect on the macroelectrode, but in the microscale they could introduce significant variation from electrode to electrode. The measurements on microelectrodes require noise shielding. The observed current levels change from microamperes to nano- and even picoamperes. It is recommended to always use the Faraday cage when working with microelectrodes. The mains power supply could potentially interfere, when current levels are in picoampere range. Battery-operated devices are recommended, as they offer much lower noise levels, than conventional potentiostats. (33)

The gold microelectrodes, sealed in glass tubes, were carefully prepared by cautious polishing with Al_2O_3 powder of particle size in the range from 1 to $0.05 \mu\text{m}$ on a wet pad. After each polishing, the electrodes were rinsed with a direct stream of ultrapure water (Milli-Q, Millipore, conductivity of $\sim 0.056 \mu\text{S/cm}$) to remove alumina completely from the electrode surface, and then were dried. The quality of the electrode surface was always inspected with an inverted, model Olympus PME3, optical microscope. Electrodes manifesting extensive scratches or imperfections were polished repeatedly to eliminate such defects. **Figures 2.4-2.7** present images of microelectrodes. Electrodes represented in **Figures 2.4** and **2.7** are suitable for electrochemical applications. Electrodes presented in **Figures 2.5** and **2.6** are damaged and the surfaces require abrading by fine sand paper prior to polishing with alumina powder.

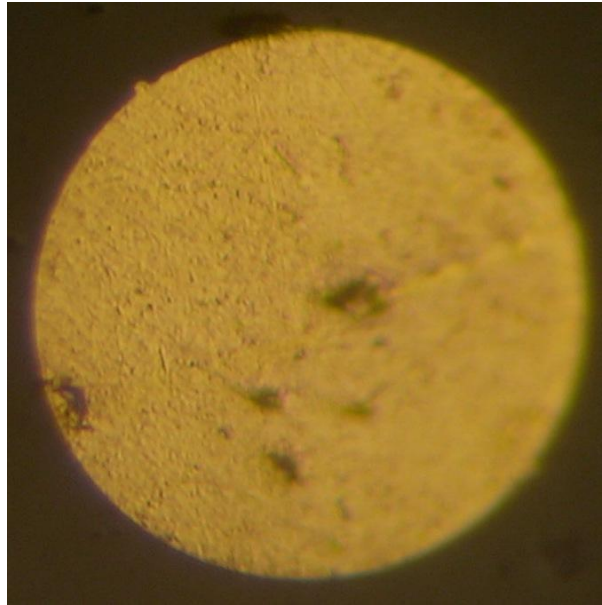


Figure 2.4 Example of smooth electrode surface (100 μm), which was accepted to be used for the experiment. Minor defect observed.

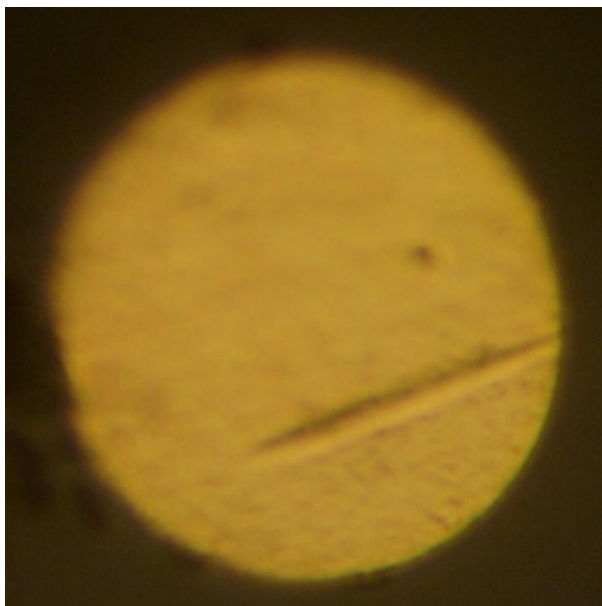


Figure 2.5 Example of an electrode with a mark, not acceptable for further processing, (100 μm)



Figure 2.6 100 μm –example of the electrode, where damage to the surface is too serious to generate satisfactory electrochemical response



Figure 2.7 25 μm –example of smooth electrode surface, no major defects

Following polishing, the electrodes were electrochemically pretreated by cycling between -0.2 and 1.35 V (vs. Ag/AgCl) in 0.1 M H_2SO_4 solution until a stable voltammogram typical for a clean gold electrode was observed. (34) An example of a satisfactory voltammogram that qualified the electrode for further processing is presented in **Figure 2.8**. Especially crucial are low currents in the range $0 - 0.5$ V. The anodic peak indicates formation of gold oxide, which is then reduced upon the cathodic sweep.

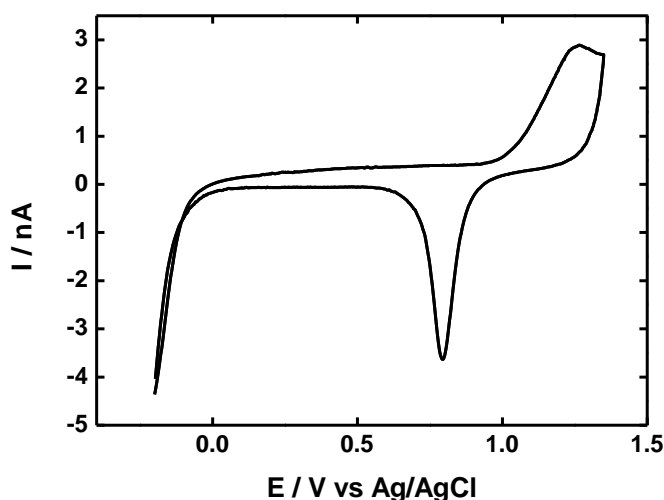


Figure 2.8 Background scan, cyclic voltammetry, $40 \mu\text{m}$ microelectrode, 0.1 M sulphuric acid. (34)

The “real” electroactive area of the gold electrode can be calculated by dividing the anodic or cathodic peak area by $390 \mu\text{C}/\text{cm}^2$ as recommended by IUPAC. (35) The roughness of the electrodes was expressed as a dimensionless parameter R_f (roughness factor) obtained by dividing the “real” surface area by the geometric area. Average surface roughness determined from anodic peak charge was: 2.30 for $25 \mu\text{m}$, 1.92 for $40 \mu\text{m}$ and 1.45 for $100 \mu\text{m}$ diameter microelectrodes. (**Table 2.1**) Roughness factor estimated for $10 \mu\text{m}$ electrodes was found to be 0.51. For the micrometer size of the gold wire achieving the disc geometry could be difficult, which means obtaining the values less than one is possible. Oxidation peak is not well defined; an average R_f estimate using a cathodic peak area yields the value of 1.31 for $10 \mu\text{m}$. Roughness values calculated from reduction peak areas are similar

to these obtained from the anodic peak for all other electrodes and are 2.16 for 25 μm , 1.81 for 40 μm and 1.56 for 100 μm diameter, respectively. (**Table 2.1B**).

Table 2.1A R_f values for gold microelectrodes estimated from gold oxidation peak area.

Electrode	100 μm (n=8)	40 μm (n=9)	25 μm (n=12)	10 μm (n=7)
Average R_f	1.45	1.92	2.30	0.51
SD	0.79	1.81	1.09	0.13
RSD	55	94	47	26
MIN	0.55	0.18	0.96	0.23
MAX	2.70	6.17	4.35	0.59
MEDIAN	1.19	1.50	2.23	0.58

Table 2.1B R_f values for gold microelectrodes estimated from gold reduction peak area.

Electrode	100 μm (n=8)	40 μm (n=9)	25 μm (n=12)	10 μm (n=7)
Average R_f	1.56	1.81	2.16	1.31
SD	0.71	1.98	1.04	0.51
RSD	46	110	48	39
MIN	0.63	0.18	0.76	0.46
MAX	2.62	6.69	4.21	1.91
MEDIAN	1.48	1.05	2.02	1.35

After electrochemical pretreatment, the electrodes were immediately rinsed with a direct stream of ultrapure water, dried with nitrogen or argon and immersed in a slowly stirred deoxygenated 10 mM ethanolic solution of cysteamine for either 20 minutes (25 and 40 μm electrodes) or 30 min (100 μm electrodes). Then, the electrodes were removed, rinsed with ethanol and dried with a gentle stream of nitrogen/argon. After these two steps a 6 μL drop containing the redox polymer (OsPVI, 2 μL of a 5 mg/ml solution in water), the PEGDGE cross-linker (2 μL of a 15 mg/ml solution in water) and amine terminated capture probe-DNA (2 μL of a

400 $\mu\text{g}/\text{ml}$ solution in water) was deposited onto the electrode surface, followed by at least 48 hours of drying in a dessicator, to form the sensing film.

The modified gold disc microelectrodes were cycled in the potential range -0.2 V to 0.6 V in a 0.02 M phosphate buffer solution ($\text{pH} = 7.4$) containing 0.15 M NaCl and 1 mM EDTA until the obtained voltammogram was stable. The sensing film was then characterized using a wide range of scan rates.

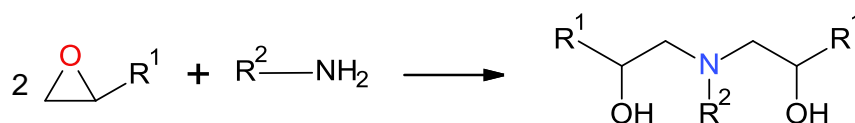
2.2.4. Detection of DNA hybridization

The hybridization assay was performed by addition of a 7 μL droplet of buffer solution (0.02 M phosphate buffer, $\text{pH} = 7.4$, with 1 M NaCl and 1 mM EDTA) containing the appropriate concentration of target DNA deposited on the sensing surface. High ionic strength buffer was used in order to reduce non-specific binding between the osmium redox polymer and negatively charged species (DNA, enzyme). Degani and Heller report that the formation of electrostatic complex between the enzyme and the osmium redox polymer is favoured at low ionic strength condition. (36) Hybridization was allowed to proceed for 30 minutes, whilst minimizing evaporation of the droplet by covering the electrode with a plastic cap, in an attempt to avoid difficulties with reproducibility. Following hybridization, a 2 μL aliquot of glucose oxidase-avidin D conjugate (50 $\mu\text{g}/\text{ml}$ solution in water) was carefully, exactly placed on the previous droplet to allow binding, over a further 30 minute period, between the biotinylated DNA now hybridized to the probe DNA in the sensing film, and the glucose oxidase-avidin D conjugate, again minimizing droplet evaporation by covering the electrode with a plastic cap. The resulting electrode was then rinsed with the hybridization buffer solution and immersed in a blank buffer solution (0.02 M phosphate buffer, $\text{pH} = 7.4$, with 0.15 M NaCl) for recording of background cyclic voltammetry and chronoamperometry traces, with all electrochemical measurements undertaken in a Faraday cage. Glucose substrate was then added to the blank solution to yield a working solution of 20 mM glucose in the buffer, and the current for the bioelectrocatalytic glucose oxidation was measured using cyclic voltammetry and chronoamperometry.

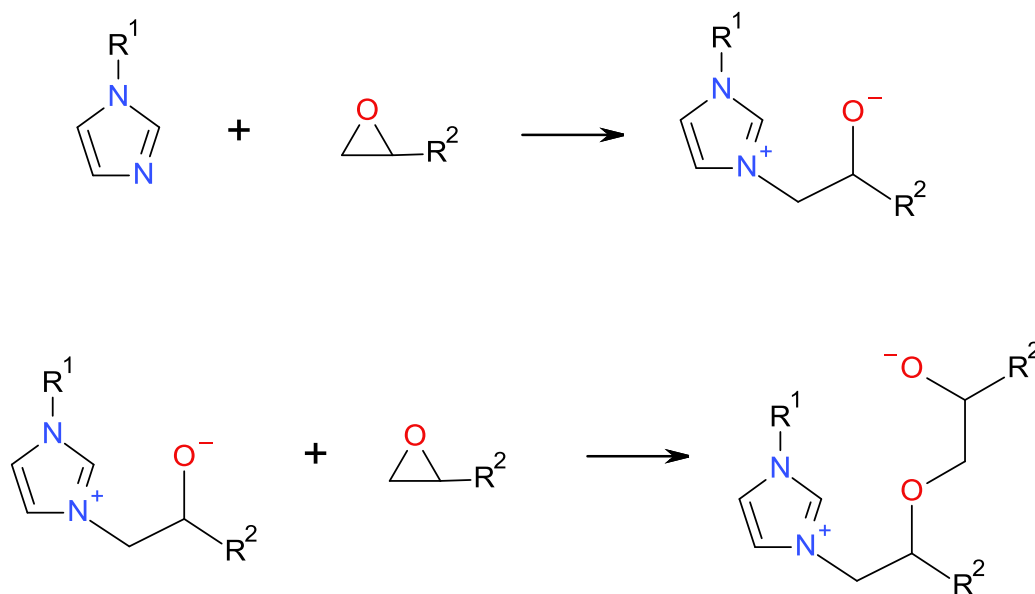
2.3. Results and Discussion

2.3.1. Voltammetry of redox polymer films on gold microelectrodes

Hydrogels containing OsPVI, DNA and PEGDGE were cured by drying for at least 48 hours, in a solid-phase reaction, epoxy crosslinking agent binds to amino- and imidazole groups as shown in **Schemes 2.1** and **2.2**.



Scheme 2.1 The mechanism of crosslinking of amino groups by epoxy-terminated molecules. Adapted from reference (37)



Scheme 2.2 The mechanism of crosslinking of imidazole groups by epoxy-terminated molecules. Mechanism proposed by Barton et al. (38)

The epoxide groups remain active for several days, so strict control over drying time is crucial for film formation. Studies on cross-linked glucose oxidase have shown an increase of the film thickness with the drying time. Also, long-term curing

might result with overcrosslinking of the enzyme within the hydrogel and consequently with diminished catalytic activity. Maximum catalytic activity of the enzyme is achieved for 24 h drying time, although films dried for 48 h present a more uniform structure. (39) An influence of drying time on biosensor response has not been the part of this study, but it might be one of the future aspects to consider.

The film drying was followed by repetitive scanning in the phosphate buffer solution to remove physisorbed species. Hydrogels were characterised by cyclic voltammetry and parameters of modified electrodes were determined using the theoretical model described in Chapter 1. (40)

The voltammograms of OsPVI/DNA films on microelectrodes exhibit well-defined oxidation and reduction peaks corresponding to the Os(II)(III) redox couple. The voltammetric curves of OsPVI films on microelectrodes are hybrids between Gaussian and sigmoidal peak shapes. CVs of lower microelectrodes sizes, such as 25 μm display the significant tailing of the peaks, which can be seen in **Figure 2.9**. A diffusional tailing contributes to the current to a lesser degree at larger microelectrode sizes to disappear completely at 2 mm electrodes. (**Figure 2.12**) Sigmoidal-shape voltammograms, which are typical for voltammetry at the solution-phase species at microelectrodes, cannot be observed. (22) These observations are in accordance with numerous literature studies on modified microelectrodes. (41-43) Rebouillat et al. (44) proposed that the type of diffusion, either radial or planar depends on thickness of the film. When the thickness of the redox polymer layer is comparable with the radius of the electrode radial diffusion of substrate throughout the film is expected. If the radius is much greater than the film thickness, planar diffusion model applies. Geng et al. (45) explains the presence of the diffusional tail by the polymer “spill over”; this is the case when redox polymer layer extends the microdisc area. Regardless of the nature of the diffusion process, analytical sensitivity of the films deposited on microelectrodes is improved comparing to the films on macroelectrodes. (43)

Also the modification of 10 μm gold microelectrodes was studied, but no Os(II)(III) redox peak can be seen. It is thought that an optimisation of the film thickness and osmium site concentration is needed to observe a semi-infinite diffusion type response. Undoubtedly, there is no particular reason why voltammetry of the redox hydrogel cannot be recorded at 10 μm disc size. Data published by Geng et al. (45), who studied films of $[\text{Ru}(\text{bpy})_3](\text{PF}_6)/\text{PEO}_{16}\cdot\text{Li}(\text{CF}_3\text{SO}_3)$ at 10 μm

Pt microelectrodes, clearly demonstrates presence of semi-infinite diffusion and the shapes of the CV curves are similar to those presented in **Figures 2.9** and **2.10**. (PEO - polyethylene oxide)

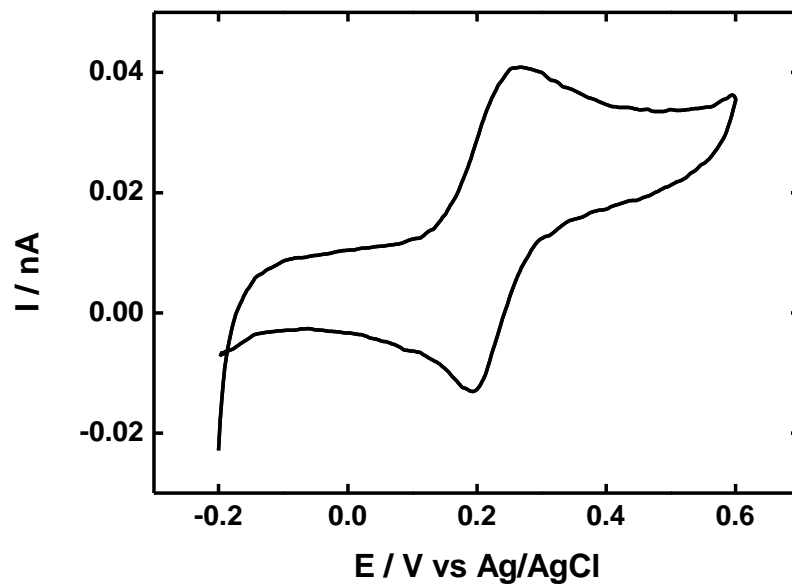


Figure 2.9 The response of the sensing film at low scan rate - 5mV/s. Electrolyte; phosphate buffer, pH 7.4, 0.15M NaCl, 1mM EDTA, 25 μ m.

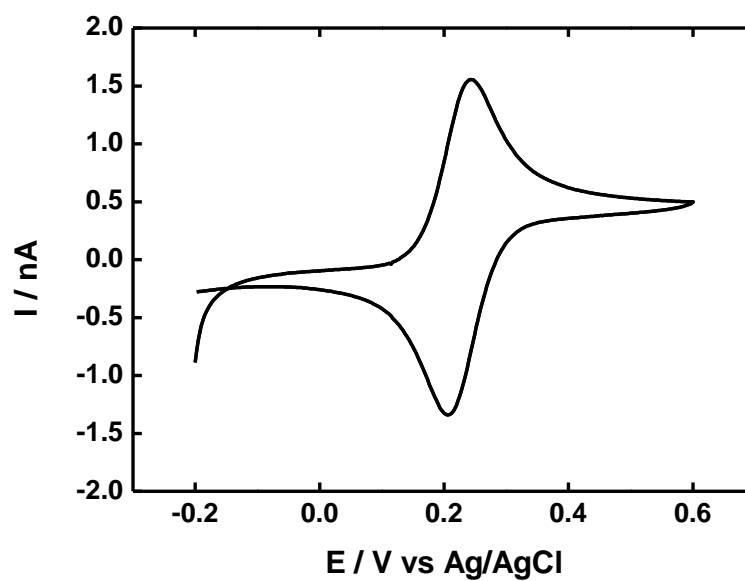


Figure 2.10 The response of the sensing film at low scan rate – 5 mV/s. Electrolyte; phosphate buffer, pH 7.4, 0.15 M NaCl, 1 mM EDTA, 40 μ m

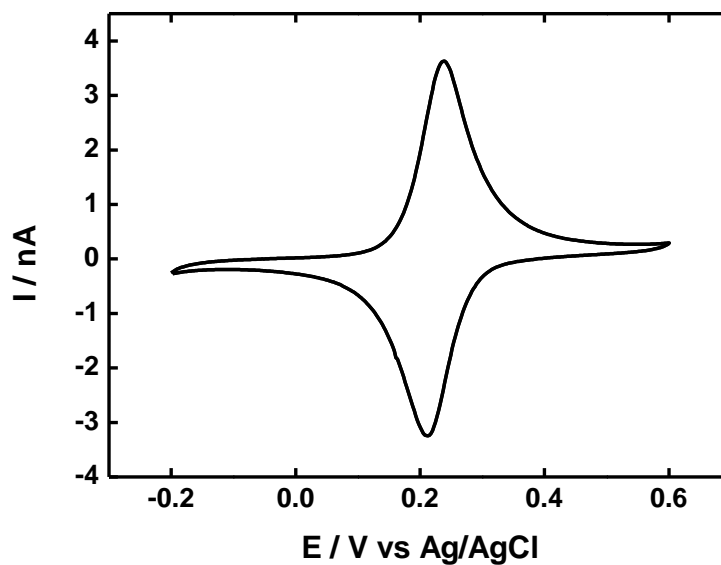


Figure 2.11 The response of the sensing film at low scan rate – 5 mV/s. Electrolyte; phosphate buffer, pH 7.4, 0.15 M NaCl, 1 mM EDTA. 100 μm microelectrode

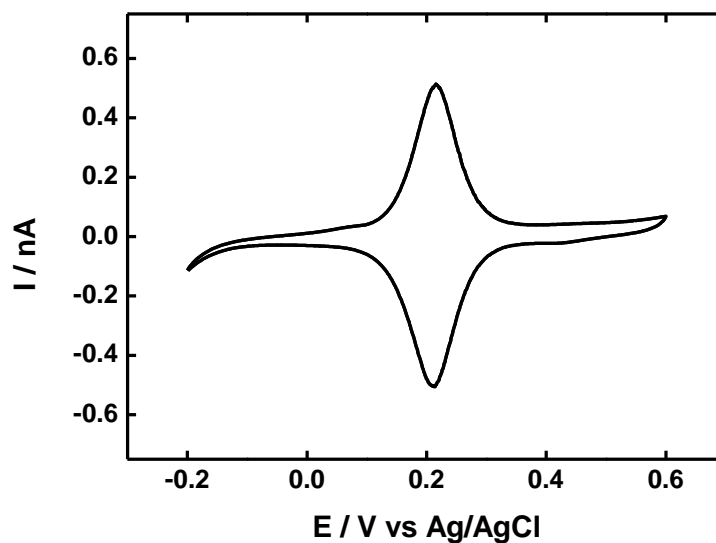


Figure 2.12 The response of the sensing film at low scan rate – 5 mV/s. Electrolyte; phosphate buffer, pH 7.4, 0.15 M NaCl, 1 mM EDTA. 2 mm macroelectrode

The voltammetric behaviour was studied at the range of scan rates. **Figure 2.13** shows the voltammograms recorded at 40 μm microelectrode between 50-500 mV/s.

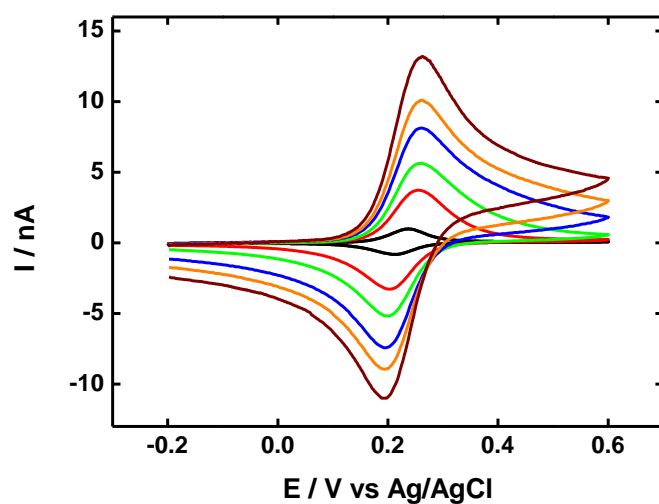


Figure 2.13 Cyclic voltammogram of OsPVI/DNA deposited on 40 μm electrode, scan rates from 50-500 mV/s

The peak currents scale linearly with the square root of scan rate 50-500 mV/s indicating semi-infinite diffusional charge transport within the sensing film at these scan rates. (Figure 2.14)

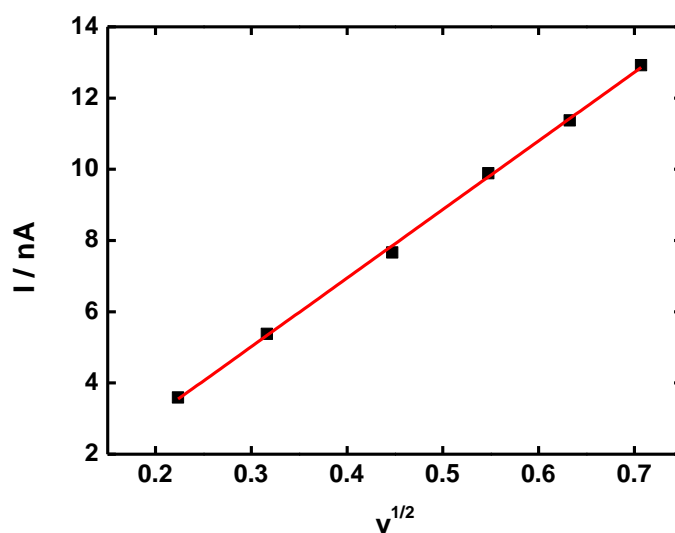


Figure 2.14 OsPVI/DNA, Peak currents plotted versus square root of the scan rate, 40 μm electrode; scan rates from 50-500 mV/s

The films were also characterized at scan rates between 2-50 mV/s. **Figure 2.15** presents cyclic voltammograms for 40 μm electrode.

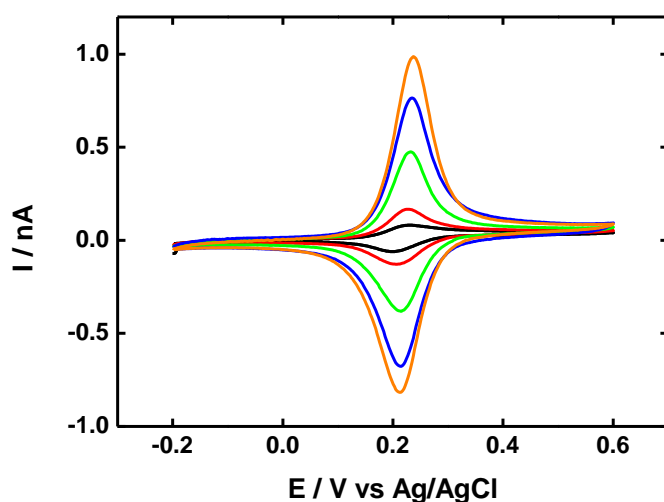


Figure 2.15 Cyclic voltammogram of OsPVI/DNA deposited on 40 μm electrode, scan rates from 2-50 mV/s

For scan rates less than 50 mV/s peak currents vary linearly with scan rate, indicating a surface confined electrochemical response, expected for such films. (Figure 2.16)

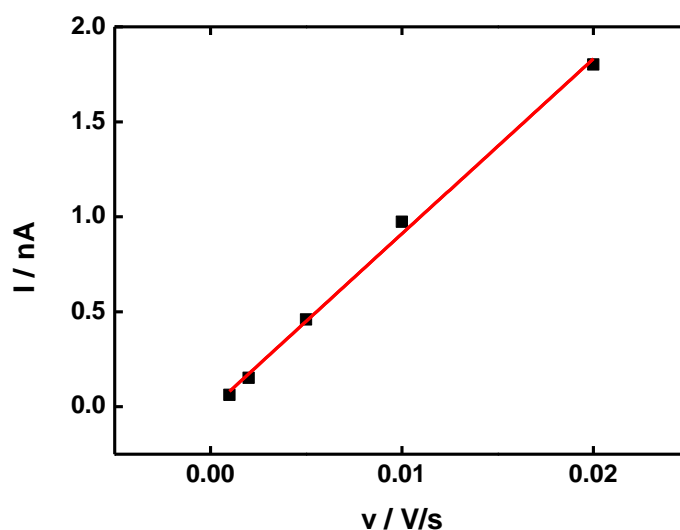


Figure 2.16 OsPVI/DNA, Peak currents plotted versus scan rate, 40 μm electrode; scan rates from 2-20 mV/s

An estimate of total osmium surface coverage (Γ_{Os}) can be evaluated by integrating the charge passed when the film is comprehensively electrolysed. (40) The slow-scan voltammogram of the sensing film on microelectrodes is a hybrid of

the Gaussian peak and the steady-state sigmoidal shaped curve, which can cause difficulties in peak area calculations. Peak areas were thus estimated by subtracting the steady state current from the overall peak area. A parameter, $D^{1/2}c$, where D is the charge transport diffusion coefficient and c is the concentration of osmium redox sites in the film, can also be evaluated from CVs at scan rates from 100 mV s^{-1} to 500 mV s^{-1} , using the Randles-Sevcik equation. (46)

The electrochemical parameters of the sensing films with the co-immobilized probe DNA were compared to films of the redox polymer alone (**Figures 2.17-2.20**) for all gold microelectrodes used and for macroelectrodes (23) and the results are shown in **Tables 2.2** and **2.3**.

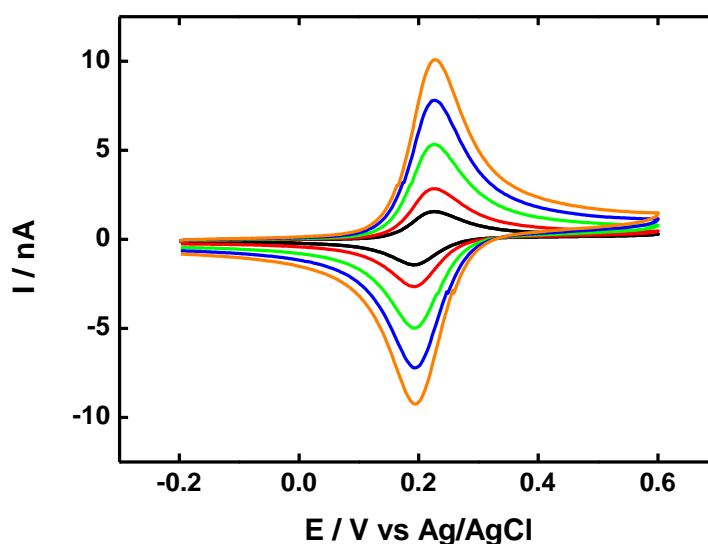


Figure 2.17 - Cyclic voltammogram of OsPVI without co-immobilised DNA deposited on $40 \mu\text{m}$ electrode, scan rates from **50-500 mV/s**

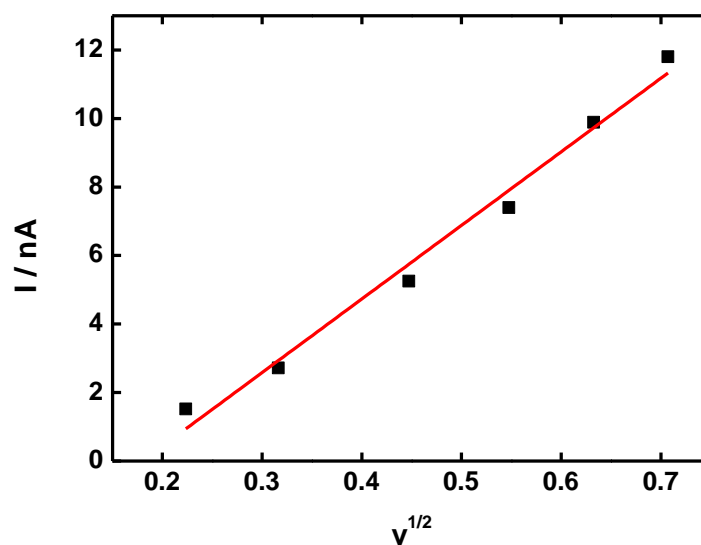


Figure 2.18 Peak currents plotted versus square root of the scan rate, of OsPVI without co-immobilised DNA deposited on 40 μm electrode; scan rates from 50-500 mV/s

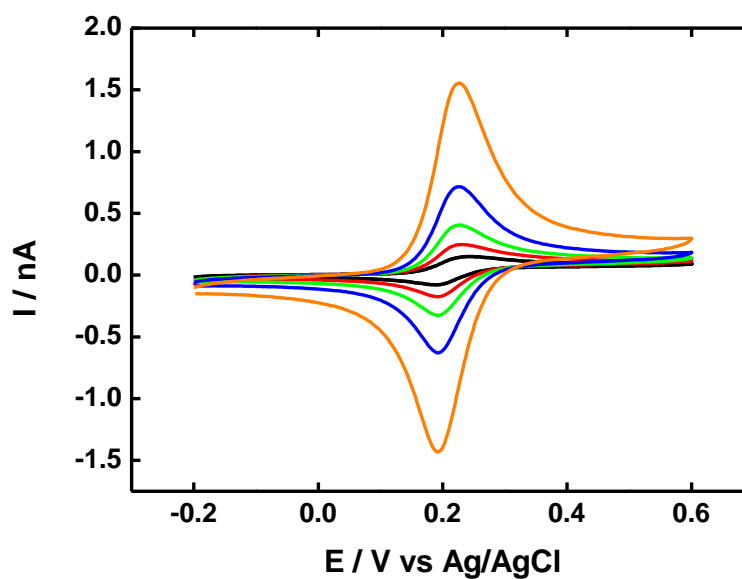


Figure 2.19 Cyclic voltammogram of OsPVI without co-immobilised DNA deposited on 40 μm electrode, scan rates from 2-50 mV/s

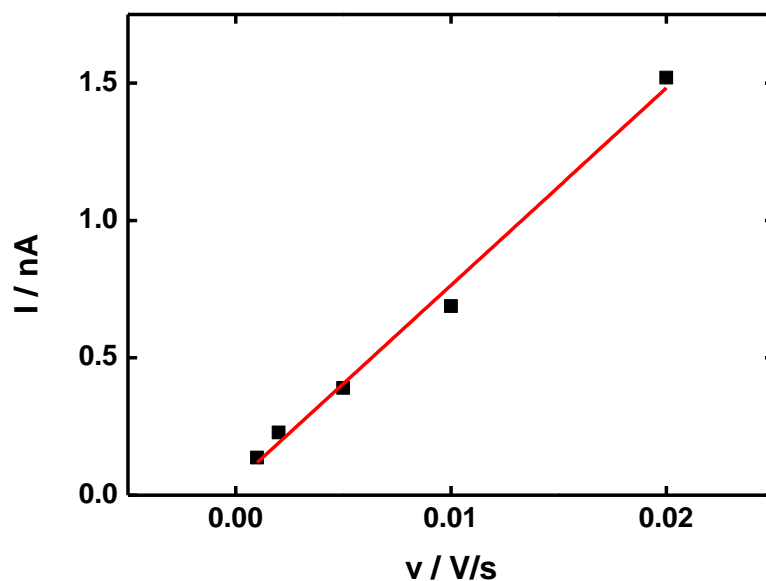


Figure 2.20 Redox polymer alone, peak currents plotted versus scan rate, of OsPVI without co-immobilised DNA deposited on 40 μm electrode; scan rates from 2-20 mV/s

Table 2.2 Parameters of the redox polymer film crosslinked with ssDNA, a-parameter estimated from **Randles-Sevcik** equation, b- surface coverage estimated from the following formula $\Gamma = Q/nFA$

Parameter	Redox polymer with DNA			
	<i>diameter of electrode</i>			
	<i>25 μm</i>	<i>40 μm</i>	<i>100 μm</i>	<i>2mm</i>
E^0 [V]	0.228	0.228	0.228	0.208
ΔE_p [V]	0.057	0.054	0.047	0.042
FWHM [V]	0.129	0.122	0.130	0.114
$D^{1/2}C$ [cm ⁻² s ^{-1/2} mol] ^a	5.85x10 ⁻⁹	5.26x10 ⁻⁹	4.33x10 ⁻⁹	5.32x10 ⁻⁹
Γ_{Os} [mol/cm ²] ^b	5.98x10 ⁻⁹	5.15x10 ⁻⁹	5.17x10 ⁻⁹	3.45x10 ⁻⁹

Table 2.3 Parameters of the redox polymer film without ssDNA, a-parameter estimated from **Randles-Sevcik** equation, b- surface coverage estimated from the following formula $\Gamma = Q/nFA$

Parameter	Redox polymer without DNA			
	<i>diameter of electrode</i>			
	<i>25 μm</i>	<i>40 μm</i>	<i>100 μm</i>	<i>2mm</i>
E^o [V]	0.227	0.209	0.208	0.206
ΔE_p [V]	0.054	0.030	0.017	0.037
FWHM [V]	0.122	0.111	0.101	0.104
$D^{1/2}C$ [cm ⁻² s ^{-1/2} mol] ^a	6.75x10 ⁻⁹	5.51x10 ⁻⁹	5.11x10 ⁻⁹	7.22x10 ⁻⁹
Γ_{Os} [mol/cm ²] ^b	1.5x10 ⁻⁸	5.42x10 ⁻⁹	2.33x10 ⁻⁹	3.51x10 ⁻⁹

A slight increase (shown in **Table 2.2**) of formal potential (E^o) of the redox polymer in the presence of the DNA capture probe could reflect both the contribution of radial diffusion at microelectrodes to the difficulty in estimating such formal potentials and an interaction between the DNA probe and the redox polymer. The increase shown in **Table 2.2** of *FWHM* upon conjugation of the DNA could also arise from both these contributions. The increase in the separation of anodic and cathodic peak potentials (ΔE_p), at this scan rate could arise because of radial diffusion contribution at microelectrodes, but is also indicative of a decrease in the rate of heterogeneous electron transfer for the DNA probe films. (**Table 2.2**) A slight decrease of the $D^{1/2}C$ parameter in the presence of the DNA probe, corresponding to a slower rate of charge transport through the film and/or a decrease in the concentration of the osmium redox centers is also evident, and has been observed previously for osmium-based redox polymer films containing co-immobilized DNA. (23) Little variation in the estimated osmium surface coverage values are observed, particularly for the films containing co-immobilized DNA. The osmium surface coverage value for these films can be used to estimate a minimum film thickness equivalent to 50 layers of the osmium complex, or ~75 nm if an estimate of 0.75 nm, from crystallographic data, is used for the radius of the osmium complex. (22) For the sensing film to be useful in DNA hybridization assay the film should be stable over at least the timeframe of the experiment (typically 1 hour). We have

previously demonstrated that tethering the probe DNA sequence and the redox polymer to the surface of a gold electrode via a self-assembled monolayer of cysteamine, can yield stable sensing films, with peak current signals decreasing by only 15% over an eight hour period. The stability of the peak current response for the sensing film tethered to the cysteamine-modified gold microelectrodes is shown in **Figures 2.21 A** and **B**. Stability was tested by periodically measuring the voltammetric peak current and storing the electrodes either in a dessicator in a dry state (**Figure 2.21 A**) or in the electrolyte/buffer (**Figure 2.21 B**) between measurements. The electrochemical signal in both cases decreased by only approximately 15 % after 140 hours demonstrating a significant improvement in stability over films tethered to macroelectrode, postulated to be a result of the careful pre-treatment and preparation procedures adopted for the sensing films on microelectrodes.

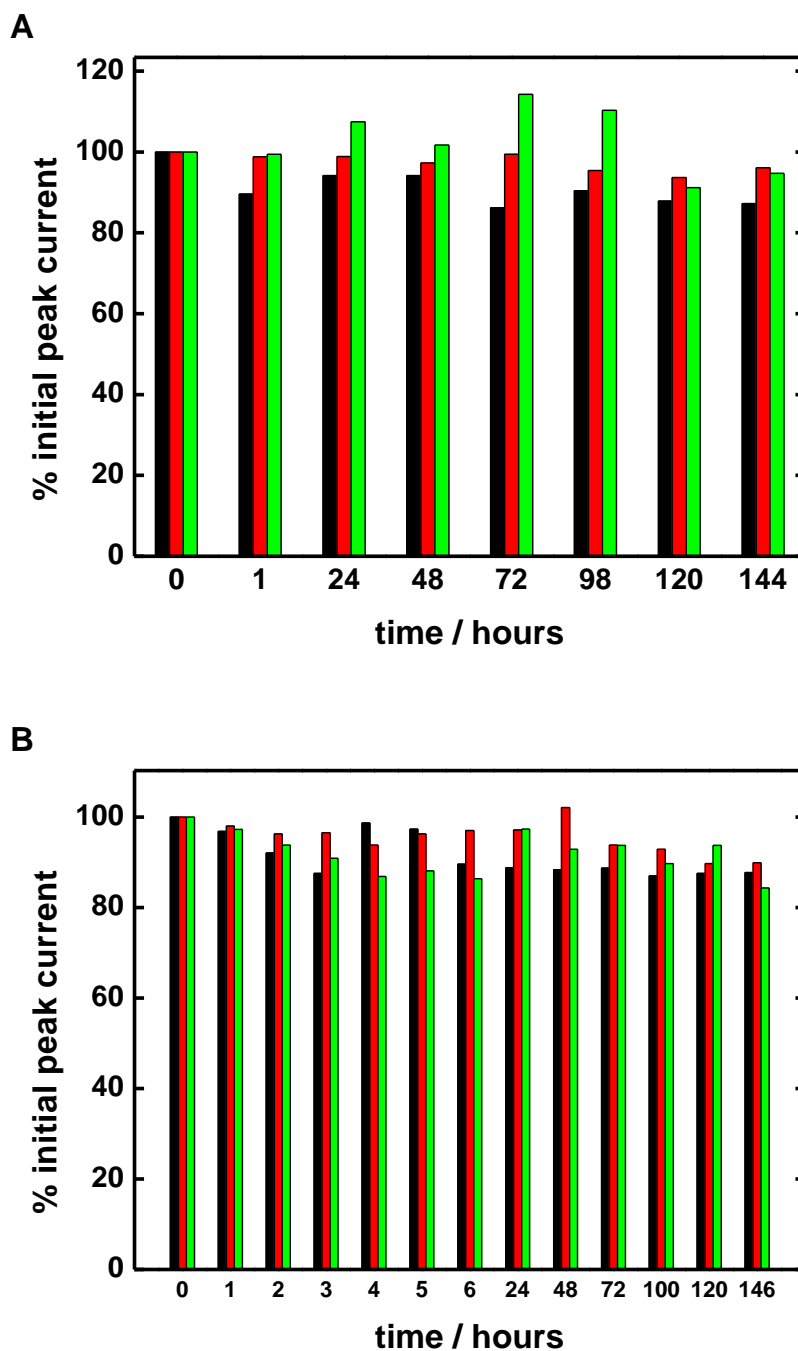


Figure 2.21 Stability of the peak current, normalized to initial peak currents (0 hours), of the sensing films at 25 μm (**black**), 40 μm (**red**) and 100 μm (**green**) diameter microelectrodes. Experimental conditions: CV, $v = 5 \text{ mV/s}$, 0.02 M phosphate buffer (pH = 7.4) with 0.15 M NaCl and 1 mM EDTA, **A**- electrodes were removed from the buffer after each measurement, rinsed with water, and stored in the dessicator, **B**- electrodes were continuously immersed in the buffer.

A simplified model of a first-order process of decrease in response can provide a measure of the response half-life, or rate constant, permitting better comparison of systems. Using this approach plots for the natural logarithm of the percentage decrease in osmium peak current decay ($40\ \mu\text{m}$) versus time, presented in **Figures 2.22 A and B**, confirm that this simple approach may be valid, as a linear response is observed.

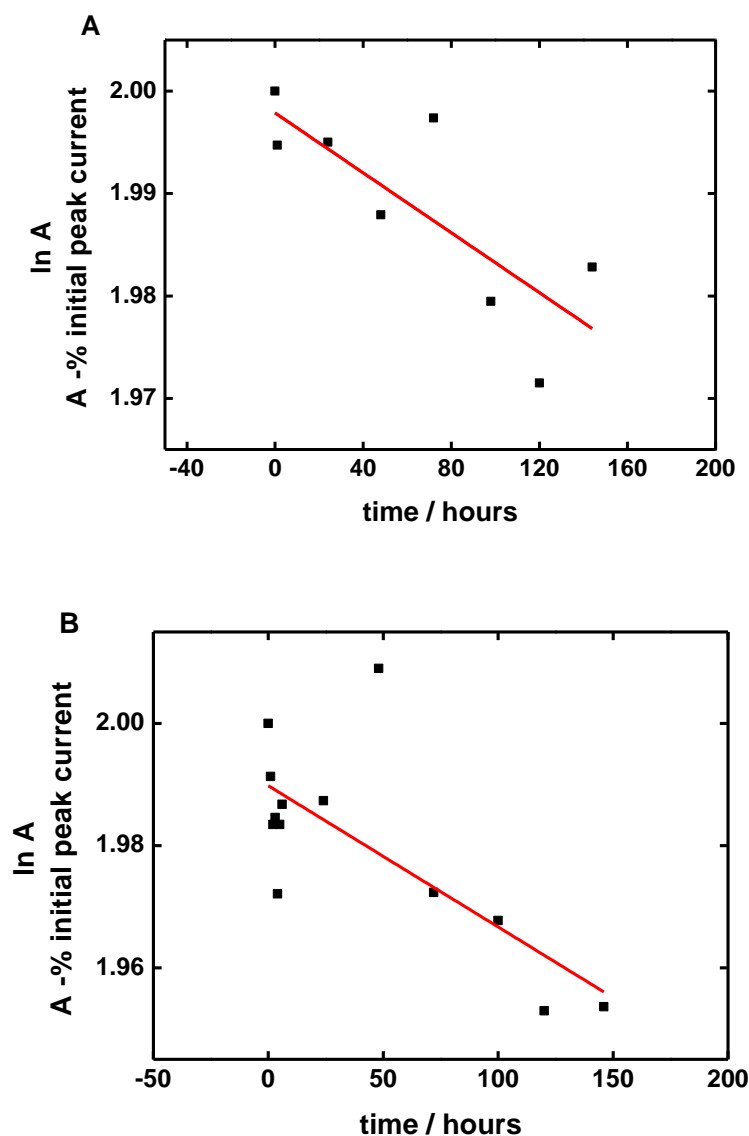


Figure 2.22 Kinetic plots (first order) for the stability of the peak current, normalized to initial peak currents (0 hours), of the sensing films at $40\ \mu\text{m}$ microelectrodes. Experimental conditions: CV, $v = 5\ \text{mV/s}$, $0.02\ \text{M}$ phosphate buffer ($\text{pH} = 7.4$) with $0.15\ \text{M}$ NaCl and $1\ \text{mM}$ EDTA, **A**- electrodes were removed from the buffer after each measurement, rinsed with water, and stored in the dessicator, **B**- electrodes were immersed in the buffer for the time of experiment.

A pseudo-first order rate constant of 0.00015 s^{-1} and a half-life of approximately 4740 h were estimated for the films stored in the dessicator. The film dissolution process was found to be faster, when the electrode was continuously immersed in the buffer with kinetic parameters as follows: $k = 0.00023\text{ s}^{-1}$ and $t_{1/2} = 2997\text{ h}$.

2.3.2. Amperometric detection of DNA hybridization

In the presence of the complementary biotinylated-DNA and glucose oxidase-avidin D conjugate we observe bioelectrocatalytic oxidation of glucose by the enzyme, mediated by the osmium redox couple. The bioelectrocatalytic current was measured using cyclic voltammetry. The steady state current value was taken at 0.35 V. Cyclic voltammograms showing bioelectrocatalytic curves for different concentrations of complementary DNA with and without glucose are displayed in **Figures 2.23, 2.24 and 2.25**. No catalytic current is observed, when a surface is reacted with biotin non-complementary DNA target. (**Figure 2.26**)

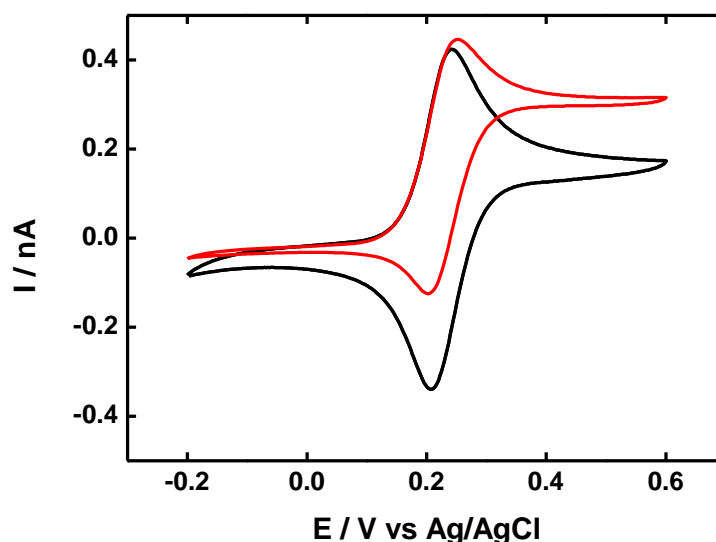


Figure 2.23 Cyclic voltammograms of the sensing film after interaction with biotinylated-target DNA and the glucose oxidase-avidin D conjugate in the absence (**black lines**) and presence (**red lines**) of 20 mM glucose. **Complementary DNA** concentration: $1.85 \times 10^{-7}\text{ M}$

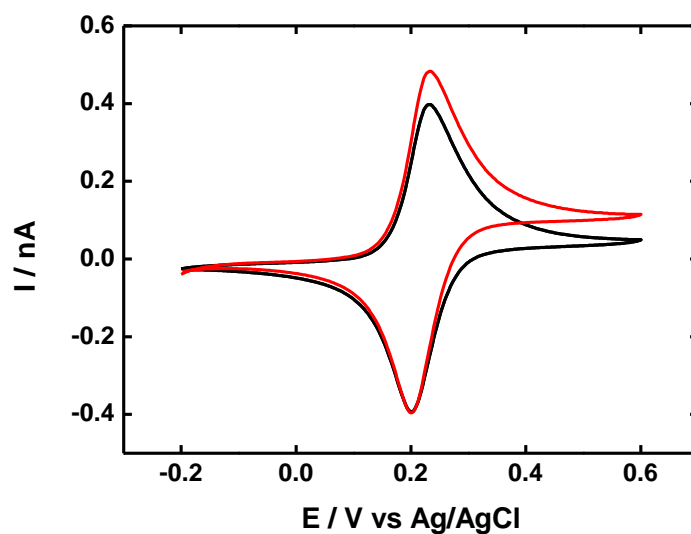


Figure 2.24 Cyclic voltammograms of the sensing film after interaction with biotinylated-target DNA and the glucose oxidase-avidin D conjugate in the absence (**black lines**) and presence (**red lines**) of 20 mM glucose. **Complementary DNA** concentration: 1.85×10^{-11} M.

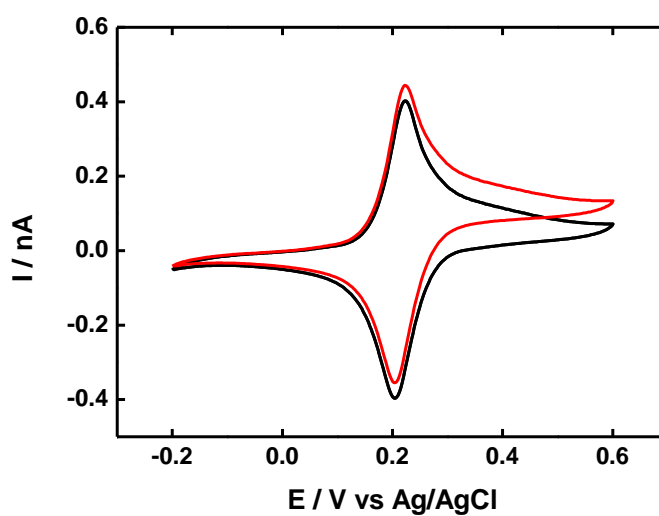


Figure 2.25 Cyclic voltammograms of the sensing film after interaction with biotinylated-target DNA and the glucose oxidase-avidin D conjugate in the absence (**black lines**) and presence (**red lines**) of 20 mM glucose. **Complementary DNA** concentration: 1.85×10^{-13} M.

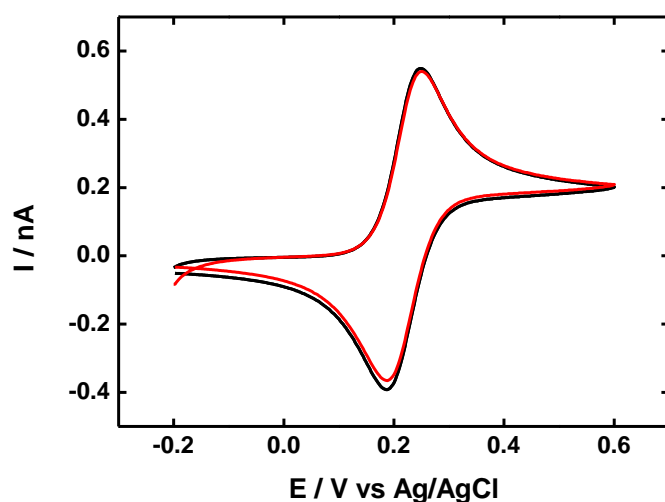


Figure 2.26 Cyclic voltammograms of the sensing film after interaction with biotinylated-target DNA and the glucose oxidase-avidin D conjugate in the absence (**black lines**) and presence (**red lines**) of 20 mM glucose. **Non-complementary DNA** concentration: 1.85×10^{-7} M.

The bioelectrocatalytic response, corresponding to the mediated oxidation of glucose, was also recorded using chronoamperometry at an applied potential of 0.35 V. The blank, background current, was measured in the buffer solution without glucose for 250 s. Measurement of the bioelectrocatalytic current was then performed following addition of 20 mM glucose to the buffer solution. A significant increase in the current intensity, corresponding to bioelectrocatalytic oxidation of glucose was observed in the presence of the complementary biotinylated-DNA. (**Figure 2.27**) The steady state response has not been fully achieved, but the decay is not significant after approximately 100 s. Studies on electrocatalytic NADH oxidation on OsPVI-modified carbon fibre microelectrode conducted by Ju and Leech showed that approximately 90 % of the steady state response is obtained in the first 10 s. (42)

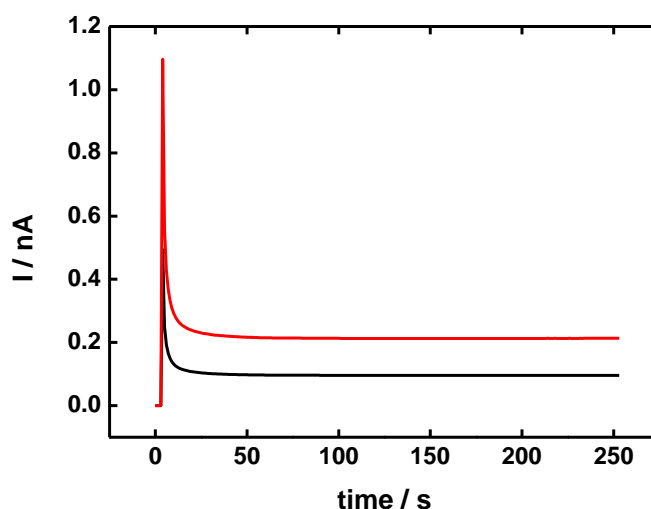


Figure 2.27 Chronoamperometric responses of the sensing film on a 40 μm diameter microelectrode after interaction with **complementary biotinylated-DNA** (1.85×10^{-7} M) and the glucose oxidase-avidin D conjugate in the absence (**black**) and presence (**red**) of 20 mM glucose.

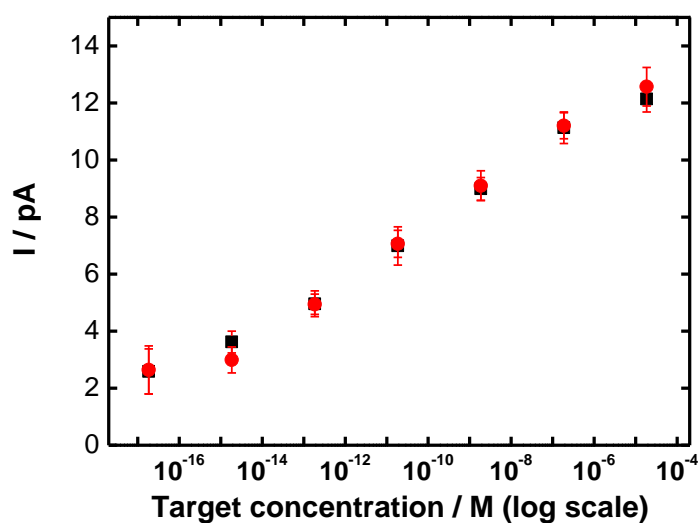


Figure 2.28 Current responses at 0.35 V corresponding to the concentration of the **complementary DNA** target sequences in 7.0 μl droplets. Concentration values are displayed using logarithmic scale. Cyclic voltammetry (**squares**) and chronoamperometry (**circles**) at the 40 μm diameter microelectrodes. Scan rate 5 mV/s; 20 mM glucose; 0.02 M phosphate buffer; pH = 7.4; 0.15 M NaCl. (n=5, first series of experiment)

The voltammetric and chronoamperometric currents scale with logarithm of complementary DNA concentration. The plots constructed by plotting current differences determined from cyclic voltammetric experiments (measured at 0.35 V in the forward scan) are presented in **Figure 2.28**. The chronoamperometry results (steady state currents measured after 250 seconds electrolysis time) as a function of DNA concentration show a similar trend. The current varies with the logarithm of the concentration of complementary target DNA sequences in the concentration range of 10^{-6} to 10^{-13} M. The estimated limit of quantification, is $\sim 4 \times 10^{-18}$ mol in a 7 μ l droplet and corresponds to a concentration of 6×10^{-13} M of target DNA in the sample estimated from the equation of the best-fit line of the calibration curve in the range of 10^{-6} to 10^{-13} M and the current for the average of the controls using non-complementary biotinylated target DNA plus 10 times the standard deviation of the controls. This limit is equivalent to the detection of $\sim 4 \times 10^{11}$ DNA copies in a one litre sample or $\sim 2.5 \times 10^6$ copies of DNA in the 7 μ L droplet, three-orders of magnitude lower than the stated limit of detection obtained for the same assay with the gold macroelectrodes. (23) An estimate of the limit of detection for this assay, using the concentration equivalent to the current signal determined for the average of the controls using non-complementary biotinylated target DNA plus 3 times the standard deviation of the controls, yields a value of 4×10^{-16} M. It should be noted that all four factors: improved signal-to-noise due to miniaturization of the gold electrodes, careful preparation of the electrode surfaces, background subtraction, and shielding from electronic noise contributed to the substantial lowering of the detection limit for this assay compared to that at 2 mm diameter gold macroelectrodes.

Experiments uncovered some issues with reproducibility for these systems, with response dependent upon preparation of electrodes. For example, the signals of the peak current for the osmium redox process for the redox polymer were found to be variable. A relative standard deviation for films prepared on 40 μ m diameter microelectrodes for the osmium redox process peak current values for DNA-modified electrodes over several months, was estimated to be 79 % for 16 measurements. (**Table 2.4**)

Table 2.4 Statistical parameters of the osmium peak currents at 40 μm electrodes

Average [A]	SD	RSD	Min.	Med.	Max.	n
1.48×10^{-9}	1.17×10^{-9}	79 %	2.35×10^{-10}	1.09×10^{-9}	4.07×10^{-9}	16

2.4. Conclusions

It was demonstrated that the analytical performance of the sensor format can be improved with miniaturisation of the gold electrodes, coupled to careful polishing of electrodes, background subtraction and shielding from electronic noise, allowing detection of femtomolar concentrations of target ssDNA using microelectrodes.

Redox polymer films on microelectrodes display much greater stability in comparison with macroelectrodes (23) and this fact also contributes to the improvement.

A major issue of the assay is its complexity. The assay procedure requires careful preparation of the sensing layers and elimination of electrical interferences. The current response is highly influenced by the production of the modified layer, which is more likely to form on smooth electrodes. (47) Microelectrodes are quite difficult to polish and a number of sensors that could be prepared in one batch is limited. Drop-coating of the modification solution is also a disadvantage of the film formation procedure. Improvements to this may be achieved by robotic dispensing and precision placements of droplets onto electrode surface or by investigation of alternate immobilization and crosslinking chemistry that can be performed in solution. For example an osmium redox polymer can be electropolymerised on carbon electrodes. (24, 43) Further efforts should thus focus on solution-phase film formation processes.

2.5. References

1. A. M. Bond, *Analyst* **119**, 1R (1994).
2. C. Beriet, D. Pletcher, *J. Electroanal. Chem.* **361**, 93 (1993).
3. A. M. Bond, M. Fleischman, J. Robinson, *J. Electroanal. Chem.* **168**, 299 (1984).
4. M. Ciszowska, Z. Stojek, S. E. Morris, J. G. Osteryoung, *Anal. Chem.* **64**, 2372 (1992).
5. J. Ghoroghchian, F. Sarfarazi, T. Dibble, J. Cassidy, J.J. Smith, A. Russell, G. Dunmore, M. Fleischmann, S. Pons, *Anal. Chem.* **58**, 2278 (1986).
6. Y. Ikariyama, S. Yamauchi, T. Yukiashi, H. Ushioda, M. Aizawa, *Bull. Chem. Soc. Jpn.* **62**, 1869 (1989).
7. J. A. Stamford, *J. Neurosci. Meth.* **17**, 1 (1986).
8. R. C. Engstrom, C. M. Pharr, *Anal. Chem.* **61**, 1099A (1989).
9. C. Holmes, G. Eisenhofer, D. S. Goldstein, *J. Chromatogr., B* **653**, 131 (1994).
10. T. Kappes, P. C. Hauser, *J. Chromatogr., A* **834**, 89 (1999).
11. J. W. Bixler, A.M. Bond, P.A. Lay, W. Thormann, P. van den Bosch, M. Fleischmann, B.S. Pons, *Anal. Chim. Acta* **187**, 67 (1986).
12. M. Sosna, G. Denuault, R. W. Pascal, R. D. Prien, M. Mowlem, *Sens. Actuators, B* **123**, 344 (2007).
13. N. S. Lawrence, L. Jiang, T. G. J. Jones, R. G. Compton, *Anal. Chem.* **75**, 2499 (2003).
14. C. M. Li, J. Zang, D. Zhan, W. Chen, C.Q. Sun, A.L. Teo, Y.T. Chua, V.S. Lee, S.M. Moochhala, *Electroanalysis* **18**, 713 (2006).
15. M. A. Baldo, S. Daniele, G. A. Mazzocchin, *Electroanalysis* **10**, 410 (1998).
16. P. R. M. Silva, M.A. El Khakani, M. Chaker, G.Y. Champagne, J. Chevalet, L Gastonguay, R. Lacasse, M. Ladouceur, *Sens. Actuators, B* **76**, 250 (2001).
17. X. Xie, D. Stüben, Z. Berner, J. Albers, R. Hintsche, E. Jantzen, *Sens. Actuators, B* **97**, 168 (2004).
18. R. J. C. Brown, M. J. T. Milton, *TrAC Trends Anal. Chem.* **24**, 266 (2005).
19. J. Buffle, M.-L. Tercier-Waeber, *TrAC Trends Anal. Chem.* **24**, 172 (2005).
20. E. A. Hutton, B. Ogorevc, S. B. Hocevar, M. R. Smyth, *Anal. Chim. Acta* **557**, 57 (2006).
21. F. Lehmann-Horn, M. Fauler, B. Holzherr, K. Jurkat-Rott, in *Cardiac Electrophysiology Methods and Models*, D. C. Sigg *et al.* Eds. (Springer US, 2010), pp. 119-134.
22. R. J. Forster, *Chem. Soc. Rev.* 289 (1994).
23. P. Kavanagh, D. Leech, *Anal. Chem.* **78**, 2710 (2006).
24. Y. Zhang, H. H. Kim, A. Heller, *Anal. Chem.* **75**, 3267 (2003).
25. N. Djellouli, M. Rochelet-Dequaire, B. Limoges, M. Druet, P. Brossier, *Biosens. Bioelectron.* **22**, 2906 (2007).
26. Z. P. Aguilar, I. Fritsch, *Anal. Chem.* **75**, 3890 (2003).
27. Z. P. Aguilar, W. R. Vandaveer, I. Fritsch, *Anal. Chem.* **71**, 3321 (2002).
28. H. Xie, C. Zhang, Z. Gao, *Anal. Chem.* **76**, 1611 (2004).
29. R. Miranda-Castro, P. de-los-Santos-Alvarez, M. J. Lobo-Castanon, A. J. Miranda-Ordieres, P. Tunon-Blando, *Anal. Chem.* **79**, 4050 (2007).
30. A. L. Ghindilis, M.W. Smith, K.R. Schwarzkopf, K.M. Roth, K. Peyvan, S.B. Munro, M. J. Lodes, A.G. Stöver, K. Bernards, K. Dill, A. McShea,

- Biosens. Bioelectron.* **22**, 1853 (2007).
31. R. J. Forster, J. G. Vos, *Macromolecules* **23**, 4372 (1990).
 32. Z. Kerner, T. Pajkossy, *J. Electroanal. Chem.* **448**, 139 (1998).
 33. J. W. Bixler, A. M. Bond, *Anal. Chem.* **58**, 2859 (1986).
 34. H. O. Finklea, S. Avery, M. Lynch, T. Furttsch, *Langmuir* **3**, 409 (1987).
 35. S. Trasatti, O. A. Petrii, *Pure & Appl. Chem.* **63**, 711 (1991).
 36. Y. Degani, A. Heller, *J. Am. Chem. Soc.* **111**, 2357 (1989).
 37. A. Bhattacharya, J. W. Rawlins, P. Ray, *Polymer grafting and crosslinking*. (John Wiley, 2009).
 38. J. M. Barton, I. Hamerton, B. J. Howlin, J. R. Jones, S. Liu, *Polymer* **39**, 1929 (1998).
 39. J. Lehr, B. E. Williamson, F. Barrière, A. J. Downard, *Bioelectrochemistry* **79**, 142 (2010).
 40. R. W. Murray, in *Electroanalytical Chemistry*, A. J. Bard, Ed. (Marcel Dekker Inc., New York, 1984), vol. 13.
 41. M. V. Pishko, A. C. Michael, A. Heller, *Anal. Chem.* **63**, 2268 (1991).
 42. H. Ju, D. Leech, *Anal. Chim. Acta* **1997**, 51 (1997).
 43. Y. Zhang, H. H. Kim, N. Mano, M. Dequaire, A. Heller, *Anal. Bioanal. Chem.* **374**, 1050 (2002).
 44. S. Rebouillat, M. E. G. Lyons, A. Flynn, *Analyst* **125**, 1611 (2000).
 45. L. Geng, R. A. Reed, M. Longmire, R. W. Murray, *J. Phys. Chem.* **91**, 2908 (1987).
 46. J. G. Vos, R. J. Forster, T. E. Keyes, *Interfacial Supramolecular Assemblies*. (John Wiley and Sons, New York, 2003).
 47. G. E. Poirier, *Chem. Rev.* **97**, 1117 (1997).

Chapter 3

**DNA detection at hydrogels prepared
via attachment of carboxymethylated
dextran to electrodes**

3.1. Introduction

Chapter 2 describes a stable and sensitive platform for the electrochemical detection of DNA hybridisation. It was demonstrated that sensing films, where a probe DNA is cross-linked to osmium-based redox polymer film on gold microelectrodes can detect tens of picomoles of target DNA. (1) There are however a few disadvantages to this method. Reproducing signals between electrodes was found to be difficult. It was postulated that detection of real samples would require an alternative approach in sensor preparation. For example, more rigorous washing and blocking sequences may be required in order to better discriminate between analyte and non-specific binding to the surfaces.

In addition, the crosslinking method used for the study in Chapter 2, is based on a solid-phase reaction between poly(ethylene glycol)bisglycidyl ether (PEGDGE) crosslinking reagent and nucleophiles, which can introduce further complications into the electrode preparation protocol. The cross-linker contains epoxide groups, which can potentially bind to amino groups and heterocyclic nitrogens contained within DNA bases (2) thus damaging the DNA structure (3) and hindering hybridisation.

In an effort to improve the analytical performance of the DNA assay, we have applied alternative reagents and immobilisation methods for hybridisation detection. In the present approach the reduction of *in-situ* generated aryldiazonium salt from p-phenylenediamine allows introduction of covalently attached arylamine to the electrode surface, replacing the cysteamine SAM and providing greater surface stability when exposed to high temperature, rigorous washing conditions, exposure to air and sonication. (4) We also replace the $[\text{Os}(2,2'\text{-bipyridine})_2(\text{polyvinylimidazole})_{10}\text{Cl}]^{+/2+}$ (OsPVI) redox polymer films, used as a matrix for co-immobilisation with ssDNA, with a carboxymethylated dextran (CMD) matrix, which provides carboxyl functional groups for subsequent immobilisation of amine-functionalised ssDNA and other affinity and signalling reagents through solution-phase carbodiimide coupling chemistry. The structure of carboxymethylated dextran subunit is presented in **Figure 3.1**. The introduction of the solution-phase carbodiimide coupling assay protocol replaces the drop coating/drying with dipping of the electrodes into larger volumes (over 20 μl), which provides greater control.

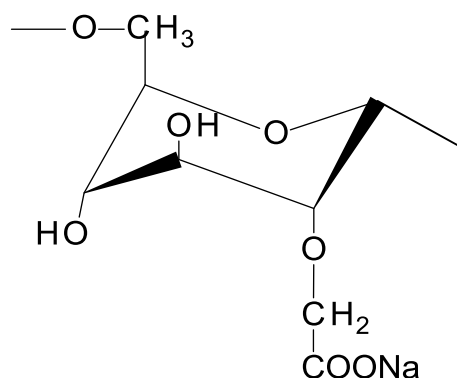


Figure 3.1 Structure of carboxymethylated dextran subunit

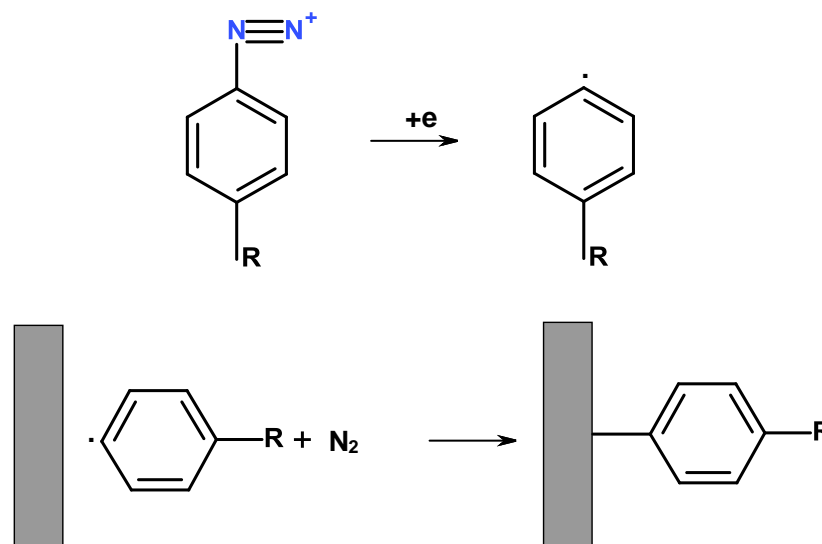
CMD was introduced in between the monolayer and the DNA to reduce non-specific binding, compared to the positively charged osmium redox polymer used in our original assay. (5) The presence of carboxylic groups allows electrostatic repulsion between the carboxyl groups and the negatively charged ssDNA strands. The hydrophilic, 3-dimensional structure of CMD reportedly facilitates diffusion of species towards the surface and displays low non-specific binding towards biomolecules. (6-8)

Studies by S.J. Wood (9) demonstrated high specificity of DNA hybridisation assays on CMD chips. In addition, it was demonstrated that the extent of non-specific binding of proteins can be reduced when CMD is coupled to a cysteamine monolayer on gold. (10, 11) CMD coated gold electrodes was also used in an amperometric immunoassay for detection of *Salmonella typhimurium*. (12)

Construction of modified electrode interfaces via reduction of aryl diazonium salts has increasingly become a viable alternative/complement to self-assembled monolayers (SAMs). Unlike the SAMs, which can form exclusively on metals, diazonium chemistry is applicable for modification of a broad range of solid electrode materials, such as glassy carbon, (13) graphite, (14) screen-printed electrodes, (15) diamond (16) and metals. (17) Films attached to an electrode surface through formation of C-C bonds, using reduction of aryldiazonium salts on carbon electrodes, are more stable than modified gold. (18-21) Mobile nature of gold atoms results in de-sorption and structural reorganisation of the thiols on the surface and limits the stability as the consequence. (22) The bond energy of the Au-S is

estimated as 170 kJ/mol, (4) comparing to covalent C-C bond energy of ~347 kJ/mol. (23)

The diazonium salt can be formed from an aromatic amine in acidic conditions in the presence of nitrite. Upon polarisation of the electrode, formation of the radical occurs and the covalent bond between the carbon and a phenyl ring is established. (Scheme 3.1)



Scheme 3.1 Mechanism of reduction of an aryl diazonium salt at a carbon electrode. Adapted from reference (4)

Fang Teh et al. (24) reported covalent grafting of DNA onto amino-benzoic acid-functionalised glassy carbon (GC) electrodes. A sensor network based on DNA immobilised on arylamine-modified carbon nanotubes and carbon nanofibers, *via* electroreduction of an aryl diazonium salt, was also described. (25) Increased stability of a copper sensor based on a peptide sensing film on glassy carbon surfaces modified by covalent grafting of aryl diazonium salts was demonstrated by Liu et al. (26) In the work by Polsky et al., aryl diazonium salt reduction is used for the formation of recognition layers in multi-analyte sensors, which allow simultaneous detection of DNA and proteins. (27, 28)

Here we aim to evaluate the feasibility of the detection platform, outlined in **Figure 3.2** for electrochemical DNA hybridisation. For this purpose we have used a recognition surface consisting of ssDNA probe (coding for *ssrA* gene of *Listeria monocytogenes*) immobilised in a CMD film attached to an electrode. In a preliminary study, a solution phase electron transfer mediator (ferrocenemethanol,

structure shown in **Figure 3.2**) was employed in favour of an immobilised mediator, in order to reduce assay complexity and to establish the principle of the scheme. Hybridisation between probe ssDNA and target biotinylated-ssDNA and the addition of the glucose oxidase:avidinD conjugate results in the current due to bioelectrocatalytic oxidation of glucose, where ferrocenemethanol in the solution-phase acts as electron transfer mediator.

Another version of this platform with a surface-bound mediator [Os(2,2'-bipyridine)₂(4-aminomethylpyridine)Cl]PF₆ co-immobilised with ssDNA on carboxymethylated dextran was also tested for the ability to detect DNA binding.

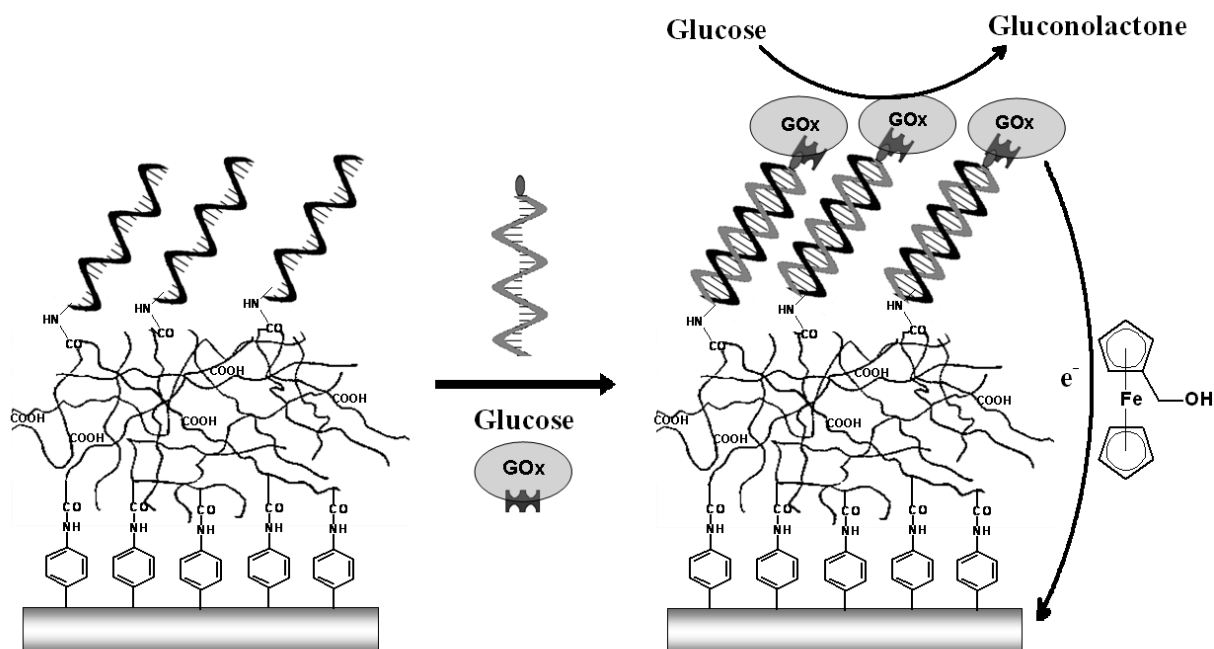


Figure 3.2 Simplified schematic of assay platform. The recognition layer at left consists of ssDNA bound within a CMD film that is anchored to the arylamine-derivatised graphite electrode. Hybridisation of **biotin-labelled target ssDNA** and addition of **glucose oxidase:avidinD**, represented by GOx, results in bioelectrocatalytic oxidation of glucose using a solution phase **ferrocenemethanol** mediator.

3.2. Experimental

3.2.1. Materials

The probe oligonucleotide sequence (5'⇒3'): NH₂-C6-ATTCGACAGGGATAGTTCGA, target oligonucleotide sequence (5'⇒3'): biotin-TCGAACTATCCCTGTCGAAT (designed from the *ssrA* gene of *Listeria monocytogenes*), control oligonucleotide sequence (5'⇒3'): biotin-ATTCGACAGGGATAGTTCGA (biotin-non-complementary) and (5'⇒3'): TCGAACTATCCCTGTCGAAT (unmodified-complementary) were purchased from MWG-Biotech. Glucose oxidase: avidinD conjugate was purchased from Vector Laboratories. [Os(2,2'-bipyridine)₂(4-aminomethylpyridine)Cl]PF₆ and [Os(2,2'-bipyridine)₂(4-aminoethylpyridine)Cl]PF₆ were synthesised according to the literature procedure.⁽²¹⁾ All other chemicals were purchased from Sigma-Aldrich and used as received.

3.2.2. Methods

The electrochemical measurements were performed using an Autolab, EcoChemie, PGSTAT12 potentiostat or a CHI 1030A multi-channel potentiostat. All experiments were carried out with a three-electrode system at room temperature. Custom-made graphite disk electrodes (3 mm diameter, constructed from graphite rods purchased from Goodfellow) were used as working electrodes, Ag/AgCl (CH Instruments) was used as a reference electrode and a platinum wire was used as a counter electrode. In all experiments, the electrochemical cell was maintained in a custom-built Faraday cage to minimize electrical noise.

3.2.3. Deposition of the sensing layer

Methods for immobilising monolayers of polymers and mediators on gold and glassy carbon electrodes are presented in the final section of the chapter. (**Table 3.8** and **3.9**)

Graphite disk electrodes were abraded using silicon carbide paper, grit P400, rinsed with ultrapure water, and dabbed with lint-free tissues to remove graphite particles. Surface derivatization to generate attached phenylamine was carried out as described previously (19-21) using electrochemical reduction; by cycling 4 times at 20 mV/s between 0.6 V and -0.4 V vs. Ag/AgCl, of a mixture of 0.5 M HCl (50 mL), 10 mM p-phenylenediamine, and 8 mM NaNO₂ maintained on an ice bath.

Electrodes were rinsed with water and sonicated for 5 min. Surface attachment of carboxymethylated dextran (CMD) was achieved by dipping the derivatized electrodes into a solution containing 50 mM EDC (N-Ethyl-N'-(3-dimethylaminopropyl)carbodiimide), 20 mM NHS (N-Hydroxysuccinimide) and 2 mg/mL CMD in ultrapure water for 2 h at room temperature following pre-activation of the CMD with the EDC/NHS solution for 1.5 h at 4 °C. The resulting CMD-modified surfaces were re-activated by immersion in EDC/NHS solution for 1 h and subsequently immersed into a probe DNA solution (30 µL, 400 µg/mL) for 15 h. After reaction with the probe DNA the electrodes were rinsed with pH 9.6 carbonate buffer to remove unreacted NHS esters, and then with distilled water. Attachment of osmium complexes was achieved through reactivation of CMD-modified graphite electrodes with EDC/NHS followed by immersion in 2.5 mg/mL solution of osmium complex in methanol-water mixture (1:1) for 15 hrs.

For sensor containing surface-confined mediator the osmium complex was reacted with CMD layer first, according to the procedure described above. The electrode was rinsed with carbonate buffer, MilliQ water and electrochemically cycled, until the CV signal was stable. Then surfaces were re-activated with EDC/NHS and the electrode was placed overnight in probe DNA solution (30 µL, 400 µg/mL).

3.2.4. Assay procedure

Sensing electrodes were dipped into plastic micro-centrifuge tubes containing solution of target DNA (500 µL, varying concentrations of DNA in 0.3 M sodium citrate, 1 M NaCl, 0.05 % SDS, 0.2 % milk powder) for 2 h at 37 °C with gentle shaking. Milk powder and SDS (sodium dodecyl sulphate) were added to reduce non-specific binding of DNA and the enzyme. (29)

After 2 hours electrodes were removed, rinsed with hybridization solution and immersed into 0.2 mg/ml glucose oxidase: avidinD solution (150 μ L) for 1 h at room temperature. The electrodes were then rinsed with hybridization solution and the catalytic current was measured by cyclic voltammetry (0 - 0.5 V vs. Ag/AgCl, 2 scans at 5 mV/s) and chronoamperometry (0.35 V, 250 s) in 0.02 M phosphate buffer containing 0.2 mM ferrocenemethanol as the mediator, in the absence and presence of 20 mM glucose.

3.2.5. Optical characterization of DNA-modified surfaces

The presence of DNA on CM Dextran films on graphite was confirmed by **Total Internal Reflectance Fluorescence (TIRF)**, microscope model: **Olympus IX81**. Microscope settings are presented in **Table 3.1**

Table 3.1 Microscope settings

Camera	Andor iXon EMCCD	Intensity	32.29%
Binning	1x1 (512x512) pixels	Exposure time	500 ms
Gain	0	EM Gain	50%
Camera temperature	-8°C (Target = - 10 °C)	Filters	TRITC for fluorescence, Free for the white light
Objective	5x/0.1 ∞ /-		

For optical determination of the surface-bound DNA a complementary DNA sequence containing Bodipy 530/550 dye in 5' position was used for hybridization. Also negative control surfaces were prepared for comparative analysis. Graphite discs were separated from the electrode body by careful cutting of the graphite rod with the scalpel. The details of the samples used for TIRF test can be found in **Table 3.2**.

Table 3.2 Description of surfaces used in TIRF experiment

Sample no	Sample description
1	Arylamine/CMD/ssDNA layer on graphite (exactly the same as the recognition layer used for amperometric detection), DNA sequence containing fluorescent tag (BODIPY 530/550) has been hybridised in the same assay procedure as in the amperometric sensor
2	Bare graphite
3	Graphite with CMD linked to phenylamine monolayer, no probe DNA attached
4	As sample 3, allowed to react with ssDNA-BODIPY 530/550 target
5	Graphite with CMD and ssDNA

3.3. Results and discussion

3.3.1. Development of the sensing layer

In an effort to select a suitable method for immobilising layers of polymers and DNA on gold and glassy carbon electrodes, control experiments using an amine terminated redox probe $[\text{Os}(2,2'\text{-bipyridine})_2(4\text{-aminoethylpyridine})\text{Cl}]\text{PF}_6$ were undertaken. (Also $[\text{Os}(2,2'\text{-bipyridine})_2(4\text{-aminomethylpyridine})\text{Cl}]\text{PF}_6$ was used.) A range of approaches was initially investigated, using the amine terminated osmium redox complex. Most of these approaches resulted in insufficient amount of redox complex detected at the surface, indicating their unsuitability for progression to immobilisation of amine-terminated DNA for a DNA hybridisation assay. These are presented in **Appendix** of the chapter. (**Table 3.8** and **3.9**)

Efforts were focused on derivatisation of carbon electrodes in order to provide a more stable anchoring of films than physisorbed (5) or Au-S-based systems (Chapter 2) used heretofore. In general, carbon electrodes were derivatised by electro-reduction of the diazonium salts produced by in situ diazotisation of p-phenylene diamine or p-aminomethylaniline. This approach can introduce amino functionality for further derivatisation by coupling of carboxymethylated dextran and the redox complex. Cyclic voltammograms recorded in the solution used for in situ

diazotisation of p-phenylenediamine, on glassy carbon electrodes, are presented in **Figure 3.3**, illustrating the presence of a peak on the first reductive cycle, corresponding to the reduction of the diazonium salt that disappears gradually upon each subsequent cycle, as reported previously. (19-21)

An estimate of the surface coverage of the amine (calculated from the area under the first diazonium reduction peak, $\Gamma = Q/ nFA$) gives $\Gamma = 2.37 \times 10^{-9} \pm 1.24 \times 10^{-9}$ mol/cm². This correlates with data published by Boland et al. (19), who reported a coverage of grafted aryl moieties to be $2 \pm 0.82 \times 10^{-9}$ mol/cm².

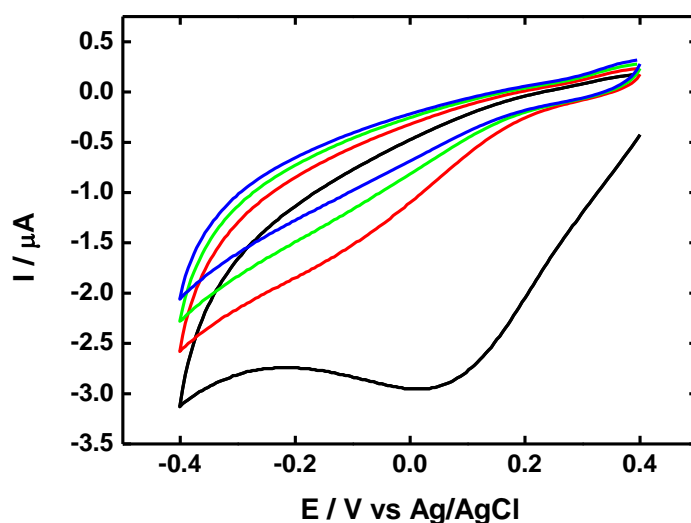


Figure 3.3 GC electrode modified with p-phenylene diamine diazonium salt. Scans from 1 to 4

A voltammogram of the glassy carbon modified with arylamine, carboxymethylated dextran and osmium complex is presented in **Figure 3.4**. Poorly defined peaks at 0.35 and 0.25 V, presumably corresponding to Os(II) to Os(III) transition can be observed. Despite relative high coverage estimated for the grafted arylamine, the coupling of the osmium complex within anchored films of the CMD does not appear to be efficient: not providing sufficient functional groups to couple significant amounts of the redox probe to films of CMD on glassy carbon electrodes.

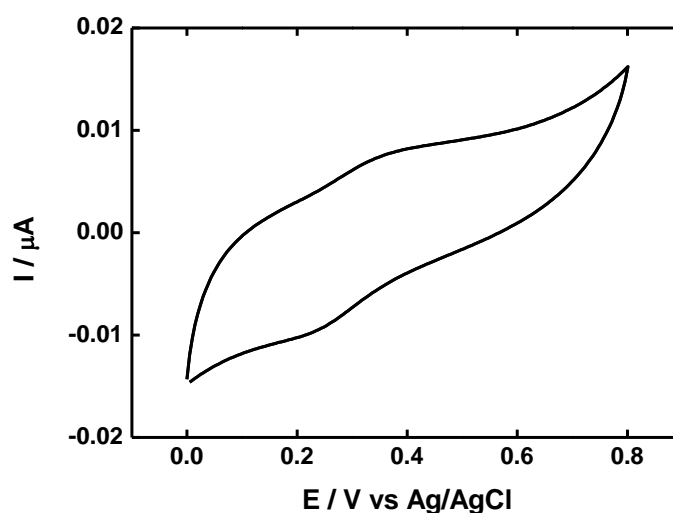


Figure 3.4 CMD with redox probe $[\text{Os}(\text{bpy})_2(4\text{-aminomethylpyridine})\text{Cl}]\text{PF}_6$ immobilized onto 3 mm **glassy carbon** electrode with arylamine surface functionalization

From all the electrode materials studied coupling of the redox probe to CMD immobilised on graphite was the only approach that yielded significant redox signals corresponding to the Os(II) to Os(III) transition. CVs in **Figure 3.5** illustrate the reductive coupling process for the diazonium salt on a graphite electrode. Two reduction peaks observed were previously observed by others, but, little is reported of their origin. (30, 31)

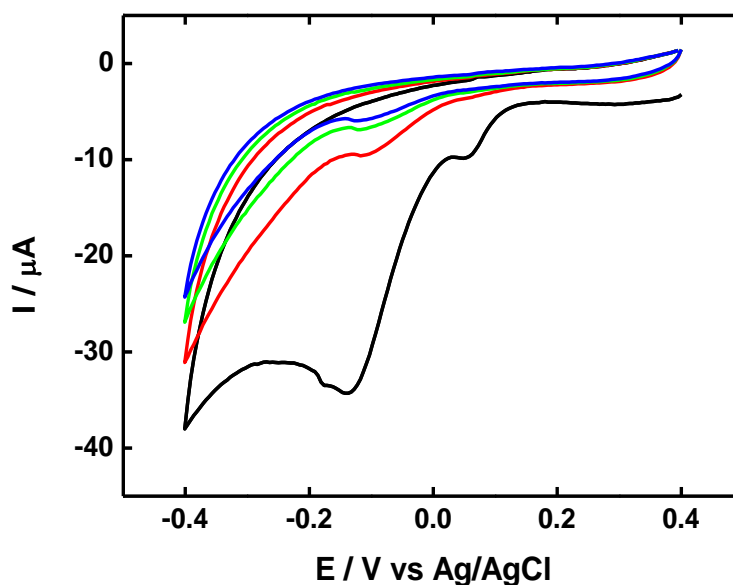


Figure 3.5 Graphite electrodes modified with **p-phenylene diamine diazonium salt**. Scans from 1 to 4.

The cyclic voltammogram at graphite electrodes derivatised via reduction of diazonium salts of p-phenylene diamine, followed by coupling carboxymethylated dextran and [Os(2,2'-bipyridine)₂(4-aminoethylpyridine)Cl] (**Figure 3.6**) displays an Os(II)/(III) redox transition, with a formal redox potential (E°) of 0.329 V vs. Ag/AgCl. The similarity of this redox potential to that observed for this complex, and analogues of this complex, in solution is indicative of similar microenvironments surrounding the complex in the highly solvated CMD film. (20)

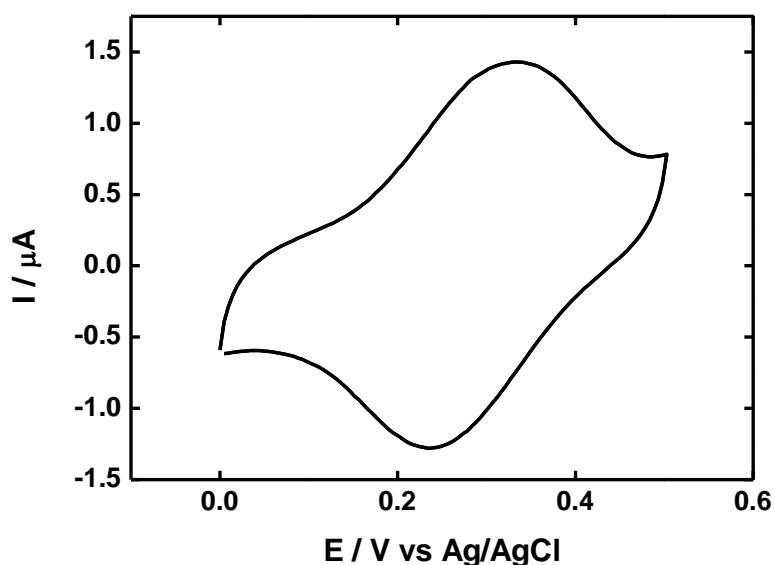


Figure 3.6 Cyclic voltammogram of the redox probe [Os(bipyridine)₂(4-aminoethylpyridine)Cl] bound within a CMD film that is anchored to the **arylamine-derivatised graphite** electrode. 20 mM phosphate buffer, pH 7.4, scan rate 5 mV/s.

An osmium surface coverage of 4×10^{-9} mol/cm² can be estimated by integration of the charge under the voltammetric wave for oxidation of the immobilised osmium redox probe. This coverage is comparable to the surface coverage of 3.5×10^{-9} mol/cm² obtained for the osmium redox polymer hydrogel films anchored to the gold macroelectrodes, used in the original DNA hybridisation assay. (5) From data on related osmium complexes, a surface coverage of $\sim 1 \times 10^{-10}$ mol/cm² is estimated for formation of complete close-packed monolayer coverage of such a complex on smooth electrodes, providing a rough estimate of films containing the equivalent of at least 40 monomolecular layers of redox complex. (32)

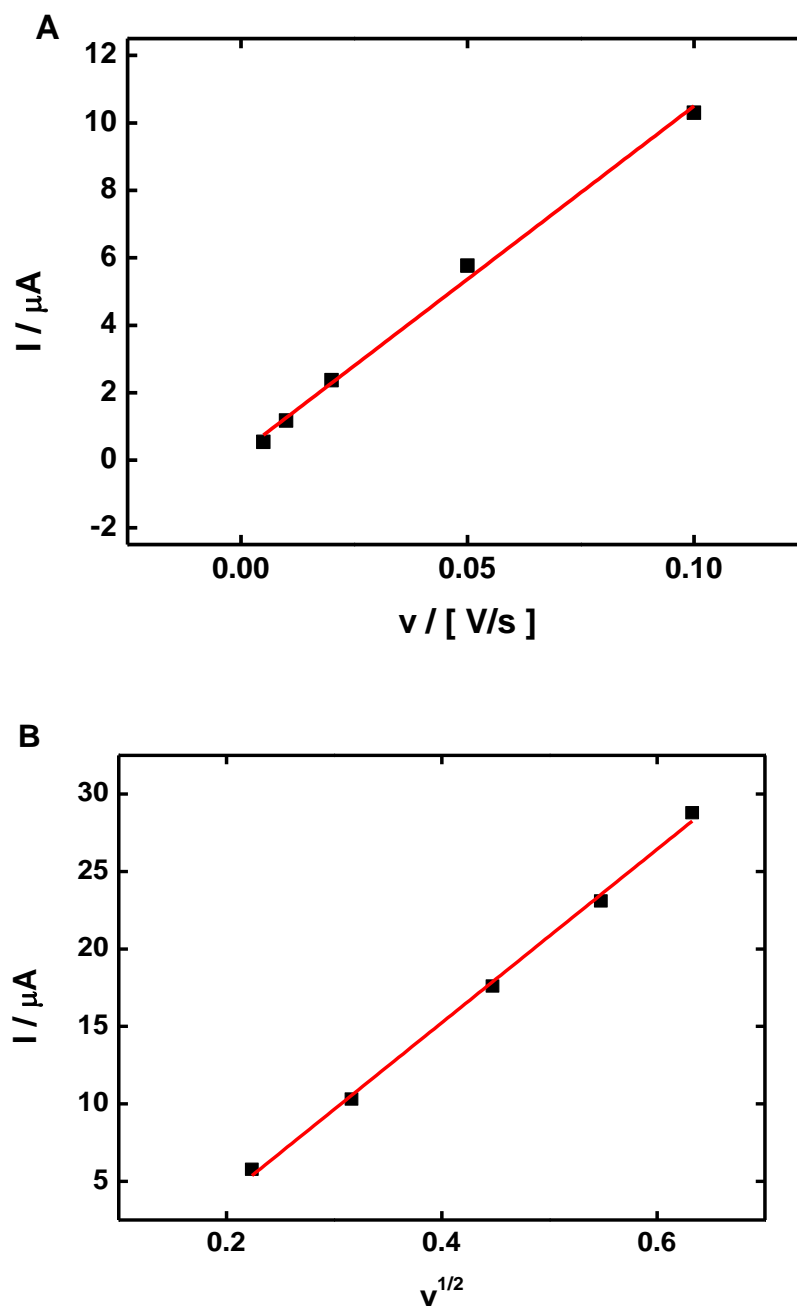


Figure 3.7 Plots of I vs v (A) and $v^{1/2}$ (B) and v for $[\text{Os}(2,2'\text{-bipyridine})_2(4\text{-aminoethylpyridine})\text{Cl}]$ coupled to **carboxymethylated dextran** on graphite electrode, phosphate buffer, pH 7.4, scan rate 5 mV/s. (33)

Cyclic voltammograms recorded at different scan rates can help probe whether the redox complex is surface attached. (33) For example, the linear trend observed when peak currents are plotted versus scan rate ($v < 100$ mV/s) in **Figure 3.7 A** are indicative of finite (bounded) diffusion, confirming that the redox complex is surface-confined. At more rapid scan rates ($v > 100$ mV/s) the peak currents scale

with the square root of the scan rate **Figure 3.7 B** as the diffusion layer does not extend entirely through the attached film (semi-infinite diffusion), in agreement with other systems containing surface-confined films of redox probes. (33)

Table 3.3 presents charge transport parameters for the osmium complex confined to carboxymethylated dextran film on graphite, extracted from the plots (**Fig 3.7**) of CV peak currents as a function of square root of the scan rate as described in Chapter 1 (**Eq. 1.3**).

Table 3.3 Film parameters of [Os(2,2'-bipyridine)₂(4-aminoethylpyridine)Cl] covalently bound to CMD film

	E^0	ΔE	FWHM	$D^{1/2}c$ [Mol cm ⁻¹ s ⁻¹]	Γ (surface coverage) [mol/cm ²]
	n = 8				n = 23
Average	0.32	0.07	0.156	3×10^{-9}	4×10^{-9}
SD	0.02	0.02	0.02	1×10^{-9}	1×10^{-9}
RSD	5 %	34 %	14 %	44 %	33 %

An average redox potential of the complex has a value of 0.329 V, which is in close to the value of 0.29 V reported by Boland et al. (19) Average peak separation is in the region of 70 mV at 5 mV/s perhaps indicative of interaction between the redox complexes within the film, as $\Delta E > 0$; supported by the divergence from the ideal FWHM of $90.6/n$ mV for the system. (33, 34) The values for $D^{1/2}c$ and Γ estimated lie within a similar range as those for redox polymer films on gold microelectrodes. (1) A DNA sensing film must possess a sufficient stability to withstand long term immersion in solutions for at least the time required to complete the hybridisation. A study on the stability of the [Os(bpy)₂(4-aminoethylpyridine)Cl]PF₆ in the CMD film is presented in **Figure 3.8**. There is a significant improvement of film stability on macroelectrodes compared to redox polymer crosslinked and anchored to cysteamine derivatised gold. (5) For example, the decrease of the redox peak signal from the [Os(bpy)₂(4-aminoethylpyridine)Cl]PF₆ complex, bound to the CMD film, is 21% after 3 days and 33% after 25 days (600 hr) compared to a 54% decrease in signal

over 24 hr previously observed for the redox polymers anchored to cysteamine pre-adsorbed on gold. (5)

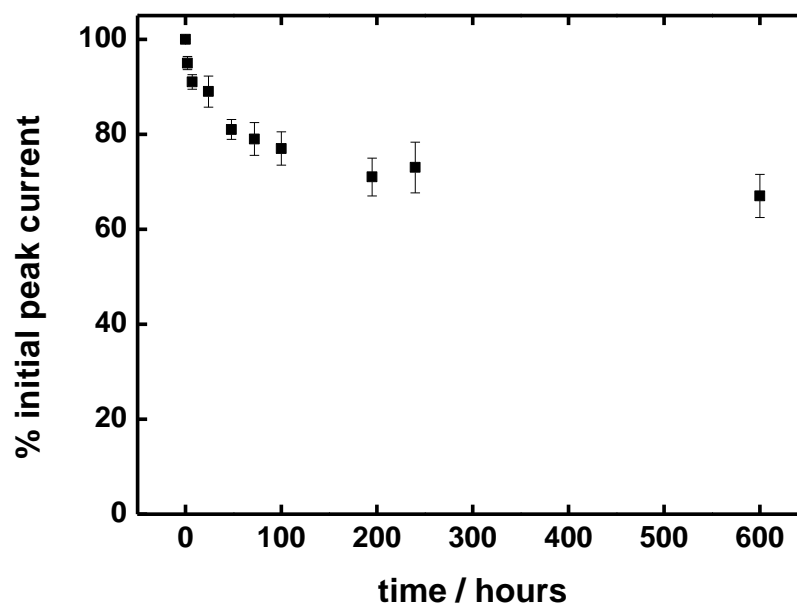


Figure 3.8 The stability of the peak current signal at the modified electrode from **Figure 3.6** as a function of time. Peak current extracted from cyclic voltammograms recorded at a scan rate **5 mV/s**, at selected time intervals and normalised to the initial peak height. Electrodes stored and analysed in 20 mM phosphate buffer, pH 7.4.

The decrease in peak height for the osmium complex can be modelled assuming a simple first order reaction process. A plot of the natural logarithm of the decrease in peak height should therefore be linear. The plot for this system, as seen on **Figure 3.9**, displays two separate linear portions.

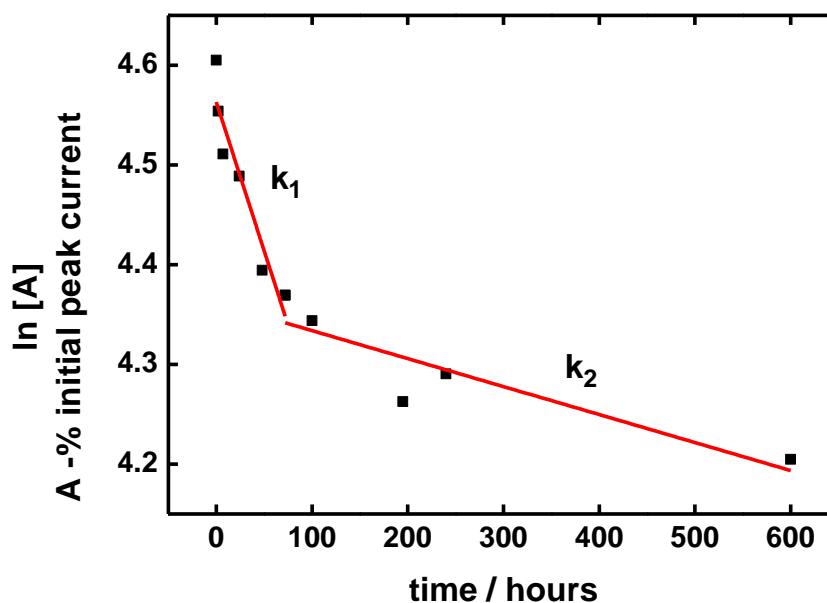


Figure 3.9 Kinetic plot (first order) for decay of osmium redox complex

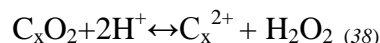
The desorption of electroactive species from modified electrodes has been extensively studied. For example, Voicu et al. (35) recorded CV signals of an electrode derivatised with 11-(ferrocenylcarbonyloxy)undecanethiol and *n*-decanethiol mixed monolayer upon long-term immersion in ethanol. The decay curves, where the redox signals of the ferrocene moiety are plotted versus time, display a fast exponential decay in the first 100 hours and then signals reach a plateau. In addition, an initial rapid decay, followed by a slower first order desorption of species from an electrode was reported for ruthenium bipyridyl complexes immobilized on silanised surface via amide bond. (36) The two processes observed for the osmium complex bound to the anchored CMD film may be attributed to a gradual desorption of a more weakly bound (physisorbed?) population from the surface, followed by a slower desorption of more strongly bound (attached) complex.

The half-life extracted from first order rate constant for the second (slower) process is approximately 2470 hours. In comparison, a half life for the osmium peak decay for redox polymer films on microelectrodes is 2997 hours, when continuously immersed in the phosphate buffer (see Chapter 2), confirming that the complex is more stably confined to the electrode surface.

3.3.2. Redox probe studies of modified surfaces

The effect of surface chemistry and microstructure of carbon electrodes on electrochemical parameters for the electrode and for redox reactions at the electrode is well-documented in literature. (37-58) The processes at carbon surface can be influenced by a variety of factors, such as presence of functional groups on carbon, (40-43, 45, 53, 55-57) crystal structure, (49) in particular the position of edge and basal planes of the graphite lattice and pH. (46) Influence of electrode roughness and physis- and chemisorption was reported on. (49)

For example, the kinetics of the some voltammetric processes in aqueous media improves upon formation of oxygen containing functional groups on glassy carbon electrode via potential cycling. (38, 50) These groups are known to be hydroquinone, carbonyl, carboxylic and hydroxyl. (37-39) A theory describing chemical reactions at carbon surfaces suggests that upon polarisation an exchange of protons between the solution and different electrode functionalities takes place; the following reaction mechanism was suggested:



Chen and McCreery reported the opposite effect; when oxygen to carbon ratio decreases, a slower kinetics of electron transfer is expected. (53) Surface modification can result in enhancement of the charging currents. (42)

The data presented in this section focuses on the effect of chemical modification on cyclic voltammetry of redox probes using a negatively charged probe - potassium ferricyanide and a positively charged probe - ruthenium hexamine chloride, dissolved in the phosphate buffer, pH 7.4. The report by Chen and Mc Creery classifies $Fe(CN)_6^{3-/4-}$ as a redox probe which is sensitive to surface modification, but not to O/C ratio. According to the same authors the redox process of $Ru(NH_3)_6^{3+/2+}$ is an outer-sphere electron transfer reaction and is not surface sensitive. (53) **Figure 3.10** shows the cyclic voltamogram of potassium ferricyanide recorded at a bare electrode, a surface modified by the in situ diazotisation and electro-reduction of p-phenylenediamine, and this surface subsequently reacted to anchor a carboxymethylated dextran film. The response of ruthenium hexamine (III) chloride at the same electrodes is shown in **Figure 3.11**.

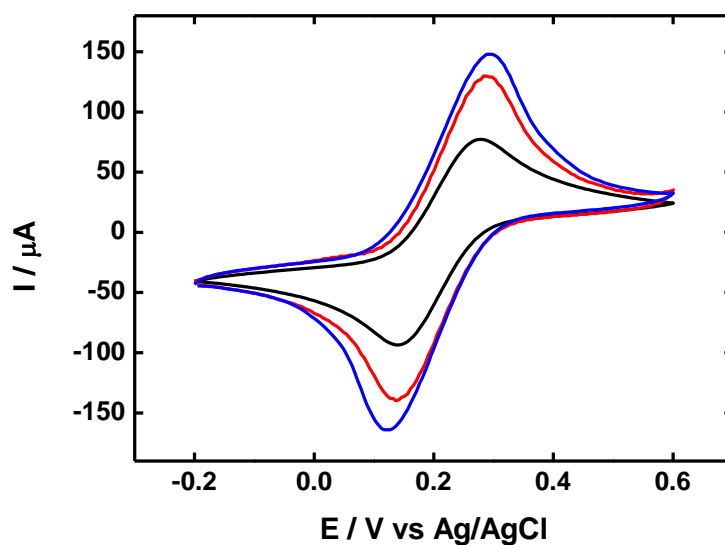


Figure 3.10 Cyclic voltammetry studies of modified electrodes, response of the **black** - bare electrode, **red**- electrode after reaction with p-phenylene diamine diazonium, **blue**- electrode with carboxymethylated dextran support. , **10 mM ferricyanide**, 20 mM phosphate buffer, pH 7.4, scan rate 50 mV/s

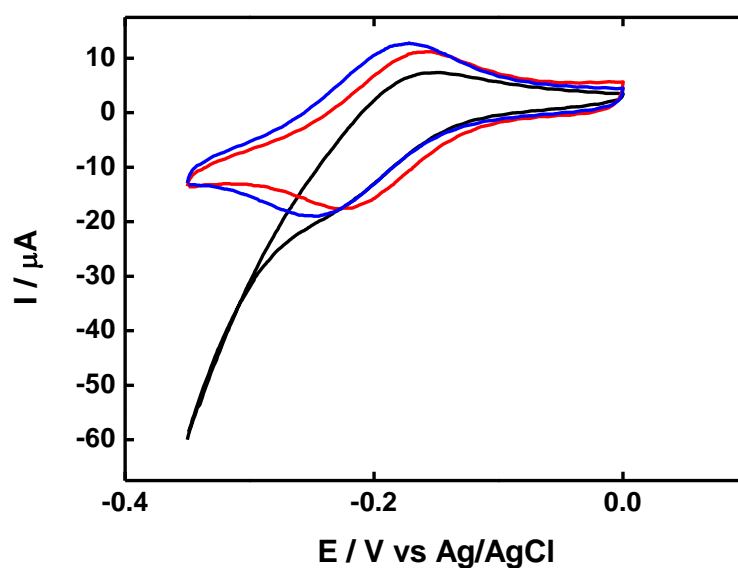


Figure 3.11 Cyclic voltammetry studies of modified electrodes, bare electrode (**black**), b- electrode after reaction with p-phenylene diamine diazonium salt (**red**), electrode with carboxymethylated dextran support (**blue**), **1 mM ruthenium hexamine (III) chloride**, 20 mM phosphate buffer, pH 7.4, scan rate 50 mV/s. The modification with diazonium salts results with disappearance of oxygen oxidation/reduction wave as well as in current increase.

In case of the ferri/ferro-cyanide redox process, a notable change in charging currents is observed upon both modifications of the electrode, as shown in Figure 3.10. If considering solution-phase pK_a values of immobilised species the CVs of redox probes cannot be influenced by protonation of amino- and carboxylic groups at neutral pH, as full protonation of benzylamine and CMD is very unlikely to happen. Known pK_a values of the modifiers are 4.6 (59) for aniline and 6.1 for CMD (60) Using **Henderson-Hasselbach** equation, (Eq. 3.1) it is possible to estimate degree of protonation of the amino- groups of the arylamine and carboxylic groups of the carboxymethylated dextran. At pH 7.4 aniline should be 0.2 % protonated and for CMD degree of protonation is 3 %.

$$pH = pK_a + \log \frac{[A^-]}{[HA]} \quad (3.1)$$

However, the above theory might not be valid for surface confined molecules. The research group of Compton reports a positive shift of pK_a by approximately 2 units for carboxyphenyl- groups coupled to graphite powder compared to benzoic acid in solution, for example. (61) Assuming a similar shift for pK_a values of amino-phenyl groups we could expect ~10 % of amino- groups to be protonated. Increased peak height for $K_3[Fe(CN)_6]$ scans could be rather attributed to accumulation of redox probe within the film, than electrostatic interactions. Zangmeister et al. examined the electrochemical behavior of chitosan modified surfaces towards potassium ferricyanide and ruthenium (III) hexamine chloride. $K_3[Fe(CN)_6]$ displays affinity towards the polysaccharide layer whilst no adsorption effect was observed for the ruthenium-based probe. (62) The CV scans for potassium ferricyanide also show increased peak-to-peak separation upon modification of the electrode surface. The experimental data published by Kariuki and McDermott illustrates that HOPG modified with 4-diazo-*N,N*-diethylaniline fluoroborate, (14) displays slightly diminished charging currents and increase in ΔE_p for potassium ferricyanide over the bare electrode. The slower kinetics of electron transfer, exemplified by the larger peak splitting, is explained by the lower number of graphite edge sites on modified electrode participating in the redox process.

The changes in CVs of ruthenium (III) hexamine chloride are rather insignificant: the response of this probe is expected not to be dependent on surface phenomena. (53) Voltammetric curves (Figure 3.11) indicate the presence of oxygen reduction wave at bare electrode, but not in case of the modified electrodes. A slight increase

in charging currents and no significant change in peak separation can be seen. Negative shift of the redox potential was clearly present after the CMD was coupled to the electrode indicating that there is a possibility of electrostatic attraction between the redox probe and the negatively charged carboxyl moieties.

Further modification of the surfaces with ssDNA and hybridisation to the complementary strand resulted in diminished peak currents for potassium ferricyanide, with broadening of the peaks. (**Figure 3.12**)

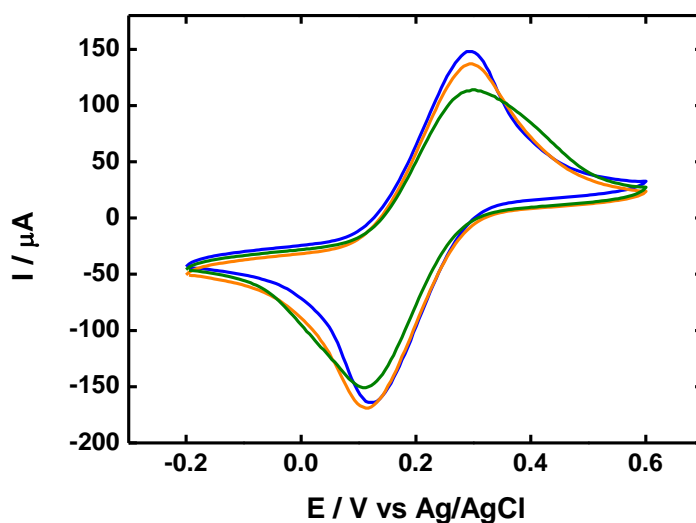


Figure 3.12 Cyclic voltammetry studies of modified electrodes; carboxymethylated Dextran support - blue, ssDNA - orange, dsDNA - green, 10 mM potassium ferricyanide, 20 mM phosphate buffer, pH 7.4, scan rate 50 mV/s

In order to explain the changes in the peak width, control experiment was undertaken. The sensor was reacted with the blank solution containing no DNA under similar conditions (0.3 M sodium citrate, 1 M NaCl, 0.05 % SDS, 0.2 % milk powder, shaking for 2 h at 37 °C) and the resulting voltammograms are presented in **Figure 3.13**. An effect similar to one observed for the surface with hybridised DNA, of decreased peak currents and increased peak width, is observed. The “background” properties of the electrode are obviously, in this case, influenced by components present in the hybridization solution and not by the presence of the dsDNA.

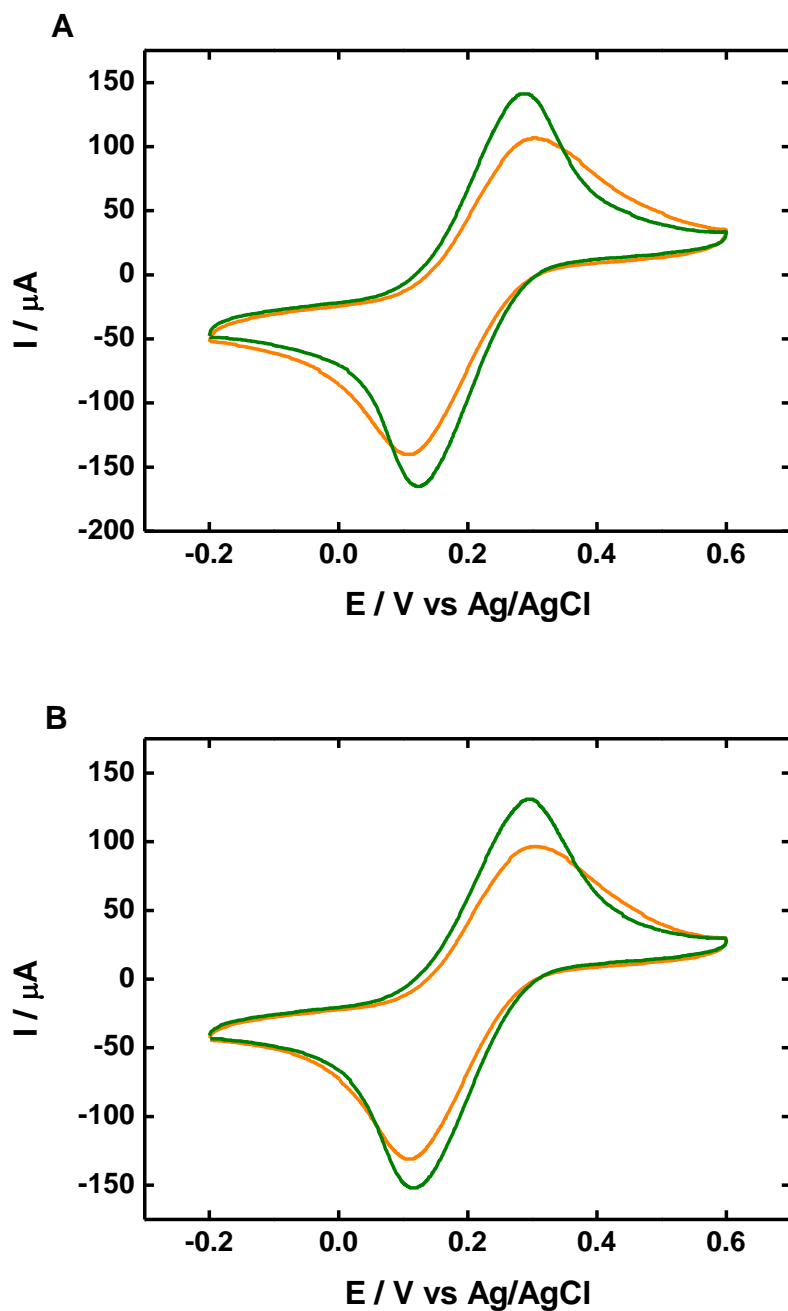


Figure 3.13 CVs comparing the films before (**green**) and after hybridisation (**orange**) A – after DNA hybridisation concentration 1.25×10^{-6} M, B- after conditioning of the electrode in hybridisation solution containing no DNA, **10 mM ferricyanide**, 20 mM phosphate buffer, pH 7.4, scan rate 50 mV/s

When a positive redox probe is used for this series of experiments, instead of ferricyanide, an increase in the charging currents upon probe coupling and hybridisation can be observed. Such an effect can be seen from the voltammograms of ruthenium (III) hexamine chloride at the DNA-modified surfaces presented in

Figure 3.14 the hybridisation procedure also results in the E° shifting towards more negative potentials.

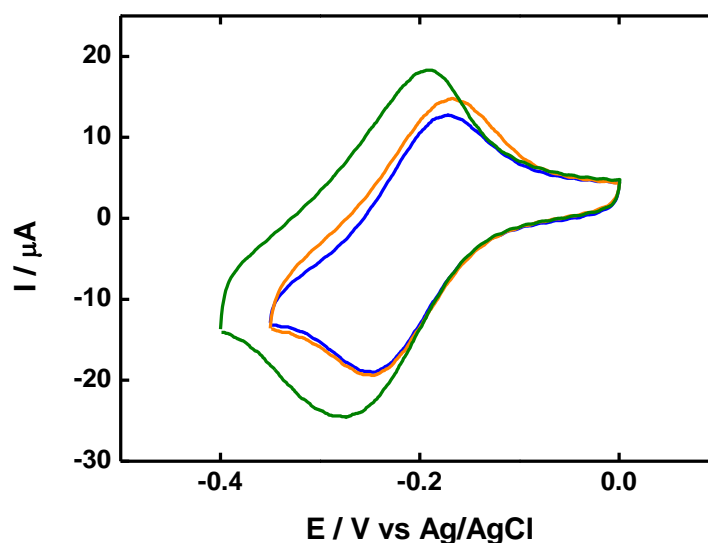


Figure 3.14 Cyclic voltammetry studies of carboxymethylated dextran support on functionalised electrodes - **blue**, ssDNA - **orange**, dsDNA - **green**, **1mM ruthenium hexamine (III) chloride**, 20 mM phosphate buffer, pH 7.4, scan rate 50 mV/s.

Such electrostatic effects on DNA modified electrodes were studied in the past. For example, signal hindering of the electrodes was observed for immobilised DNA in the presence of a negative redox probe and the opposite effect when a positively charged redox complex was used. (63, 64)

3.3.3. Optical characterization of DNA-modified surfaces

In this study, we have used a recognition surface consisting of ssDNA probe (coding for *ssrA* gene of *Listeria monocytogenes*) immobilised in a CMD film at an arylamine derivatised graphite electrode, depicted in **Figure 3.2**. The presence of ssDNA on carboxymethylated dextran surface has been confirmed by the use of Total Internal Reflectance Fluorescence (TIRF) spectrophotometry. In this case, hybridization of the target containing a fluorescent tag (BODIPY 530/550) with the modified graphite surface results in a 25 % increase in TIRF intensity (1 in **Table 3.4**), when compared to TIRF signals recorded with the control, unmodified, surfaces. (2-5 in **Table 3.4**)

Table 3.4 Average fluorescence intensities for different modified graphite samples. (5 areas of the sample considered, 3 images taken on each). Detailed description of samples is contained within experimental part

Sample	Average intensity
1	1327
2	1049
3	1068
4	1089
5	1033

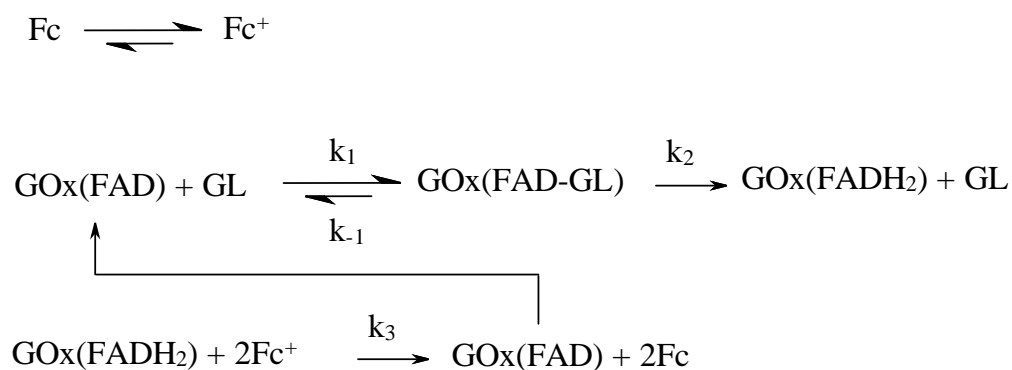
3.3.4. Amperometric detection of DNA hybridization with ssDNA grafted onto CM Dextran with ferrocenemethanol as diffusional mediator

In the present studies, it was elected to employ a solution phase electron transfer mediator (ferrocenemethanol) in favour of an immobilised mediator, in an attempt to reduce variability in signal between films on electrodes and to establish the principle of the scheme. Surface-confined glucose oxidase displays excellent catalytic activity in the presence of solution-phase ferrocenemethanol. (65)

Similar strategies based on the use of solution-phase mediator have been reported. For example, Won et al. (66) detected mutations of the breast cancer susceptibility gene using glucose oxidase amplification and ferrocenedicarboxylic acid as the mediator. Pividori et al. (67) performed amperometric dot-blot type DNA analysis using HRP and hydroquinone. HRP amplification with methylene blue as diffusional mediator has been used by Loaiza et al. (68) The use of an osmium based complex in solution for mediation of HRP has also been reported. (69)

Hybridisation between probe ssDNA and target biotinylated-ssDNA and addition of the avidinD-glucose oxidase conjugate results in bioelectrocatalysis in the presence of glucose, using ferrocenemethanol as electron mediator. For example, a slow-scan CV, recorded in the absence of glucose, and presence of ferronecenmethanol mediator, following the hybridisation assay protocol at the CMD films containing ssDNA probe, shows a reversible redox signal, characteristic of the

ferrocenemethanol response, with a formal potential of 0.23 V vs. Ag/AgCl (**Figure 3.15**). In the presence of 20 mM glucose a sigmoidal catalytic curve is observed, (70) due to the biocatalytic oxidation of glucose by glucose oxidase (GOx) with the ferrocenemethanol acting as a mediator. The mechanism of catalytic process, presented below, is similar to that presented in Chapter 2, except that the solution-phase ferrocenemethanol is the mediator instead of the surface-confined osmium complex.



Scheme 3.2 Mechanism of catalytic oxidation of glucose mediated by ferrocenemethanol. The scheme was adapted from reference (71)

Assuming the above mechanism the surface coverage of electroactive enzyme can be estimated from the kinetic equation (**Eq. 3.2**), as reported by Zhang et al. (71)

$$\frac{1}{I_{\text{cat.}}} = \frac{1}{2FS\Gamma_E^0} \left(\frac{1}{k_3[\text{Fc}]} + \frac{1}{k_2} + \frac{1}{k_{\text{red.}}[\text{GL}]} \right) \quad (3.2)$$

Where:

$I_{\text{cat.}}$ – catalytic current

F – Faraday constant

S – electrode area

Γ_E^0 – enzyme coverage

$[\text{Fc}]$ – concentration of ferrocenemethanol

$[\text{GL}]$ – concentration of glucose

k_2 - 700 s⁻¹

k_3 - 1.2 x 10⁷ M⁻¹s⁻¹

$k_{\text{red.}}$ - $k_1k_2/(k_{-1}+k_2) = 1.1 \times 10^4$ M⁻¹s⁻¹

The coverage of the enzyme was calculated from the currents obtained when using the target DNA concentration of 5×10^{-6} M. A value of 5.9×10^{-12} mol/cm² was obtained, which is equivalent to ~ 3.5 monomolecular layers of the active enzyme, given that a monolayer of enzyme corresponds to a coverage of 1.7×10^{-12} mol/cm². (72) When considering the high porosity of graphite and the three-dimensional nature of carboxymethylated dextran films, it is reasonable to assume that more than a single monolayer of enzyme can be coupled to DNA bound to CMD-derivatised electrodes. For example, the osmium complex described in the previous sections is a much smaller molecule (7 \AA , $\sim 1.5 \text{ nm}^2$ (73)) than the enzyme ($\sim 100 \text{ nm}^2$ (72)) and the coverage obtained for coupling that onto the CMD-derivatised electrode is 11 times greater than that observed for binding of the enzyme.

For comparison, Zhang et al. report coverage of 7.8×10^{-12} mol/cm² for a single layer of glucose oxidase immobilised onto PDDA/gold nanoparticle/PDDA via electrostatic interactions. (71)

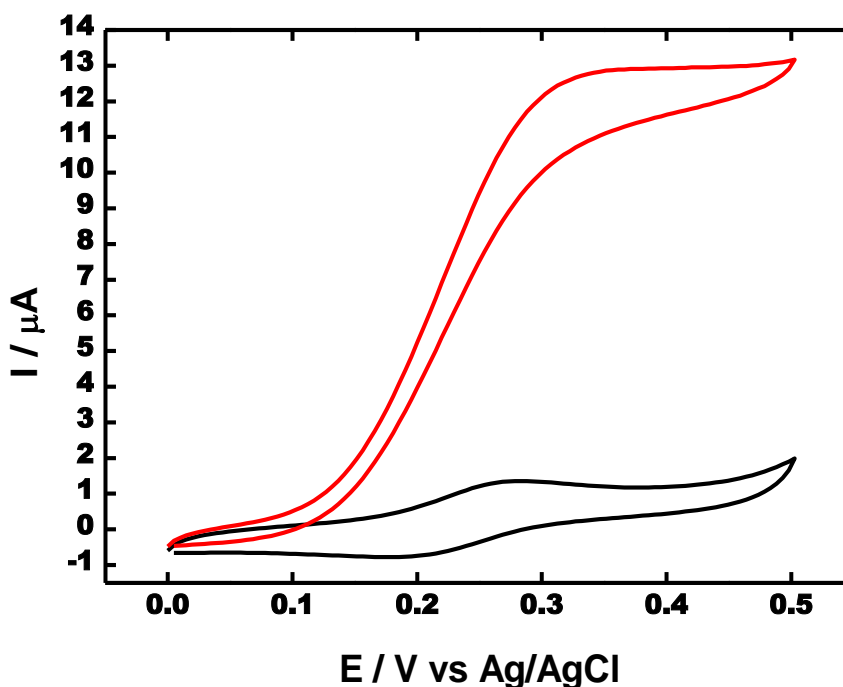


Figure 3.15 Slow scan, 5 mV/s, CVs recorded in 20 mM phosphate buffer, pH 7.4, containing 0.2 mM ferrocenemethanol and 20 mM glucose, for hybridisation assays performed at probe DNA bound within a CMD film that is anchored to the arylamine-derivatised graphite electrode. Signals obtained for interaction with 5×10^{-6} M biotin-labelled complementary DNA in presence (solid, red) and absence (black) of glucose.

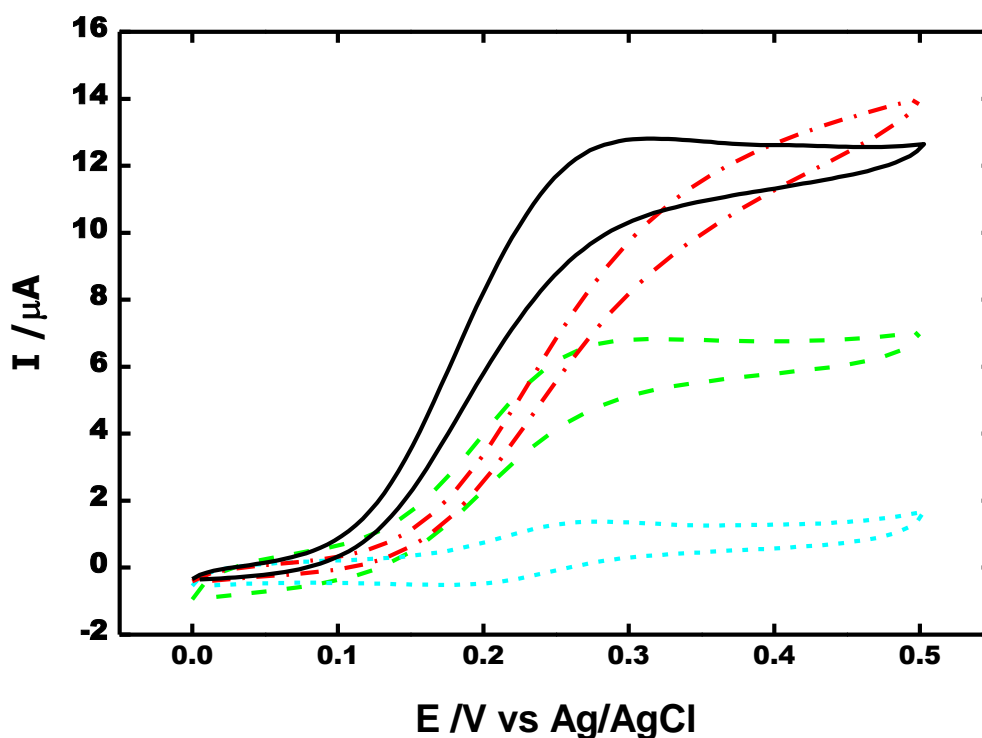


Figure 3.16 Slow scan, 5 mV/s, CVs recorded in 20mM phosphate buffer, pH 7.4, containing 0.2 mM ferrocenemethanol and 20 mM glucose, for hybridisation assays performed at probe DNA bound within a CMD film that is anchored to the arylamine-derivatised graphite electrode. Signals obtained for interaction with 5×10^{-6} M biotin-labelled complementary DNA in presence (solid, black) and absence (dash-dot, red) of SDS and milk powder; and complementary DNA without biotin-label in presence (short dash, cyan) and absence (long dash, green) of SDS and milk powder

The use of a covalently anchored support (CMD) containing bound ssDNA allows introduction of more rigorous washing conditions in contrast to systems based on thiolated gold electrodes, (1, 5) due to increased stability of films. We have thus been able to investigate the use of blocking agents, which are widely used in DNA assays, (29) in an effort to reduce the extent of non-specific binding at electrode surfaces. In this case sodium dodecyl sulfate (SDS) and milk powder were added to the hybridisation solution in order to reduce non-specific binding of DNA strands and the glucose oxidase-avidinD conjugate. When SDS and milk powder are not present, the signal, following performance of the hybridisation assay protocol using target DNA that is complementary to the immobilised probe DNA, but that does not have the biotin tag necessary to allow subsequent binding of glucose oxidase-

avidinD conjugate to elicit the biocatalytic oxidation of glucose, is nonetheless 57% that obtained using the biotin-labelled complementary DNA target, indicative of a strong non-specific binding of the enzyme conjugate to the CMD film. (**Figure 3.16**) The presence of the SDS and milk powder in the assay protocol reduces this signal due to non-specific binding of enzyme conjugate to 2% of that obtained with the biotin-labelled complementary DNA target, **Figure 3.16**. Using this assay format, the signal corresponding to a control assay using biotin-labelled, though non-complementary DNA, target is used, represents only 8 % of that obtained using biotin-labelled complementary DNA target (**Figure 3.17**).

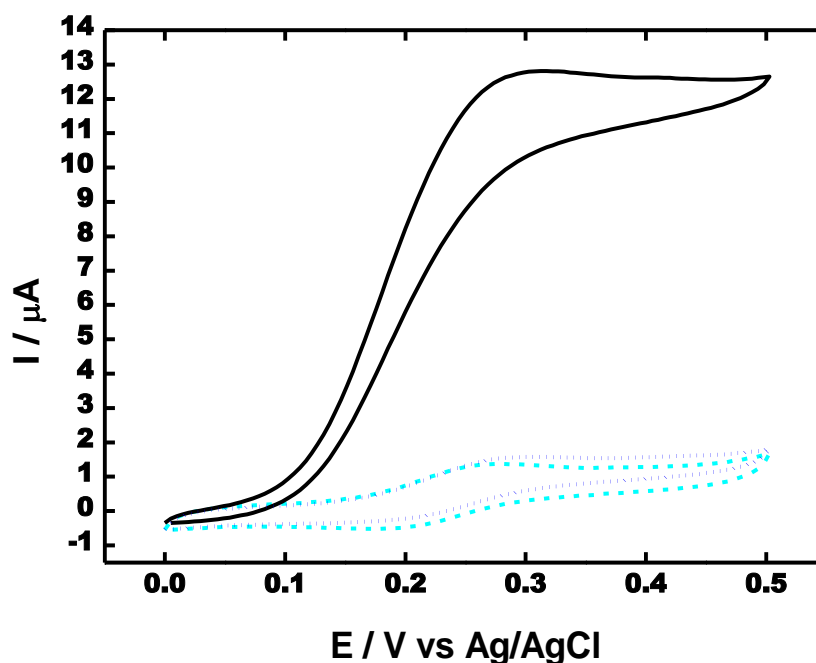


Figure 3.17 Slow scan, 5 mV/s, CVs recorded in 20mM phosphate buffer, pH 7.4, containing 0.2 mM ferrocenemethanol and 20 mM glucose, for hybridisation assays using SDS and milk powder performed at probe DNA bound within a CMD film that is anchored to the arylamine-derivatised graphite electrode. Signals obtained for interaction with 5×10^{-6} M biotin-labelled complementary DNA (solid, black) complementary DNA without biotin-label (short dash, cyan) and biotin-labelled non-complementary DNA (dot, blue).

As was the case previously (chapter 2), (1, 5, 74-78) chronoamperometric responses, obtained by applying potentials that are positive of the redox potential of the mediator, at the electrodes following performance of the hybridisation protocols result in steady-state signals for glucose oxidation (**Figure 3.18**).

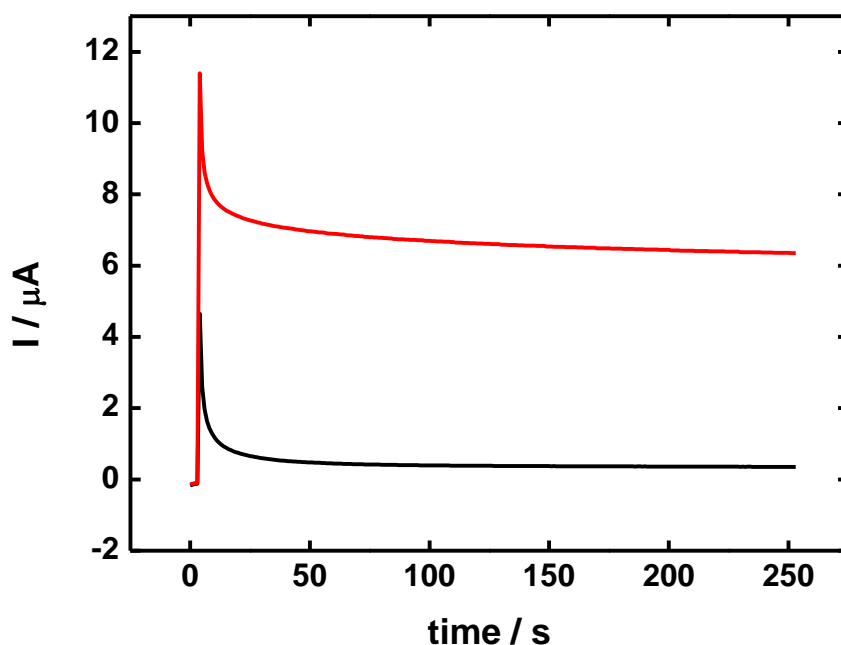


Figure 3.18 Chronoamperogram, 0.35 V applied for 250 s, recorded in 20 mM phosphate buffer, pH 7.4, containing 0.2 mM ferrocenemethanol for hybridisation assays using 5×10^{-6} M biotin-labelled complementary target DNA at probe DNA bound within a CMD film that is anchored to the arylamine-derivatised graphite electrode in the presence (black) and absence (red) of 20 mM glucose.

Both the amperometric (Figure 3.19A) and CV (Figure 3.19B) signals scale in proportion to the target DNA concentration over a concentration range of 2.5×10^{-6} M to 3×10^{-7} M

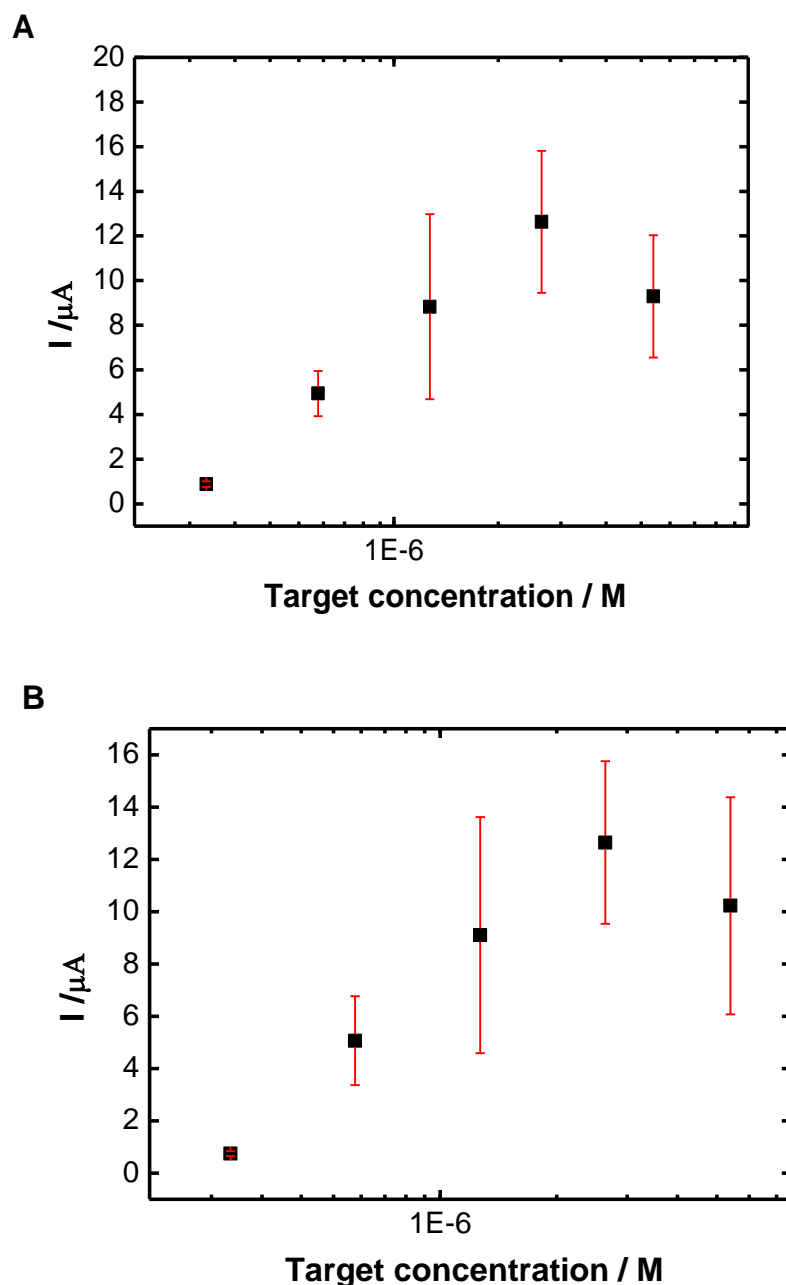


Fig 3.19 Calibration plots of current versus target DNA concentration from the chronoamperometry, 0.35 V (A) and CV (B) results, $n = 5$

The dose-response curve regression is typical for quantitative analysis of ssDNA. (74-78) A **detection limit**, estimated using IUPAC method, was evaluated as 3×10^{-7} M, which is equivalent to 0.15 nanomoles of target DNA in the 500 μL sample volume at the 3 mm-diameter graphite electrode. Relative standard deviation for a single concentration measurement (using 1.25×10^{-6} M of DNA target) is 13 %, $n = 5$, in a batch of electrodes prepared in one experiment, but 46 %, $n = 5$, when

electrode preparation and calibration studies are carried out on different days with new solutions being prepared before each experiment and new stock DNA solution being used. This highlights the requirement for a rigorous approach to production of the films on electrodes, to decrease the RSD below 13%, and of stringent controls on the storage and usage of reagents.

An alternate approach to improvement in the precision of the assays would be to use the same hybridization surface for each assay concentration. Thus sensor recovery was tested by immersion, following completion of the assay, of the electrodes in 0.25 M sodium hydroxide. Subsequent performance of the hybridization protocol at the regenerated electrodes resulted in signals that represented only 60 % of that of the initial signal, probably due to dissolution of the CMD layer under these harsh conditions. The comparison of signals from subsequent hybridizations is shown in **Figure 3.20**.

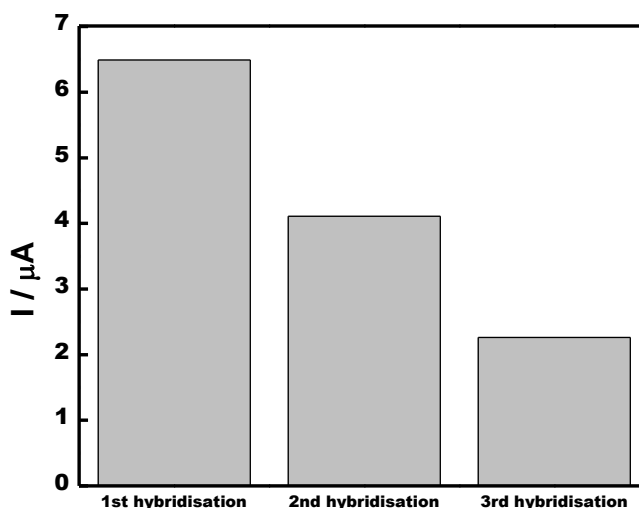


Figure 3.20 A chronoamperometric signal recorded for concentration of $1.85 \times 10^{-5} \text{M}$, initial signal and after recovery. The electrode was immersed in 0.25M NaOH, 3M NaCl for 1h and in phosphate buffer, pH 7.4 for 30 min.

The analytical parameters, though not as impressive as those reported for other amplified systems, (79-82) nonetheless demonstrate the feasibility of the proposed approach.

An effort has been made in order to try establishing a relationship between the electrode area, concentration of mediator and the output signal. The study has

however shown that the irreproducibility of the data is not related to any one of these factors alone, as evident from the comparison of R^2 values for the linear fit of current versus logarithm of concentration presented in **Table 3.5**.

Table 3.5 R^2 values for linear section of I vs log c plot for the original and treated data

Normalisation procedure	R^2 – Cyclic voltammetry	R^2 -Chronoamperometry
Untreated data	0.9970	0.9997
Data divided by ferrocenemethanol peak current	0.9847	0.9834
Data divided by $D^{1/2}c$ from ferrocenemethanol probe study	0.9452	0.9242
Data divided by electrode area (from capacitance)	0.9607	0.9656
Data divided by diazonium salt reduction peak area	0.7132	0.6661

3.3.5. Amperometric detection of DNA hybridization with ssDNA grafted onto CM Dextran with osmium redox complex co-immobilised at the electrode surface

Similar methodology has been applied for development of the sensor containing immobilised mediator - osmium(2,2'-bipyridine) 4-aminomethylpyridine and ssDNA in an effort to provide a simpler test protocol. In addition, because the oxidised form of ferrocene has been shown to be unstable in aqueous media, (83) the osmium-based mediator was considered a more suitable choice, as its stability in Os(III) oxidation state is relatively greater. (84) In the present approach the osmium complex was attached to the CMD anchored to the electrode first via EDC/NHS coupling, followed by re-activation of the carboxylic groups of the CMD with EDC/NHS and subsequent attachment of NH_2 -DNA. Then, the same hybridisation protocol was applied as for the surfaces without the osmium complex described in

previous section. Characterisation of the modified surfaces, CMD layer with immobilised osmium complex and CMD layer containing osmium complex and ssDNA, were studied using cyclic voltammetry and a comparison of CV parameters of films is presented in **Table 3.6**.

Table 3.6 Film parameters obtained from cyclic voltammetry studies of [Os(bpy)₂(4-aminoethylpyridine)Cl] bound within a CMD film that is anchored to the arylamine-derivatised graphite electrode before and after modification with ssDNA

Parameters	Osmium complex only (n=4)	Osmium complex + ssDNA (n=4)
E^0 (V)	0.303 ± 0.014	0.259 ± 0.009
ΔE_p at 0.005 V/s (V)	0.09 ± 0.018	0.073 ± 0.014
FWHM at 0.005 V/s	0.169 ± 0.028	0.168 ± 0.007
$D^{1/2}C$ (cm ⁻² s ^{-1/2} mol)	$2.4 \times 10^{-9} \pm 1.7 \times 10^{-9}$	$1.49 \times 10^{-9} \pm 4.6 \times 10^{-10}$
Γ_{Os} (mol/cm ²) at 0.005 V/s, $\Gamma = Q/nFA$	$1 \times 10^{-8} \pm 8.8 \times 10^{-9}$	$2.54 \times 10^{-9} \pm 8.7 \times 10^{-10}$

A significant drop in redox potential (44 mV) is observed when ssDNA is present at the electrode surface. Del Pozo et al. has studied voltammetry of [Os(bpy)₃]²⁺ on gold electrodes with pre-adsorbed DNA and has shown that from CV of the complex, both in solution and adsorbed on DNA-modified surface, a negative potential shift by approximately 120 mV. (85) The change in the E^0 was related to electrostatic interactions between the complex and the DNA. As for the data presented in Chapter 2, $D^{1/2}c$ and surface coverage of osmium sites decreased marginally when DNA is present within the film. The decrease, however, is not significant, as it lies within the standard deviation of the measurement.

A study was undertaken to demonstrate the ability of the immobilised [Os(bpy)₂(4-aminoethylpyridine)Cl]PF₆ to mediate oxidation of glucose by GOx. In this experiment glucose oxidase and the redox mediator were coupled in one step with the resulting CV shown in **Figure 3.21**. The appearance of a sigmoidal catalytic wave in the presence of glucose substrate indicates that the immobilised complex is capable of accepting electrons from co-immobilised GOx, and mediating electron transfer to the electrode surface.

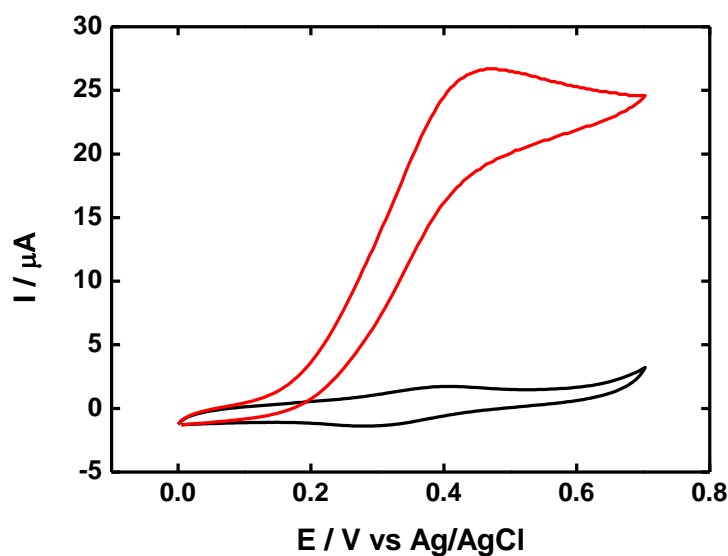


Figure 3.21 GOx and osmium complex bound within carboxymethylated Dextran layer voltammograms recorded in the phosphate buffer, no glucose (**black**) and in the presence of 20 mM glucose (**red**)

For preparation of films that could be used in the DNA hybridisation assay, both the mediator and the ssDNA were attached in separate reaction steps. This layer displays catalytic activity in the presence of complementary DNA only (**Figure 3.22** and **3.23**) and no significant response is generated when the electrode was reacted with biotin non-complementary DNA (**Figure 3.24**) and unmodified complementary DNA (**Figure 3.25**). Efforts have been made to attach DNA and the complex in one step, but these sensors did not yield sufficient signals upon hybridisation and enzyme coupling.

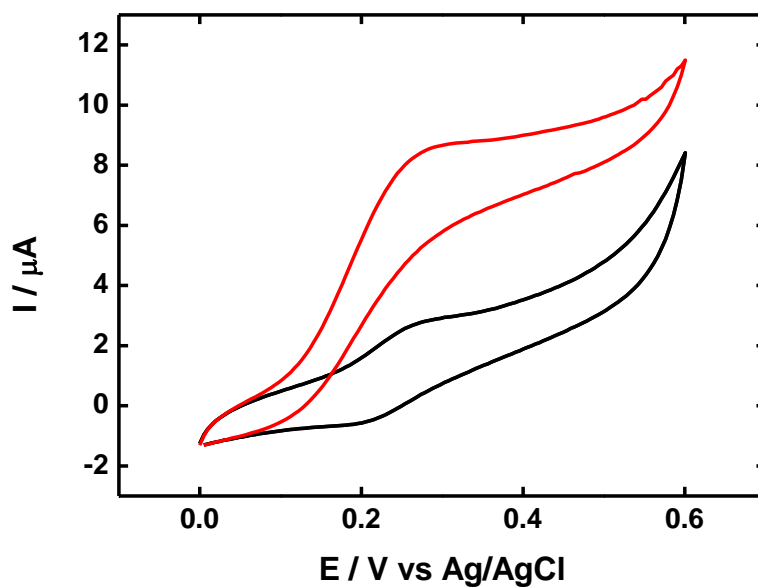


Figure 3.22 Cyclic voltammetry, **biotin-complementary DNA**, $5 \times 10^{-6} \text{ M}$, $[\text{Os}(\text{bpy})_2(4\text{-aminomethylpyridine})\text{Cl}]\text{PF}_6$ and DNA attached to CMD, no glucose (**black**), with 20 mM glucose (**red**)

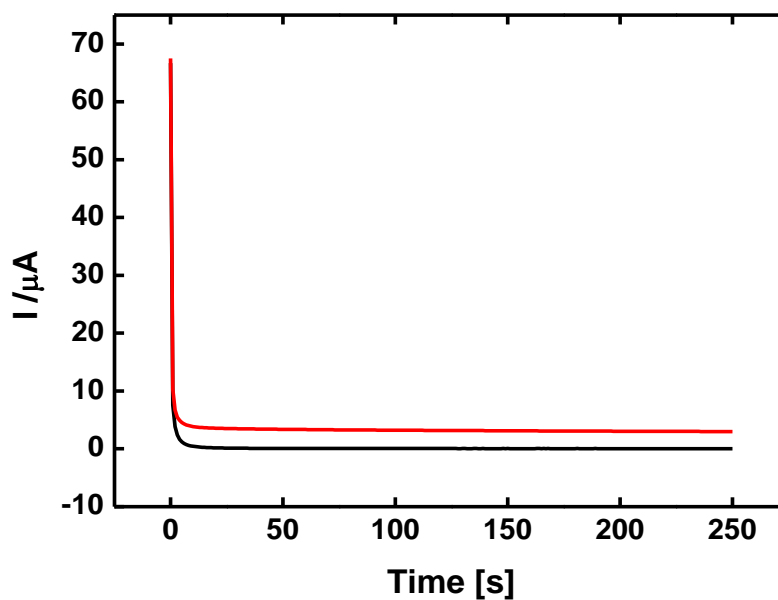


Figure 3.23 Chronoamperometry, **biotin-complementary DNA**, $5 \times 10^{-6} \text{ M}$, osmium complex and DNA attached to CMD, no glucose (**black**), 20 mM glucose (**red**). Potential was held at 0.4 V.

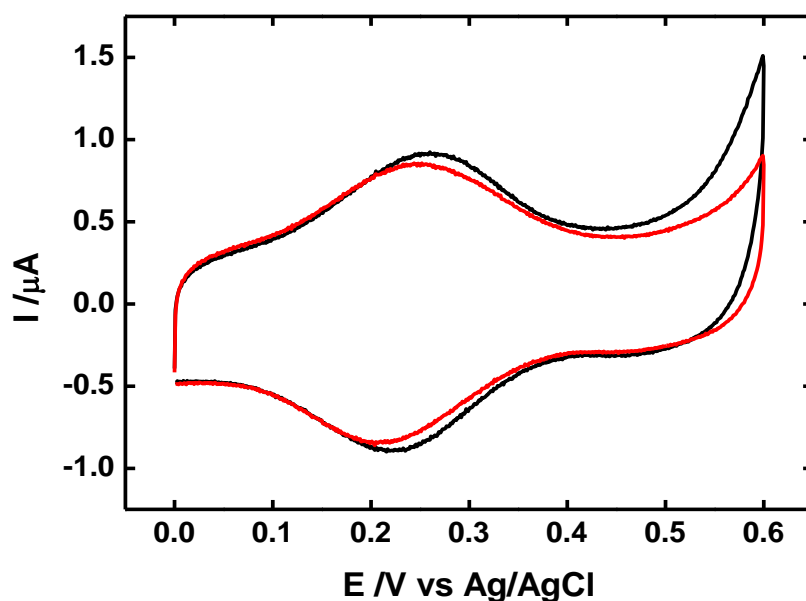


Figure 3.24 Cyclic voltammetry, **biotin non-complementary DNA**, $5 \times 10^{-6} \text{M}$, osmium complex $[\text{Os}(\text{bpy})_2(4\text{-aminomethylpyridine})\text{Cl}]\text{PF}_6$ and DNA attached to CMD, no glucose (**black**), with 20 mM glucose (**red**)

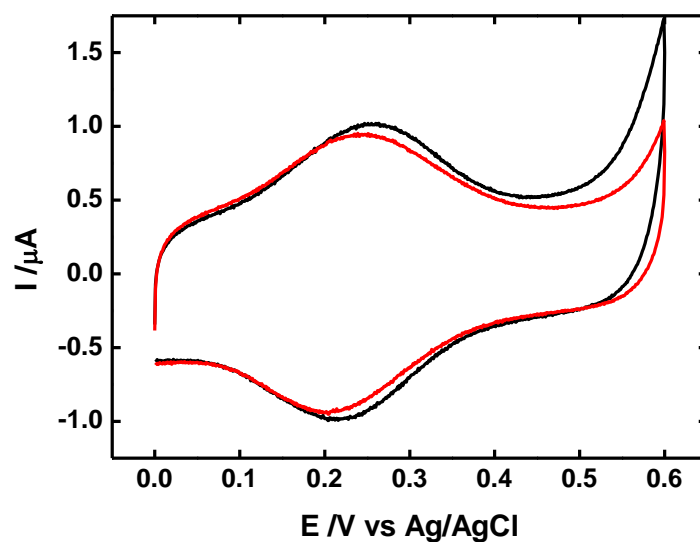


Figure. 3.25 Cyclic voltammetry, unmodified DNA, $5 \times 10^{-6} \text{M}$, osmium complex $[\text{Os}(\text{bpy})_2(4\text{-aminomethylpyridine})\text{Cl}]\text{PF}_6$ and DNA attached to CMD, no glucose (**black**), with 20 mM glucose (**red**)

The catalytic current values obtained using DNA hybridization sensors formed by consecutive immobilization of redox complex and ssDNA were plotted versus logarithm of the target DNA concentration. (**Figure 3.26**) The currents scale with the

logarithm of the DNA concentration, but significant outlier points are present. It is postulated that introduction of further complexity in the sensor preparation protocols by moving to a surface bound mediator has an impact on the variation in quantities of immobilised ssDNA.

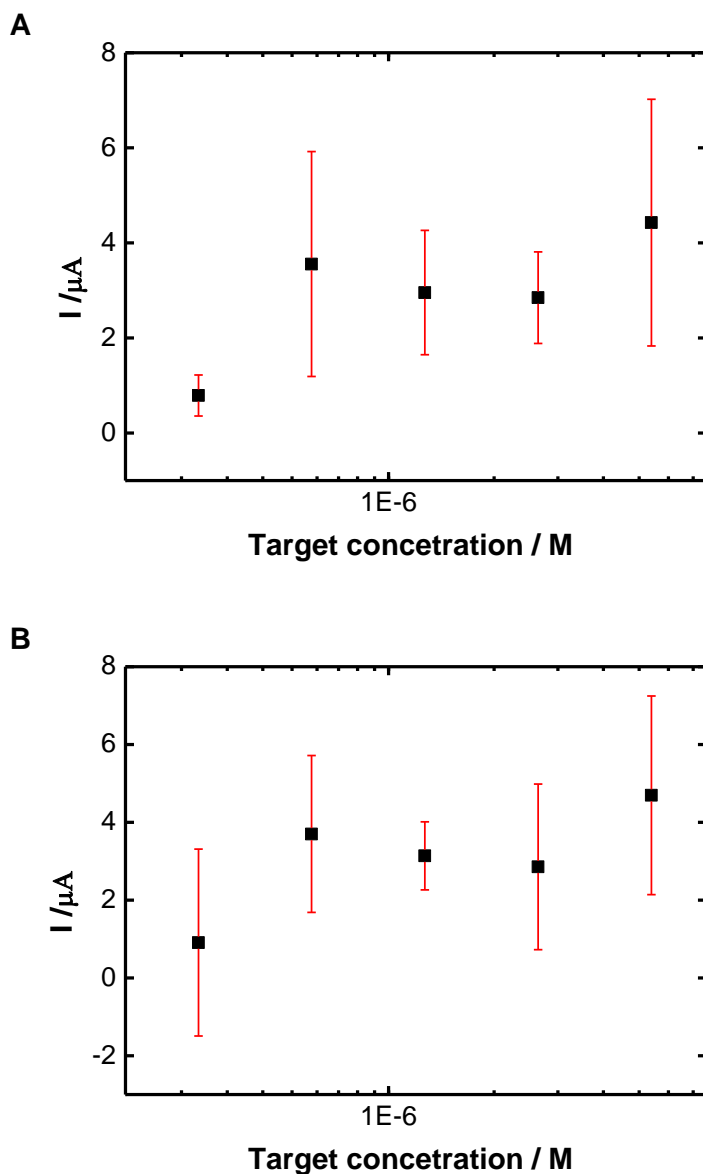


Fig 3.28 Calibration plots of current versus target DNA concentration from the chronoamperometry (A) and cyclic voltammetry (B), 0.4 V, $n = 4$

Introducing a surface bound mediator not only means less control over the amount of the probe ssDNA immobilised, and subsequently number of strands which are available for hybridisation, but also the difficulty in providing the same concentration of redox complex for the mediation of electrocatalytic reaction.

Attempts at normalization of catalytic signals show, however, that the signals are not solely dependent on the surface concentration of osmium sites. No significant improvement in the trend was gained by normalising the catalytic current values versus osmium peak current values or the charge extracted from the slow scan rate CV for the osmium redox couple. In contrast, when dividing the data by $D^{1/2}c$ the R square value improved slightly for CV and chronoamperometry data. (Table 3.7) This might suggest that the sensor signal is affected by this parameter through effects on either diffusion coefficient or the concentration of redox sites, influenced by film thickness/swelling, (86) and interactions with the solvent (87) and ions. (88)

Table 3.7 - osmium complex $[\text{Os}(\text{bpy})_2(4\text{-aminomethylpyridine})\text{Cl}]\text{PF}_6$ and DNA attached to CMD, original and normalised data for series of 4 experiments

Normalisation procedure	R ² - Cyclic voltammetry	R ² - Amperometry
None	0.6930	0.7013
Dividing by osmium peak current	0.6725	0.6645
Dividing by osmium peak charge	0.6246	0.6173
Dividing current by $D^{1/2}c$	0.7982	0.7837

3.4. Conclusions

A range of surface modification methods was investigated in this chapter. A general procedure involved introducing amino- functionality on gold or carbon electrode, and subsequent electrode modification with layer of polymer and then osmium redox complex. Smoother electrodes, such as gold and glassy carbon, did not provide sufficient surface coverage of the redox probe in cyclic voltammetry experiments to warrant investigation as surfaces for DNA hybridisation sensors using this approach.

We then demonstrated that CMD films coupled to graphite surfaces possessing grafted arylamine can be applied to develop a platform DNA assay based on amplified amperometric bioelectrocatalysis. The fact that the platform is based on covalent bonding of the layers allows leeway in performing experiments at higher temperatures, opening up the possibility for use of temperature gradient - based detection of single point mutations. (89) In contrast to the system developed in Chapter 2, all immobilisation and detection steps are carried out in solution phase

with a view to apply the detection platform to a microfluidic flow system, permitting variation in the hybridisation conditions (temperature, ionic strength etc). Initial study on the development of the sensor with DNA and redox mediator co-immobilised onto carboxymethylated dextran surface has been successful, although better reproducibility has been gained when using a solution-phase mediator.

Although the assay detection limit is high, the assay protocol lends itself well to an automated high-throughput microfluidic approach. Using smoother electrode materials may improve reproducibility of the assay, but with a trade-off of decreased signal intensities. Use of mass-produced screen-printed carbon electrodes should be considered, because they are inexpensive, they have low background currents, wide potential window and high reproducibility of currents. (90) Preparing sensors on the base of low cost disposable electrodes could potentially give also an opportunity to perform analysis of multiple samples.

3.5. References

1. J. Hajdukiewicz, S. Boland, P. Kavanagh, A.M. Nowicka, Z. Stojek, D. Leech, *Electroanalysis* **21**, 342 (2009).
2. T. Ohara, R. Rajagopalan, A. Heller, *Anal. Chem.* **65**, 3512 (1993).
3. B. Wang, I. Jansson, J. Schenkman, J. Rusling, *Anal. Chem.* **77**, 1361 (2005).
4. J. J. Gooding, *Electroanalysis* **20**, 573 (2008).
5. P. Kavanagh, D. Leech, *Anal. Chem.* **78**, 2710 (2006).
6. S. Lofas, B. Johnsson, *J. Chem. Soc., Chem. Commun.*, 1526 (1990).
7. B. Johnsson, S. Löfås, G. Lindquist, *Anal. Biochem.* **198**, 268 (1991).
8. S. Lofas, *Pure & Appl. Chem.* **67**, 829 (1995).
9. S. Wood, *Microchem. J.* **20**, 330 (1993).
10. D. Pallarola, L. Domenianni, G. Priano, F. Battaglini, *Electroanalysis* **19**, 690 (2007).
11. G. Priano, D. Pallarola, F. Battaglini, *Anal. Biochem.* **362**, 108 (2007).
12. F. T. Salam, I.E. Tothill, *Biosens. Bioelectron.* **24**, 2630 (2009).
13. M. Delamar, R. Hitmi, J. Pinson, J. M. Saveant, *J. Am. Chem. Soc.* **114**, 5883 (1992).
14. J. K. Kariuki, M. T. McDermott, *Langmuir* **15**, 6534 (1999).
15. M. Dequaire, C. Degrand, B. Limoges, *J. Am. Chem. Soc.* **121**, 6946 (1999).
16. J. Wang, M. A. Firestone, O. Auciello, J. A. Carlisle, *Langmuir* **20**, 11450 (2004).
17. A. Benedetto, M. Balog, P. Viel, F. Le Derf, M. Sallé, S. Palacin, *Electrochim. Acta* **53**, 7117 (2008).
18. M. D'Amour, D. Bélanger, *Phys. Chem. B* **107**, 4811 (2003).
19. S. Boland, F. Barrière, D. Leech, *Langmuir* **24**, 6351 (2008).
20. S. Boland, P. Jenkins, P. Kavanagh, D. Leech, *J. Electroanal. Chem.* **626**, 111 (2009).
21. S. Boland, F. K., D. Leech, *Electrochim. Acta* **54**, 1986 (2009).
22. G. Poirier, *Chem. Rev.* **97**, 1117 (1997).
23. G. Savage, *Carbon-Carbon Composites*. (Springer- Verlag, Heidelberg, ed. 1st, 1993).
24. H. Teh, H. Gong, X. Dong, X. Zeng, A. Lai Kuan Tan, X. Yang, S. Ngim Tan, *Anal. Chim. Acta* **551**, 23 (2005).
25. C. Lee, S. Baker, M. Marcus, W. Yang, M. Eriksson, R. Hamers, *Nano letters* **4**, 1713 (2004).
26. G. Liu, Q. Nguyen, E. Chow, T. Böcking, D. Hibbert, J.J. Gooding *Electroanalysis* **18**, 1141 (2006).
27. R. Polsky, J. Harper, D. Wheeler, D. Arango, S. Brozik, *Angew. Chem. Int. Ed.* **47**, 2631 (2008).
28. R. Polsky, J. Harper, D. Wheeler, S. Brozik, *Electroanalysis* **20**, 671 (2008).
29. S. Primrose, R. Twyman, R. Old, *Principles of Gene Manipulation and Genomics*. (Wiley-Blackwell, Oxford, ed. 6th, 2001).
30. M. Delamar, G. Désarmot, O. Fagebaume, R. Hitmi, J. Pinson, J. Saveant *Carbon* **35**, 801 (1997).
31. P. A. Brooksby, A. J. Downard, *Langmuir* **20**, 5038 (2004).
32. R. J. Forster, L. R. Faulkner, *J. Am. Chem. Soc.* **116**, 5444 (1994).
33. R. W. Murray, in *Electroanalytical Chemistry*, A. J. Bard, Ed. (Marcel Dekker Inc., New York, 1984), vol. 13.
34. A. P. Brown, F. C. Anson, *Anal. Chem.* **49**, 1589 (1977).

35. R. Voicu, R. Boukherroub, V. Bartzoka, T. Ward, J.T.C Wojtyk, D.D.M. Wayner, *Langmuir* **20**, 11713 (2004).
36. H. D. Abruna, T. J. Meyer, R. W. Murray, *Inorg. Chem.* **18**, 3233 (1979).
37. V. L. Snoeyink, W. J. Weber, *Environmental Science & Technology* **1**, 228 (1967).
38. B. D. Epstein, E. Dalle-Molle, J. S. Mattson, *Carbon* **9**, 609 (1971).
39. W. J. Blaedel, R. A. Jenkins, *Anal. Chem.* **46**, 1952 (1974).
40. J. F. Evans, T. Kuwana, *Anal. Chem.* **49**, 1632 (1977).
41. R. C. Engstrom, *Anal. Chem.* **54**, 2310 (1982).
42. R. C. Engstrom, V. A. Strasser, *Anal. Chem.* **56**, 136 (1984).
43. M. Noel, P. N. Anantharaman, *Analyst* **110**, 1095 (1985).
44. Y. Oren, A. Soffer, *J. Electroanal. Chem.* **186**, 63 (1985).
45. T. Nagaoka, T. Sakai, K. Ogura, T. Yoshino, *Anal. Chem.* **58**, 1953 (1986).
46. D. Golub, Y. Oren, A. Soffer, *J. Electroanal. Chem.* **227**, 41 (1987).
47. T. Nagaoka, T. Fukunaga, T. Yoshino, I. Watanabe, T. Nakayama, S. Okazaki, *Anal. Chem.* **60**, 2766 (1988).
48. D. Golub, A. Soffer, Y. Oren, *J. Electroanal. Chem.* **260**, 383 (1989).
49. R. L. McCreery in *Electroanalytical chemistry*, Bard, A.J., Ed. (Marcel Dekker Inc., New York, 1991), vol. 17.
50. L. J. Bjelica, L. S. Jovanovic, *Electrochim. Acta* **37**, 371 (1992).
51. K. R. Kneten, R. L. McCreery, *Anal. Chem.* **64**, 2518 (1992).
52. C. A. Leon y Leon, J. M. Solar, V. Calemma, L. R. Radovic, *Carbon* **30**, 797 (1992).
53. P. Chen, R. L. McCreery, *Anal. Chem.* **68**, 3958 (1996).
54. S. S. Barton, M. J. B. Evans, E. Halliop, J. A. F. MacDonald, *Carbon* **35**, 1361 (1997).
55. Q. Chi, W. Göpel, T. Ruzgas, L. Gorton, P. Heiduschka, *Electroanalysis* **9**, 357 (1997).
56. T.-C. Kuo, R. L. McCreery, *Anal. Chem.* **71**, 1553 (1999).
57. M. A. Montes-Morán, D. Suárez, J. A. Menéndez, E. Fuente, *Carbon* **42**, 1219 (2004).
58. G. Pognon, T. Brousse, D. Bélanger, *Carbon* **49**, 1340 (2011).
59. H. C. Brown, D.H. McDaniel, O. Hafliger in *Determination of Organic Structures by Physical Methods*, E. A. Braude, F. C. Nachod, Eds. (Academic Press, New York, 1955).
60. R. Zhang, M. Tang, A. Bowyer, R. Eissenthal, J. Hubble, *Biomaterials* **26**, 4677 (2005).
61. P. Abiman, A. Crossley, G. G. Wildgoose, J. H. Jones, R. G. Compton, *Langmuir* **23**, 7847 (2007).
62. R. A. Zangmeister, J. J. Park, G. W. Rubloff, M. J. Tarlov, *Electrochim. Acta* **51**, 5324 (2006).
63. K. Hashimoto, K. Ito, Y. Ishimori, *Anal. Chem.* **66**, 3830 (1994).
64. A. B. Steel, T. M. Herne, M. J. Tarlov, *Anal. Chem.* **70**, 4670 (1998).
65. C. Bourdillon, C. Demaille, J. Moiroux, J. Savéant, *J. Am. Chem. Soc.* **117**, 11499 (1995).
66. B. Won, H. Yoon, H. Park, *Analyst* **133**, 100 (2008).
67. M. Pividori, A. Merkoçi, S. Alegret, *Biosens. Bioelectron.* **16**, 1133 (2001).
68. O. Loaiza, S. Campuzano, A. Guzmán-Vázquez de Prada, M. Pedrero, J. Pingarrón, *Sens. Actuators, B* **132**, 250 (2008).

69. N. Djellouli, M. Rochelet-Dequaire, B. Limoges, M. Druet, P. Brossier, *Biosens. Bioelectron.* **22**, 2906 (2007).
70. N. Anicet, C. Bourdillon, J. Moiroux, J.-M. Saveant, *J. Phys. Chem. B* **102**, 9844 (1998).
71. S. Zhang, W. Yang, Y. Niu, Y. Li, M. Zhang, C. Sun, *Anal. Bioanal. Chem.* **384**, 736 (2006).
72. C. Bourdillon, C. Demaille, J. Gueris, J. Moiroux, J. M. Saveant, *J. Am. Chem. Soc.* **115**, 12264 (1993).
73. K. Takada, H. D. Abruña, *J. Phys. Chem.* **100**, 17909 (1996).
74. F. Pröll, B. Möhrle, M. Kumpf, G. Gauglitz, *Anal. Bioanal. Chem.* **382**, 1889 (2005).
75. M. U. Ahmed, K. Idegami, M. Chikae, K. Kerman, P. Chaumpluk, S. Yamamura, E. Tamiya, *Analyst* **132**, 431 (2007).
76. L. De Stefano, P. Arcari, A. Lamberti, C. Sanges, L. Rotiroti, I. Rea, I. Rendina, *Sensors* **7**, 214 (2007).
77. M. Koets, T. van der Wijk, J. van Eemeren, A. van Amerongen, M. Prins, *Biosens. Bioelectron.* **24**, 1893 (2009).
78. W. Liao, J. Ho, *Anal. Chem.* **81**, 2470 (2009).
79. M. Dequaire, A. Heller, *Anal. Chem.* **74**, 4370 (2002).
80. Y. Zhang, H. Kim, A. Heller, *Anal. Chem.* **75**, 3267 (2003).
81. Y. Zhang, A. Pothukuchy, W. Shin, Y. Kim, A. Heller, *Anal. Chem.* **76**, 4093 (2004).
82. F. Berti, S. Laschi, I. Palchetti, J. Rossier, F. Reymond, M. Mascini, G. Marrazza, *Talanta* **77**, 971 (2009).
83. J. R. Lenhard, R. W. Murray, *J. Am. Chem. Soc.* **100**, 7870 (1978).
84. E. M. Kober, J. V. Caspar, B. P. Sullivan, T. J. Meyer, *Inorg. Chem.* **27**, 4587 (1988).
85. M. V. Del Pozo, C. Alonso, F. Pariente, E. Lorenzo, *Biosens. Bioelectron.* **20**, 1549 (2005).
86. R. J. Forster, J. G. Vos, *Electrochim. Acta* **37**, 159 (1992).
87. G. Inzelt, *Electrochim. Acta* **34**, 83 (1989).
88. G. Inzelt, L. Szabo, *Electrochim. Acta* **31**, 1381 (1986).
89. R. G. H. Cotton, *Mutat. Res. Fundam. Mol. Mech. Mutagen.* **285**, 125 (1993).
90. V. Rao, M. Sharma, P. Pandey, K. Sekhar, *World J. Microbiol. Biotechnol.* **22**, 1135 (2006).

Appendix

Table 3.8 Immobilisation of monolayers of polymers and osmium complex on thiolated gold surface

<p>Procedure</p> <ul style="list-style-type: none"> • Gold electrode immersed into 20 mM cysteamine in absolute EtOH - 5h. • After 5h electrode was removed, rinsed with EtOH, water and dried in the air. • 5% glutaraldehyde in water - 0.5h • Droplet containing : 20µl 2mg/ml [Os(bpy)₂(4-aminomethylpyridine)Cl]PF₆ in acetonitrile, 20µl 20 mg/ml PAA in water, 20 µl 25% glutaraldehyde in water was deposited over the electrode surface. • Allowed to react 20h at RT. <p>Result Insufficient surface coverage</p>	
<p>Procedure</p> <ul style="list-style-type: none"> • 20 mM cysteamine solution in absolute EtOH for 5h. • After 5 h electrode was removed, rinsed with EtOH, water and dried in the air. • Solution containing 0.25 M EDC, 0.5M NHS, 20 mg/ml CM Dextran in pH 5.5 Hepes buffer activated in the fridge for 2h. • Droplet containing: 20 µl of CM Dextran/EDC/NHS solution, 2 mg/ml [Os(bpy)₂(4-aminomethylpyridine)Cl]PF₆ in acetonitrile, 20µl 11 mg/ml PAA in water, was deposited over the electrode surface. • Allowed to react 20 h at RT. <p>Result Insufficient surface coverage</p>	

Procedure	<ul style="list-style-type: none">• Dry gold electrode immersed into 20 mM ethanolic cysteamine solution for 1 h.• After 2 h electrode was removed, rinsed with EtOH, water and dried in the air.• Solution containing 0.02M EDC, 0.05M NHS, 2 mg/ml CMD in HEPES buffer pH 5.5 (pre-activated in the fridge for 2 h, 50μl droplet) was deposited onto the surface plus 50 μl 10 mg/ml [Os(bpy)₂(4-aminomethylpyridine)Cl]PF₆ in acetonitrile• Allowed to react overnight at RT.
Result	Insufficient surface coverage
Procedure	<ul style="list-style-type: none">• Dry gold electrode immersed into 20 mM ethanolic cysteamine solution for 1h.• After 1h electrode was removed, rinsed with EtOH, water and dried in the air.• Solution containing 0.02 M EDC, 0.05 M NHS, 1 mg/ml CMD in HEPES buffer pH 5.5 (pre-activated in the fridge for 1 h, 50 μl droplet) was deposited onto the surface plus 50 μl 10 mg/ml [Os(bpy)₂(4-aminomethylpyridine)Cl]PF₆ in acetonitrile• Allowed to react overnight at RT.
Result	Insufficient surface coverage
Procedure	<ul style="list-style-type: none">• Dry gold electrode immersed into 20 mM ethanolic cysteamine solution for 2h.• After 1h electrode was removed, rinsed with EtOH, water and dried in the air.• Solution containing 0.02 M EDC, 0.05 M NHS, 2 mg/ml CMD in HEPES buffer pH 5.5 (pre-activated in the fridge for 1 h, 50 μl droplet) was deposited onto the surface plus 50 μl 10 mg/ml [Os(bpy)₂(4-aminomethylpyridine)Cl]PF₆ in acetonitrile• Allowed to react overnight at RT
Result	Insufficient surface coverage

Procedure	<ul style="list-style-type: none">• Gold macroelectrodes immersed in DTSP in dry DMSO (10 mM) – 40 min.• Electrode was immersed in 600 μl containing: 200 μl 10 mg/ml [Os(bpy)₂(4-aminomethylpyridine)Cl]PF₆ in acetonitrile, 200 μl PAA 11 mg/ml in water, 200 μl DTSP 0.5 mg/ml in acetonitrile• Allowed to react overnight.
Result	Insufficient surface coverage
Procedure	<ul style="list-style-type: none">• Gold macroelectrodes immersed in DTSP in dry DMSO (10 mM) – 40 min.• Electrode was immersed in 500 μl of solution containing:• 250 μl 10mg/ml [Os(bpy)₂(4-aminomethylpyridine)Cl]PF₆ in acetonitrile, 250 μl PAA 11 mg/ml in water• Allowed to react overnight.
Result	Insufficient surface coverage
Procedure	<ul style="list-style-type: none">• Gold electrodes treated with 10 mM cysteamine.• CM Dextran 2 mg/ml, 50 mM NHS, 20 mM NHS, pH 5.5 HEPES buffer activated in the fridge for 2 hours.• The electrode with cysteamine monolayer was modified with the following mixture: 20 μl Dextran/EDC/NHS solution, 20 μl 20 mg/ml [Os(bpy)₂(4-aminomethylpyridine)Cl]PF₆ in acetonitrile, 10 μl PAA 10 mg/ml• Allowed to react overnight.
Result	Insufficient surface coverage

Procedure	<ul style="list-style-type: none">• Gold electrodes treated with 10 mM cysteamine for 2 hours.• The electrode with cysteamine monolayer was modified with the following mixture: 20 μl PAA 11mg/ml in water, 20 μl 20 mg/ml [Os(bpy)₂(4-aminomethylpyridine)Cl]PF₆ in acetonitrile, 10 μl DTSP 10 mg/250 ml DTSP in DMSO
Result	Insufficient surface coverage
Procedure	<ul style="list-style-type: none">• Electrodes treated with 10 mM cysteamine for 1.5 hours.• CM D 2 mg/5ml, 50 mM NHS, 20 mM NHS, pH 5.5 HEPES buffer has been activated in the fridge for 2 hours.• The electrode with cysteamine monolayer was modified with the following mixture: 20 μl Dextran/EDC/NHS solution, 20 μl 20 mg/ml [Os(bpy)₂(4-aminomethylpyridine)Cl]PF₆ in acetonitrile• Allowed to react overnight
Result	Insufficient surface coverage
Procedure	<ul style="list-style-type: none">• Gold electrodes treated with 10 mM cysteamine for 2 hours.• The electrode with cysteamine monolayer modified as follows: 40μl 20 mg/ml [Os(bpy)₂(4-aminomethylpyridine)Cl]PF₆ in acetonitrile, 8 μl PAA 10 mg/ml in water, 32 μl pH 9.6 carbonate buffer, 20 μl of 25 % glutaraldehyde in water
Result	Insufficient surface coverage

Table 3.9 Results on immobilisation of layers of polymers and osmium complex on glassy carbon electrodes functionalised via reduction of aryl diazonium salts

Procedure	<ul style="list-style-type: none"> • Solution containing 90 mls HCl, 120 μl p-aminoethylaniline (8 mM), 720 μl 0.5M NaNO₂ (10 mM) was allowed to react 5 min. at 0°C in darkness with gentle stirring. • GC electrode was swept between 0.6 and (-0.6V), 4 scans at 20 mV/s, rinsed with H₂O and sonicated for 5 min. • CM Dextran (0.4 mg/ml), 50 mM EDC, 20 mM NHS in pH 5.5 HEPES buffer were activated in the fridge for 1.5 h. • 50 μl droplet placed over electrode for 2 hours • Electrode was rinsed with carbonated buffer (0.85 M, pH 10), then HEPES buffer, pH 7.4. • Surfaces were then reactivated using 50 mM EDC, 20 mM NHS in pH 5.5 HEPES buffer solution for 1.5 h. • After re-activation 50 μl of [Os(bpy)₂(4-AMP)Cl]PF₆, 5 mg/ml in acetonitrile was deposited onto the electrode surface and was allowed to react overnight in darkness for 10 h. • After removal electrode was rinsed with pH 5.5 buffer and water.
Result	Insufficient surface coverage
Procedure	<ul style="list-style-type: none"> • Solution containing 90 mls HCl, 120 μl p-aminomethylaniline, (8 mM) 800 μl 0.5M NaNO₂ (10 mM) was allowed to react 5 min. at 0°C in darkness with gentle stirring. • GC electrode was swept between 0.6 and (-0.6V), 4 scans at 20 mV/s, rinsed with H₂O and sonicated for 5 min. • CM Dextran (2mg/ml), 50 mM EDC, 20mM NHS in pH 5.5 HEPES buffer were activated in the fridge for 2h. • Electrode immersed into EDC/NHS/ CM Dextran solution for 2h. • Electrode was immersed into carbonated buffer (0.85M, pH 10) for 30 min. • Surfaces were then reactivated using 50 mM EDC, 20 mM NHS in pH 5.5 HEPES buffer solution for 2h in the fridge. • After re-activation electrode was immersed into solution of [Os(bpy)₂(4-AMP)Cl]PF₆, 5 mg/ml in acetonitrile and was allowed to react overnight in darkness for 12h. • After removal electrode was rinsed with pH 5.5 buffer and water.
Result	Insufficient surface coverage

Procedure	<ul style="list-style-type: none">• Solution containing 100 mls HCl, 108 mg p-phenylenediamine (10 mM), 800 μl 1M NaNO₂ (8 mM) was allowed to react 5 min. at 0° C in darkness with GC gentle stirring.• GC electrode was swept between 0.6 and (-0.6V), 4 scans at 20 mV/s, rinsed with H₂O and sonicated for 5 min.• Dextran (2 mg/ml), 50 mM EDC, 20 mM NHS in pH 5.5 HEPES buffer were activated in the fridge for 2 h.• Electrodes were immersed into EDC/NHS/ CM Dextran solution for 2 h.• Surfaces were then reactivated using 50 mM EDC, 20 mM NHS in pH 5.5 HEPES buffer solution for 2 h in the fridge.• After re-activation electrode was immersed into solution of [Os(bpy)₂(4-AMP)Cl]PF₆, 5 mg/ml in HEPES buffer-acetonitrile mixture (9:1) and was allowed to react overnight in darkness for 12h.• After removal electrode was rinsed with pH 5.5 buffer and water.
Result	Insufficient surface coverage Procedure was repeated using water or phosphate buffer, pH 5.5 instead of HEPES buffer was tested, but similar results were obtained

Table 3.10 Roughness data for glassy carbon and graphite electrodes

Electrode	Method	Average capacitance [$\mu\text{F}/\text{cm}^2$]	Rf	n	Min.	Max.	Med.	RSD [%]
Glassy carbon	Capacitance	10.4	0.87	45	0.28	1.89	0.76	46.5
Glassy carbon – electrochemically pre-treated	Capacitance	17.17	1.07	8	0.79	1.39	0.99	22.0
Glassy carbon	Cyclic voltammetry 0.2 mM ferrocenemethanol phosphate buffer, pH 7.4		1.77	6	1.72	1.83	1.77	2.0
Glassy carbon	Cyclic voltammetry 10 mM ferrocene NaClO ₄ , methanol, Ag/Ag ⁺ reference electrode		3.91	46	2.10	7.00	3.81	26.4
Graphite	Capacitance	624.5	39	194	4.07	107.4	36.29	44.3
Graphite	Cyclic voltammetry 10 mM ferrocene NaClO ₄ , methanol, Ag/Ag ⁺ reference electrode		1.66	26	0.52	2.55	1.90	37.4
Graphite	10 mM potassium ferricyanide, phosphate buffer, pH 7.4		1.73	13	1.10	2.43	1.56	21.8

Table 3.11 Roughness data for gold and platinum electrodes

Electrode	Method	Average capacitance [$\mu\text{F}/\text{cm}^2$]	Rf	n	Min.	Max.	Med.	RSD [%]
Platinum	Oxygen adsorption		3.3	6	1.43	5.17	3.44	39.8
Platinum	Hydrogen adsorption		3.44	6	1.18	5.5	3.55	46.7
Gold	Oxygen adsorption		1.99	62	0.87	3.42	1.92	35
Gold	Capacitance	53.46	3.34	4	2.78	4.83	2.88	29.7
Gold	Cyclic voltammetry 0.2 mM ferrocenemethanol phosphate buffer, pH 7.4		1.98	6	1.81	2.06	2.01	5.1

Chapter 4

Electrochemistry of screen-printed electrodes and their application to DNA hybridization sensor

4.1. Introduction

Screen-printing is a widely established technique for producing substrates for electrochemical sensors and biosensors. Manufacturing of screen-printed electrodes (SPEs) generally involves printing of the conductive inks, containing carbon, gold or platinum on either plastic or ceramic substrate and adding a polyester insulation layer. In addition, electrodes could be designed with a silver/silver chloride pseudo-reference electrode and counter electrode printed either with carbon or silver ink. There is great potential for ink modification: metal nanoparticles, (1) carbon nanotubes (2) chemical reagents (3) or enzymes (4) can be easily incorporated into the ink. Especially graphite-based inks are preferred over other materials due to their distinct electrochemical properties, such as low background currents and wide potential window. For instance, a catalytically active electrode could be prepared by printing mediator, enzyme and conductive paste blend. (5) Most of methodologies reported for modification of SPEs are no different from those applied to solid electrodes and involve adsorption, (6) formation of organised monolayers, (7) coating with polymer (8) or gel, (9) crosslinking (10) and electropolymerisation. (11) A combined approach of electrode preparation, by both printing of the catalyst and ink surface derivatisation was reported where an enzyme was attached to a polymer matrix deposited on ink/mediator composite. (5, 12-15)

A flexible electrochemical cell design is another advantage offered by screen-printed electrodes: they have a potential to be integrated with disposable micro-volume cells, multiwell plates and flow systems. (16-18)

Chemical and biological sensing is the most common application of screen-printed electrodes. SPE-based sensors for detection of glucose, (15, 19-22) pesticides, (23) heavy metals, (24) gases, (25) enzyme-specific substrate, (25) antigens, (26) DNA (27) and whole cells (28) are reported in scientific literature. Since screen-printed electrodes can be mass-produced at relatively low cost; they have potential to be commercialised, with many disposable sensors being already available on the market. Especially glucose sensors have a long history of commercialisation.

Several publications devoted to electrochemistry of DNA on screen-printed electrodes have appeared in recent years. Marazza et al. developed a DNA hybridization assay, where a biotinylated probe DNA is attached to a SPE surface

containing pre-adsorbed avidin. Electrochemical signals corresponding to intercalation of daunomycin were measured using differential pulse voltammetry. (29) The same research group published an application of gold screen-printed electrodes to enzyme-amplified assays. In this particular case thiolated DNA was immobilized via gold-thiol chemistry on SPEs. (30, 31) Use of screen-printed electrode arrays for detection of *Listeria monocytogenes* sequence has also been explored. (32) Marquette et al. prepared a genosensor based on electrochemically activated screen-printed carbon electrodes modified with ssDNA via carbodiimide coupling. The hybridisation event was detected using chemiluminescence and electrochemical impedance spectroscopy. (33)

We reported, in Chapter 3, on a DNA hybridisation sensor where the sensing films are deposited onto graphite disc electrodes. (34) Micromoles of DNA could be detected with this system: however the macroscopic, hand-assembled graphite disk electrodes employed in the study resulted in poor reproducibility of the signals, where a relative standard deviation as high as 40 % was obtained. It is expected to achieve an improvement of the assay by translating it to electrodes which are characterised by high reproducibility of electroactive surface areas. Use of screen-printed electrodes may therefore improve the assay precision.

In this chapter several aspects of screen-printed electrode electrochemistry were evaluated. First, screen printed electrodes from a variety of sources were examined for electroactivity towards standard redox probes in solution. Then, electrodes were subject to modification with aryl diazonium salts, anchoring of carboxymethylated dextran support and covalent coupling of osmium redox probe or DNA, as described earlier in Chapter 3. Electroanalytical performance of DNA hybridization sensor on SPE substrates was then investigated.

4.2. Experimental

4.2.1. Materials and reagents

The probe oligonucleotide sequence (5'⇒3'): NH₂-C6-ATTTCGACAGGGATAGTTTCGA, target oligonucleotide sequence (5'⇒3'): biotin-TCGAACTATCCCTGTCGAAT (designed from the *ssrA* gene of *Listeria monocytogenes*), control oligonucleotide sequences (5'⇒3'): biotin-ATTTCGACAGGGATAGTTTCGA (biotin-non-complementary) and (5'⇒3'): TCGAACTATCCCTGTCGAAT (unmodified-complementary) were purchased from MWG-Biotech. Glucose oxidase-avidinD conjugate was purchased from Vector Laboratories. The redox complex, [Os(2,2'-bipyridine)₂(4-aminomethylpyridine)CIPF₆] was synthesised according to literature procedures. (35) All other chemicals were purchased from Sigma-Aldrich and used as received.

Screen-printed graphite electrodes from the following sources were used: Kanichi Research, Dropsens, Gwent (sensor type BE2030408D9), as well as from University College Cork (UCC) and Cranfield University. Images of the SPEs are presented in **Figure 4.1**. Most of them were designed as three electrode systems with Ag/AgCl paste reference electrode and screen-printed auxiliary electrode made from either carbon (Kanichi, Dropsens, Gwent, Cranfield) or silver (UCC). In addition, in order to facilitate incubation of the electrode in the vial with the DNA solutions, custom-designed single working electrode strips were purchased from Kanichi.

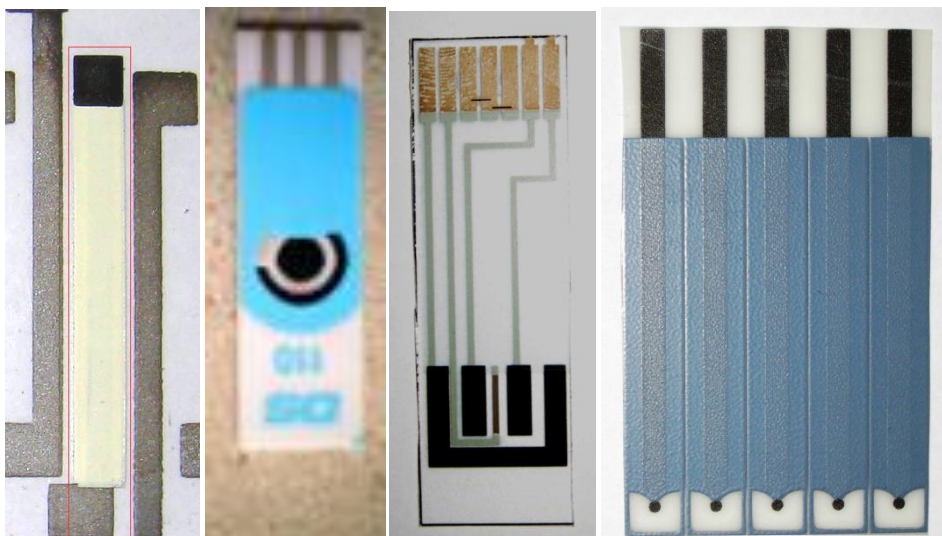


Figure 4.1 Images of screen printed electrodes: from the left; UCC electrode (red frame indicates a working electrode used in the study), Dropsens, Cranfield and Kanichi electrodes. Image of Gwent electrode is not available, but the configuration was similar to that of Dropsens SPE

For electrodes without a printed reference and counter electrode, external reference electrode Ag/AgCl (3M KCl) in a glass body (CH Instruments) was used and a platinum wire was used as counter electrode. For studies in methanol the potential was measured versus non-aqueous Ag/Ag⁺ reference electrode with internal electrolyte composition of 0.1 M AgNO₃ and 0.1 M Et₄NClO₄ in acetonitrile.

4.2.2. Instrumentation and techniques

The electrochemical measurements were performed using an Autolab, EcoChemie, PGSTAT12 potentiostat or a CHI 1030A multi-channel potentiostat using a three-electrode cell at room temperature. In all experiments, the electrochemical cell was maintained in stainless steel Faraday cage to minimise electrical noise.

Screen-printed electrodes were subjected to multiple cycles between 0 - 0.6V in the supporting electrolyte solution at a scan rate 100 mV/s to ensure an adequately reproducible background signal was observed. Then electrodes were characterised by running a background scan in potassium chloride or phosphate buffer solution over

the same potential range as for the electrochemical pre-treatment. Cyclic voltammograms were recorded in solutions of redox probes: potassium ferricyanide, ferrocenemethanol and ferrocene.

4.2.3. Estimation of electrochemically active surface area

The roughness of the electrode can be described by a dimensionless parameter R_f (*roughness factor*), which is defined as the ratio of electrochemically active area and the geometric area.

An estimate of electrode area can be obtained from electrochemical responses of solutions of redox probes, using the Randles-Sevcik equation. (**Eq. 4.1**) In this case peak currents from a series of voltammetric experiments of potassium ferricyanide solutions in the range of scan rates (20-500 mVs) were plotted versus \sqrt{v} and the slope of the curve was used for the calculations. The diffusion coefficient of potassium ferricyanide of $1.04 \times 10^{-6} \text{ cm}^2 / \text{s}$. was estimated from cyclic voltammograms using a platinum electrode (1 mm diameter).

$$I_p = 2.69 \times 10^5 n^{\frac{3}{2}} A D^{\frac{1}{2}} c v^{\frac{1}{2}} \quad (4.1)$$

An alternate approach to estimation of electrode areas is to measure the capacitance current, and assume a normalisation capacitance for different types of electrodes. For our capacitance study the data from a background CV scan in base electrolyte was used. (**Figure 4.2**) The capacitance was computed from cyclic voltammogram using **Equation 4.2**

$$C_{total} = \frac{1}{2} \left(\frac{|i_a| + |i_c|}{\nu} \right) \quad (4.2)$$

Where: C_{total} - capacitance of the electrode area

I_a - absolute value of anodic current in the middle range of the curve

I_c - absolute value of cathodic current in the middle range of the curve

ν - scan rate

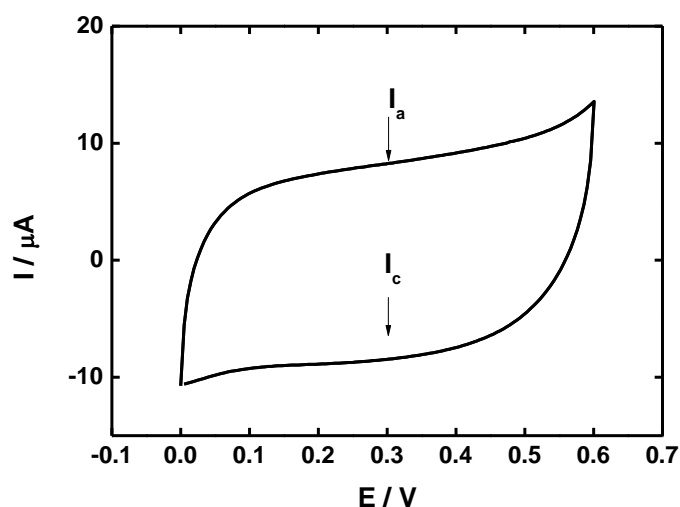


Figure 4.2 Typical background of the graphite electrode, I_a and I_c indicate current values used to estimate capacitance

The normalised capacitance estimated for a smooth mercury electrode is $16 \mu\text{F}/\text{cm}^2$. Assuming that all the area of mercury electrode is electroactive the capacitance values were divided by this value to estimate the electrochemically active area of carbon electrodes. (36)

4.2.4. Preparation and characterization of electrodes

Surface derivatisation of screen-printed electrode was achieved by the formation of the diazonium salt of p-phenylene diamine in the presence of hydrochloric acid and sodium nitrite as described in Chapter 3. Derivatised electrodes were rinsed with water and sonicated for 5 min. Carboxymethylated dextran was attached by dipping of the derivatised electrodes into a solution containing 50 mM EDC (N-ethyl-N'-(3-dimethylaminopropyl)carbodiimide), 20 mM NHS -

(N-hydroxysuccinimide) and 2 mg/mL CMD in ultrapure water for 2 h at room temperature, following pre-activation of the CMD with the EDC/NHS solution for 1.5 h at 4 °C. The resulting CMD-modified surfaces were re-activated by immersion in EDC/NHS solution for 1 h and subsequently immersed into a probe ssDNA solution (20 µL, 50 µg/mL) for 15 h. After reaction with the probe ssDNA the electrodes were rinsed with pH 9.6 carbonate buffer to remove unreacted NHS esters, and then with distilled water.

For some electrodes, osmium redox complexes, with free amine functional groups, were coupled to the CMD-modified graphite electrodes using EDC/NHS activation, followed by immersion in 2.5 mg/mL solution of osmium complex in methanol-water mixture (1:1) for 15 hrs.

4.2.5. Detection of DNA hybridization

Sensing electrodes were dipped into plastic micro-centrifuge tubes containing solution of target DNA (500 µL, varying concentrations of DNA in 0.3 M sodium citrate, 1 M NaCl, 0.05 % SDS, 0.2 % milk powder) for 2 h at 37 °C with gentle shaking. After 2 hours electrodes were removed, rinsed with hybridisation solution and immersed into 0.2 mg/ml glucose oxidase: avidinD solution (150 µL) for 1 h at room temperature. The electrodes were then rinsed with hybridisation solution and the catalytic current was measured using cyclic voltammetry (0 - 0.5 V vs. Ag/AgCl, 2 scans at 5 mV/s) and chronoamperometry (0.35 V, 250 s) in 0.02 M phosphate buffer containing 0.2 mM ferrocenemethanol as mediator, in the absence and then presence of 20 mM glucose.

4.3. Results and discussion

4.3.1. Basic electrochemistry of screen-printed electrodes

Screen-printed graphite electrodes were evaluated and compared using voltammetric techniques. The electrodes were first tested in a supporting electrolyte solution of either phosphate buffer or potassium chloride and subsequently their electrochemical reactivity towards potassium ferricyanide and ferrocenemethanol redox probes was examined.

Initially electrodes manufactured by the research group in University College Cork were tested. Originally the screen-printed strip was a three-electrode system, but the working electrode was separated and used with external reference and counter electrodes in order to reduce silver contamination. A background scan of a single working electrode, showing silver oxidation/reduction peaks is presented in **Figure 4.3**. A cyclic voltammogram recorded in potassium ferricyanide solution is shown in **Figure 4.4**. The poorly defined oxidation/reduction wave indicates “sluggish” kinetics of electron transfer. (37) In contrast, when a neutral redox probe, such as ferrocenemethanol is employed, a well defined oxidation/reduction couple as shown in **Figure 4.5**, is observed. Similarly shaped CV curves were obtained using ferrocene in non-aqueous solvent. (**Figure 4.6**).

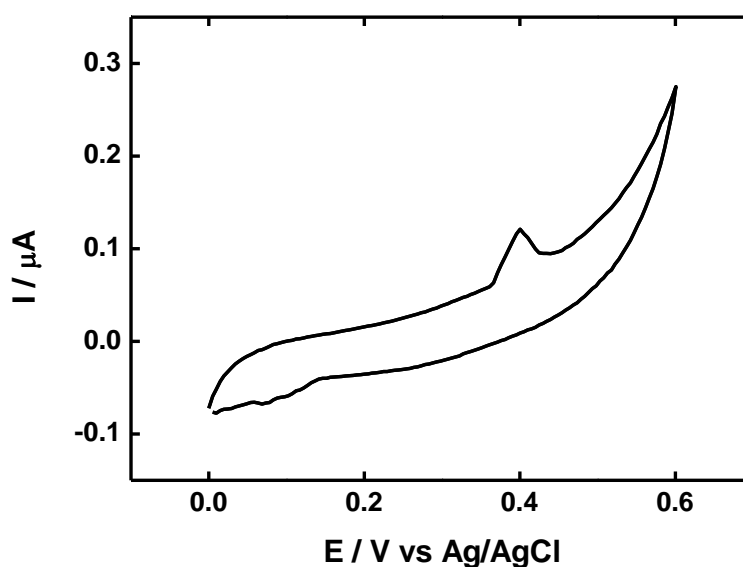


Figure 4.3 Cyclic voltammogram recorded 0.1M KCl at a scan rate of 100 mV/s using the screen printed graphite electrode, sourced from UCC, 4 x 4 mm square, **background**, as working electrode.

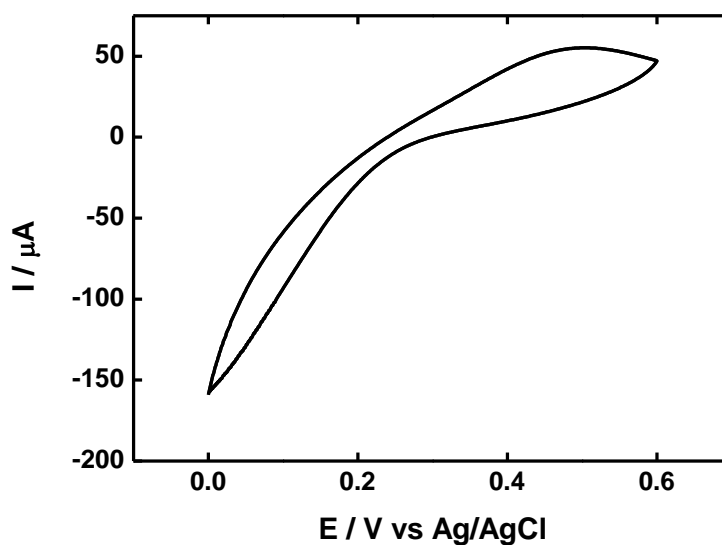


Figure 4.4 Screen-printed graphite electrode from UCC, square, 4 x 4 mm, 10 mM ferricyanide, other conditions as in Figure 4.3.

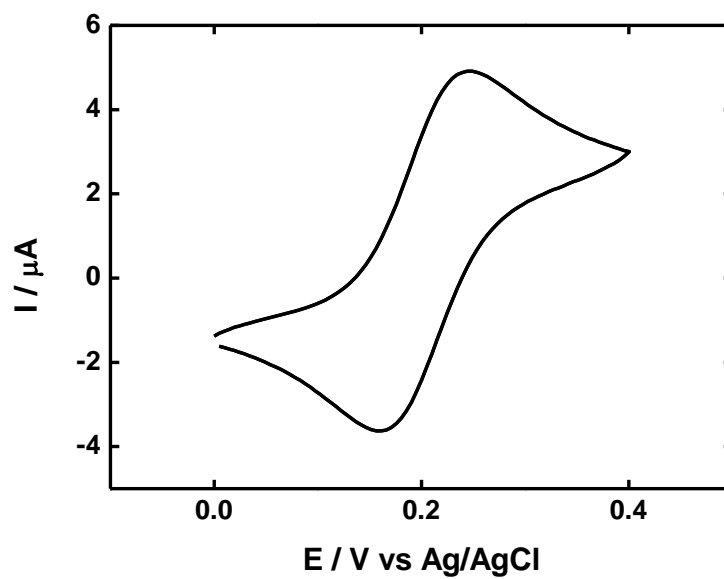


Figure 4.5 Screen-printed graphite electrode from UCC, square, 4 x 4 mm, 0.2 mM ferrocenemethanol in phosphate buffer solution, scan rate 100 mV/s

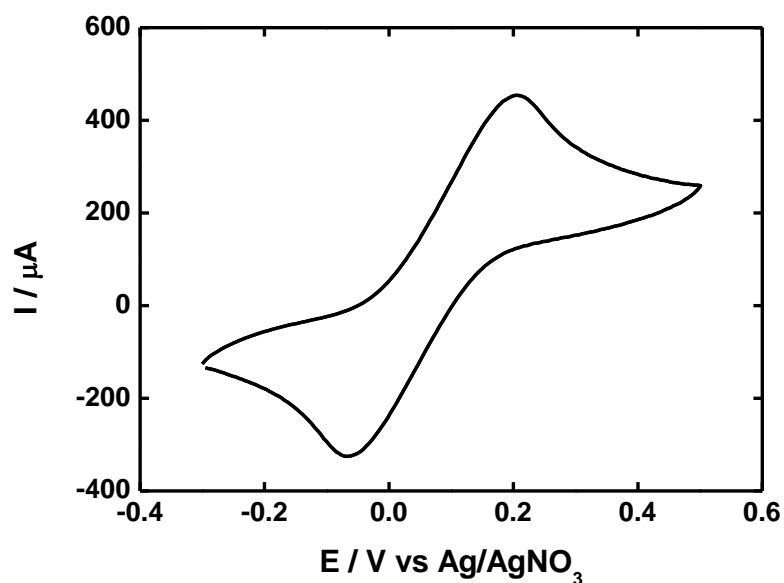


Figure 4.6 Screen-printed graphite electrode from UCC, square, 4 x 4 mm, scan rate 100 mV/s, 10 mM ferrocene in MeOH, 0.1 M LiClO₄, Ag/Ag⁺ non-aqueous reference electrode

Potassium ferricyanide, is a useful indicator of the electrochemical activity and ink parameters, such as carbon to binder ratio. Inks with the higher binder content often display poor reversibility, when tested with K₃Fe(CN)₆. As the graphite is negatively charged, the voltametric scans of positive redox probes, e.g. hexaammineruthenium(III) chloride can show a reversible redox couple in the absence of reversibility for potassium ferricyanide. (38)

Figure 4.7 presents a background scan of Cranfield screen-printed electrode. Clearly no major contaminants are present. Again, slow kinetics for oxidation of potassium ferricyanide was observed. (**Figure 4.8**) Once again, unlike for ferricyanide, ferrocenemethanol voltammetry yields oxidation/reduction waves, which are clearly distinguishable from the baseline. (**Figure 4.9**)

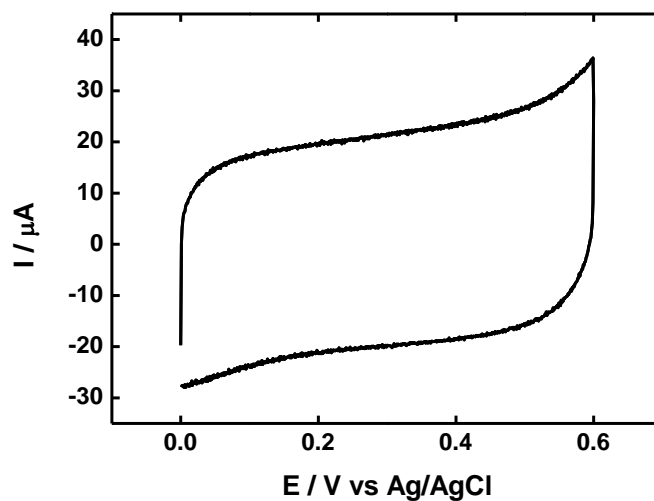


Figure 4.7 Screen-printed graphite electrodes from **Cranfield** University, rectangular, 4 x 7 mm, Ag/AgCl pseudo-reference electrode, graphite counter electrode, **background**, 0.1 M KCl

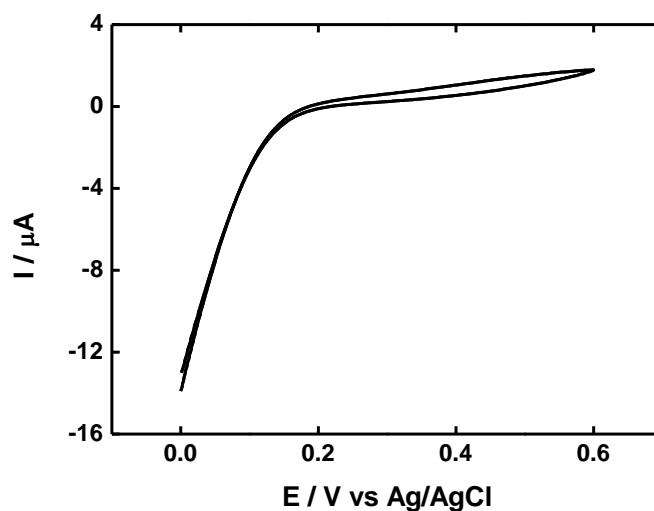


Figure 4.8 Screen-printed graphite electrodes from **Cranfield** University, rectangular, 4 x 7 mm, Ag/AgCl pseudo-reference electrode, graphite counter electrode, **10 mM potassium ferricyanide** in 0.1M KCl, scan rate 100 mV/s

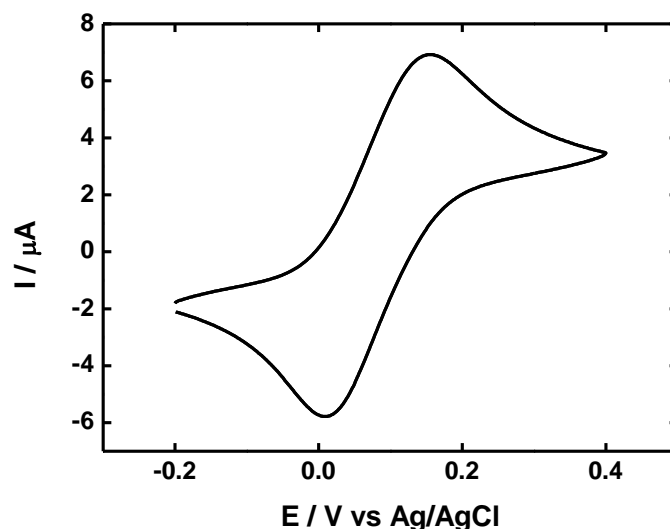


Figure 4.9 Screen-printed graphite electrodes from **Cranfield** University, rectangular, 4 x 7 mm, on strip Ag/AgCl pseudo-reference electrode, graphite counter electrode, **0.2 mM ferrocenemethanol** in 0.1M KCl

The electrochemical performance of screen-printed electrodes was extensively studied in the past and it is common to find that most of carbon inks fail to produce a satisfactory voltammogram for potassium ferricyanide. (17, 38-42) For instance Gornall et al.(38) studied electroactivity of inks purchased from GEM and Dupont for application to microelectrode arrays. For both inks a clear ferricyanide redox couple has not been observed with only an anodic peak being apparent.

Peak-to-peak splitting data extracted from CVs of ferrocenemethanol (UCC, Cranfield) and ferrocene (UCC) are displayed in **Table 4.1**. Peak separation values for ferrocenemethanol scan at UCC electrodes is 68 mV and is relatively close to an ideal reversible value of $54/n$ mV. (37) Ferrocene in non-aqueous environment displays non-reversible behaviour with peak-to-peak splitting being 348 mV in magnitude. Non-aqueous electrolytes are often characterised by high resistance and slow electron transfer in these solutions could be expected. (43) Peak separation value observed for ferrocenemethanol scan at the Cranfield electrode is 130 mV and indicates slower kinetics for this electrode compared to the UCC electrode.

Table 4.1 Redox potentials and peak separation for UCC and Cranfield screen-printed electrodes.

Electrode	Redox probe	E_{pa}	E_{pc}	ΔE_p
UCC	ferrocenemethanol	0.237	0.169	0.068 ± 0.007
UCC	ferrocene	0.213	-0.052	0.348 ± 0.01
Cranfield	ferrocenemethanol	0.13	0.003	0.127 ± 0.029

Further studies involved testing of electrodes from commercial sources in an effort to confirm sourcing of mass-produced electrodes. Electrodes were sourced from Gwent Electronics, Dropsens, and Kanichi Research. Background scans of the screen printed electrodes are presented in **Figures 4.10-4.12**. The Kanichi electrodes are characterised by relatively higher capacitive currents compared to the other two.

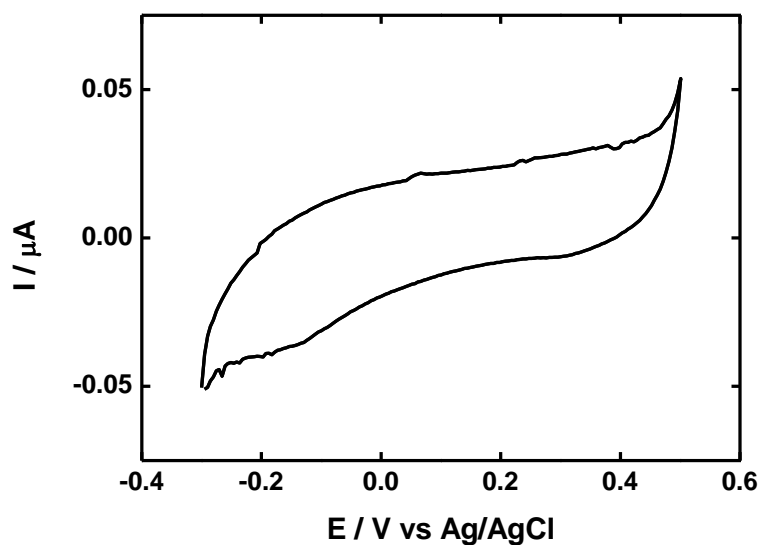


Figure 4.10 Screen-printed graphite electrode from **Gwent** Electronics, $\phi = 1$ mm, Ag/AgCl pseudo-reference electrode, graphite auxiliary electrode, **background**, 20 mM phosphate buffer, pH 7.4

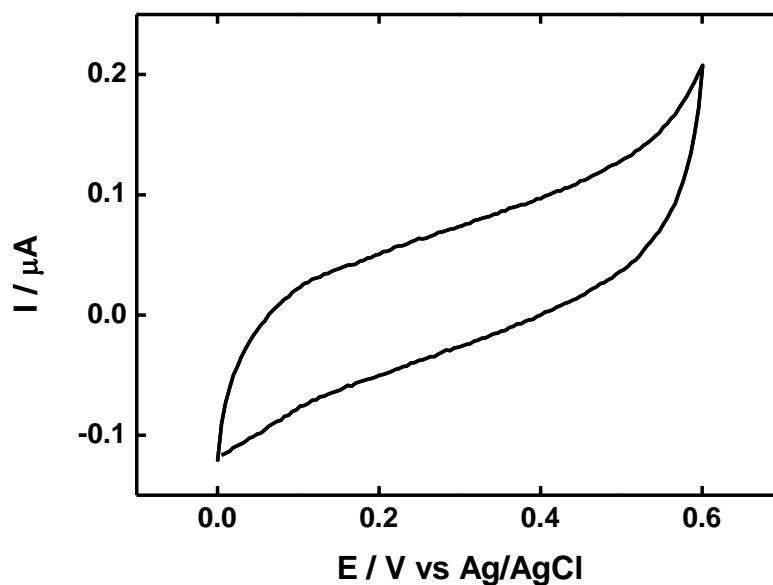


Figure 4.11 Screen-printed graphite electrodes - **Dropsens**, $\phi = 3\text{mm}$, Ag/AgCl pseudo reference electrode, graphite auxiliary electrode, **background** 0.1M KCl,

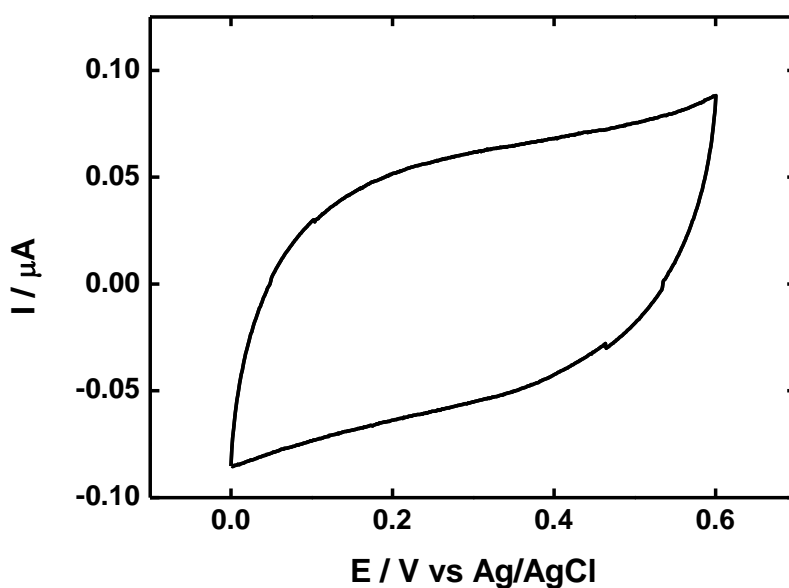


Figure 4.12 Screen-printed electrodes, **Kanichi** research, single working electrode $\phi = 1\text{mm}$, external reference and counter

In contrast to the results presented in the earlier section of this chapter, electrodes produced by Gwent Electronics, Dropsens, and Kanichi research show significant

electrochemical activity towards potassium ferricyanide as shown in **Figures 4.13, 4.14 and 4.15.**

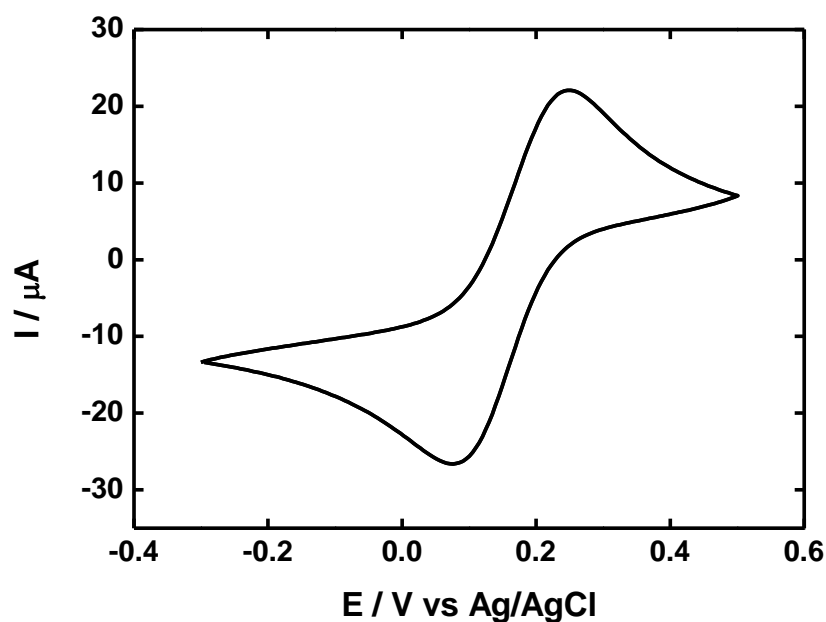


Figure 4.13 Screen-printed graphite electrode from **Gwent Electronics**, $\phi = 1$ mm, **10 mM potassium ferricyanide**, 20 mM phosphate buffer, pH 7.4

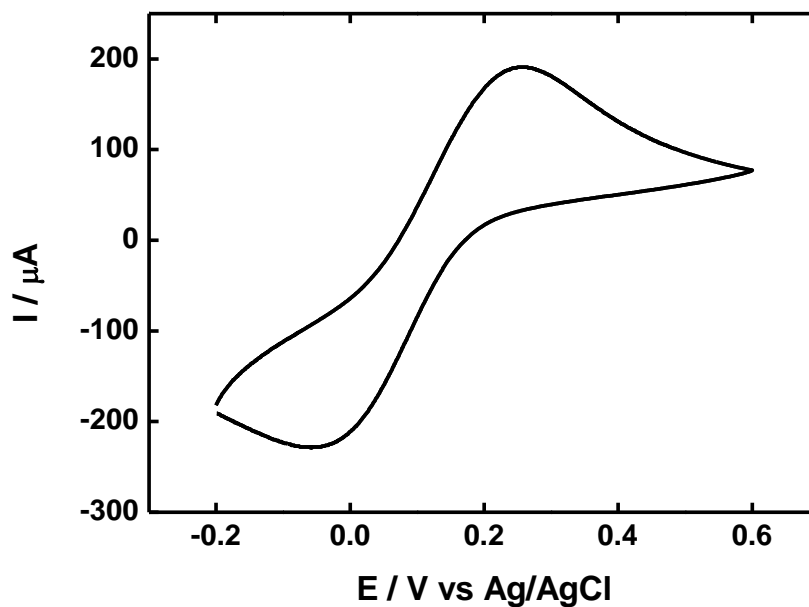


Figure 4.14 Screen-printed graphite electrodes from **Dropsens**, $\phi = 3$ mm, Ag/AgCl pseudo reference electrode, graphite auxiliary electrode, **10 mM potassium ferricyanide** in 0.1M KCl

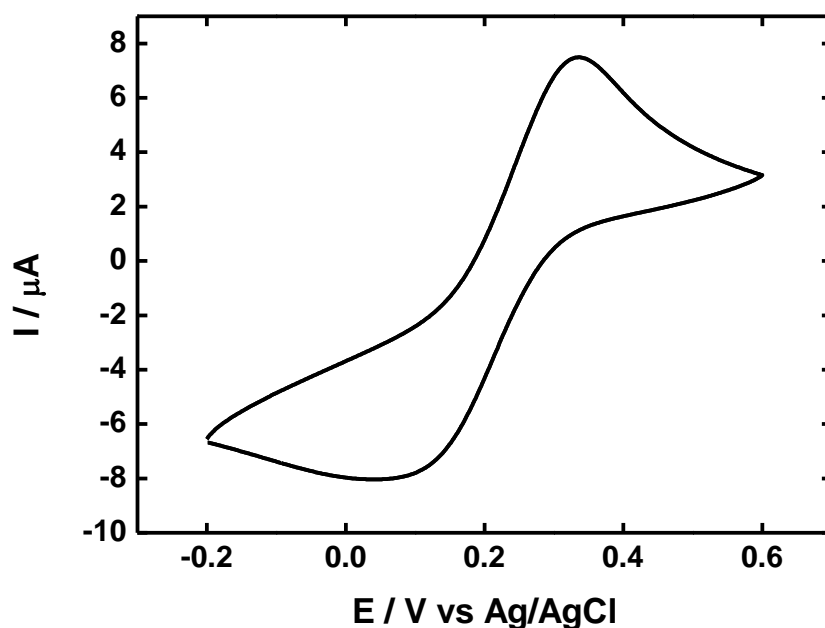


Figure 4.15 Screen-printed electrodes, **Kanichi** research, single working electrode, external reference and counter electrode, cyclic voltammetry, **10 mM potassium ferricyanide**, scan rate 100 mV/s, 20 mM phosphate buffer, pH 7.4.

Cyclic voltammetry scans were recorded at scan rates 100-500 mV/s for the Dropsens and Kanichi electrodes and the peak currents were plotted versus the square root of the scan rate. Randles-Sevcik plots (I vs $v^{1/2}$) of Dropsens and Kanichi electrodes (**Figures 4.16-4.17**) show non-linear trend at higher scan rates, which is most likely caused by the limitations of kinetics. (44)

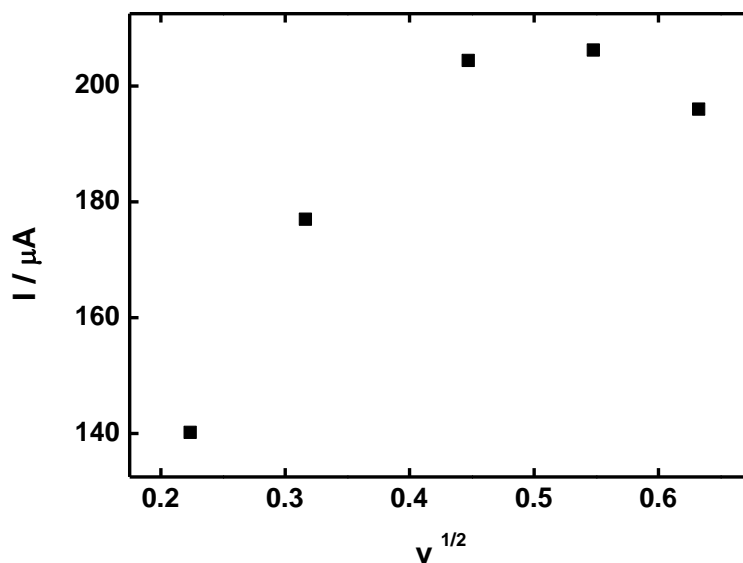


Figure 4.16 Screen-printed graphite electrodes from **Dropsens**, peak currents plotted as a function of square root scan rate, $\varphi = 3$ mm, Ag/AgCl pseudo reference electrode, graphite auxiliary electrode, **10 mM potassium ferricyanide** in 0.1M KCl,

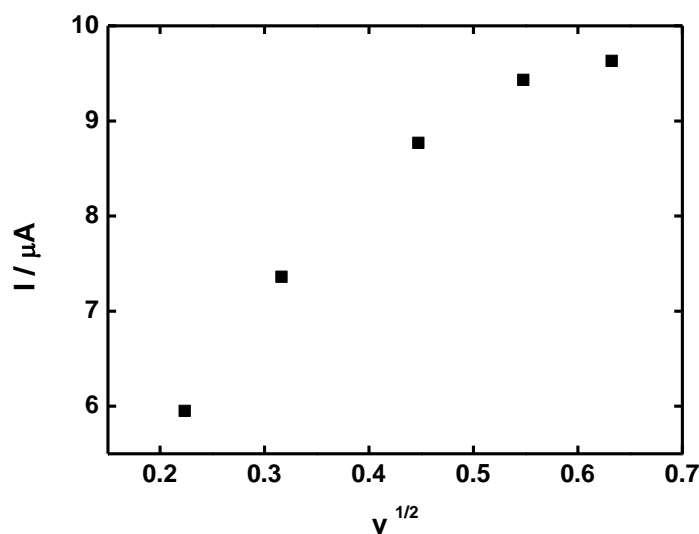


Figure 4.17 Screen-printed electrodes, **Kanichi** research, single working electrode, external reference and counter electrode, Cyclic voltammetry, **10 mM potassium ferricyanide**, Current plotted versus square root of the scan rate, 20 mM phosphate buffer, pH 7.4.

The data compiled for Gwent Electronics, Dropsens, and Kanichi electrodes are compared in **Table 4.2**. The electroactive areas of the electrodes were calculated by

capacitance method and also from the slope of the linear portion of Randles-Sevcik plot.

Table 4.2 Roughness values determined from background capacitive currents and from fericyanide redox current in CV, and the oxidation/reduction potentials and peak separation for potassium ferricyanide cycling at screen-printed electrodes

	Roughness capacitance	Roughness potassium ferricyanide			
	Average	Average	Ea	Ec	ΔE_p 100mV/s
Gwent	0.12±0.07	nd	0.296	0.022	0.274
Dropsens	0.14±0.06	0.34±0.06	0.187	0.019	0.168±0.011
Kanichi	5.08±1.2	0.49±0.06	0.326	0.086	0.241±0.024

Gwent and Dropsens electrodes yield roughness values lower than 1 for the electrode areas estimated from the capacitance measurements. The roughness values presented in **Table 4.2** correspond to capacitance of $\sim 4 \mu\text{F}/\text{cm}^2$. In comparison, the capacitance of glassy carbon electrodes could lie within 8-20 $\mu\text{F}/\text{cm}^2$ range. ⁽⁴⁵⁾ A calculation of the roughness based on the background scans of 3 mm glassy carbon electrodes yielded the value of 0.46 ($7.4 \mu\text{F}/\text{cm}^2$), when taking the average of eight electrodes. Glassy carbon electrodes polarised at extreme anodic and cathodic potentials following the protocol described by Blaedel and Jenkins (46) yield roughness values of 1.07, illustrating the sensitivity of roughness determination using capacitance values to surface history and pre-treatment procedures. Because carbon inks contain non-conductive components, such as resin binder, background currents of SPEs could reach lower values than in case of conventional carbon electrodes. Several methods of improving performance of the inks were reported, including pre-anodisation, (47, 48) treatment with oxygen (49) or argon plasma. (41) Ghamouss et al. reported that a screen-printed electrode treated with argon plasma showed an increase in capacitance from 1.6 to 32 $\mu\text{F}/\text{cm}^2$ and after second treatment the value reached 400 $\mu\text{F}/\text{cm}^2$. (41) Also electron transfer properties of the electrode

are significantly changed: exposure of an electrode to argon plasma improved the shape of voltammetric curves for potassium ferricyanide cycling.

The areas of Dropsens and Kanichi electrodes estimated from a redox probe study are less than geometric area. Even so, peak separations at $v = 100$ mV/s exceed the theoretical value of $\Delta E_p > 59$ mV/n indicating slow electron transfer kinetics, and thus the difficulty with using the Randles-Sevcik equation to estimate such areas. (37)

4.3.2. Formation of redox films on screen-printed electrodes

Initial experiments with modification of screen-printed electrodes were carried out using UCC sourced screen-printed electrodes. In an approach similar to described in chapter 3 for modification of graphite disc electrodes the electrodes were derivatised via reduction of *in situ* generated diazonium salts from p-phenylene diamine, followed by covalent coupling of the carboxymethylated dextran and redox complex $[\text{Os}(\text{bpy})_2(4\text{-AMP})\text{Cl}]\text{PF}_6$. A cyclic voltammogram of the resulting electrode, showing Os(II)/(III) redox transition, is shown in **Figure 4.18**. The system is however unsuitable for use at slow scan rates - contamination of the working electrode area with silver results in distorted voltammograms, as seen in **Figure 4.19**.

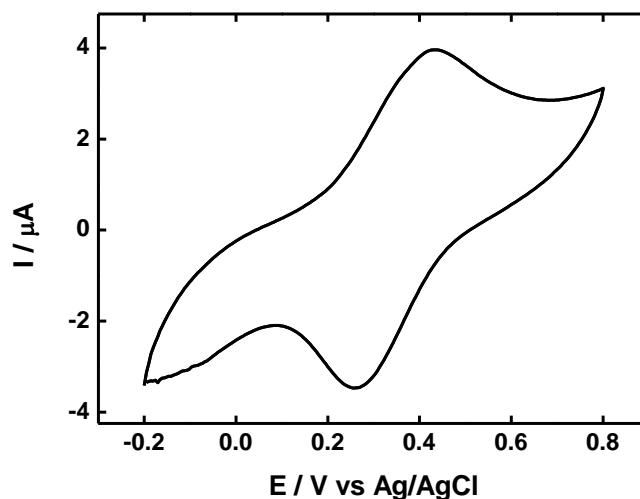


Figure 4.18 Immobilization of **p-phenylenediamine, CM Dextran** and redox probe $[\text{Os}(\text{bpy})_2(4\text{-AMP})\text{Cl}]\text{PF}_6$ on UCC screen-printed electrodes, 20 mM phosphate buffer, pH = 7.4, $v = 100 \text{ mV/s}$

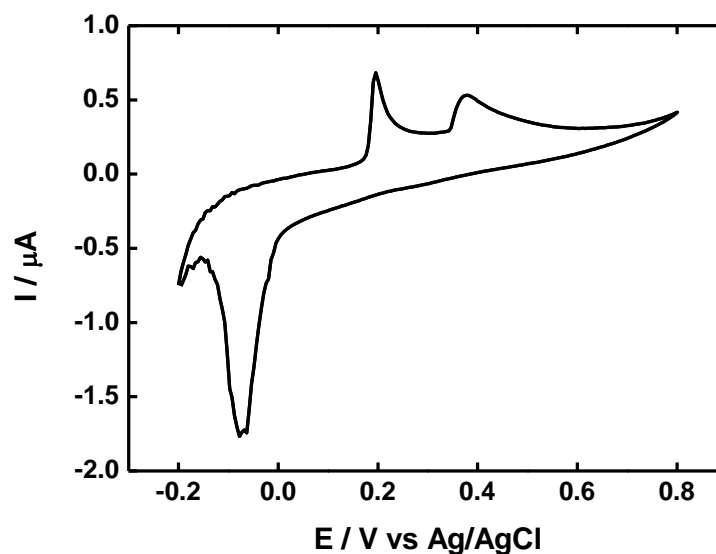


Figure 4.19 Immobilization of **p-phenylenediamine, CM Dextran** and redox probe $[\text{Os}(\text{bpy})_2(4\text{-AMP})\text{Cl}]_3\text{PF}_6$ on UCC screen-printed electrodes, 20 mM phosphate buffer, pH = 7.4, $v = 5 \text{ mV/s}$

In a further study, SPEs sourced from Kanichi were examined towards use in carboxymethylated dextran and osmium complex based layer formation. The electrode was chosen due to its satisfactory performance towards potassium ferricyanide redox cycling. Another reason for choosing Kanichi electrodes was that

a single working electrode configuration became available. It is reasonable to assume that no silver is going to interfere with the measurement in the absence of reference electrode, especially as the conducting path of the working electrode was printed with carbon only. This design also allows incubation in the plastic microcentrifuge tube during the DNA assay, using a low volume of solution.

As in Chapter 3, the electrodes were modified via reduction of *in situ* generated diazonium salt of p-phenylene diamine. The CVs for reduction of the diazonium salt at the electrode surface display a clear, single peak. (**Figure 4.20**) This behaviour is comparable with that observed on a glassy carbon electrode. (See **Figure 3.3** in Chapter 3) The introduced amino functional groups were then used to chemically attach carboxymethylated dextran via an amide bond, with subsequent attachment of the amine-functionalised osmium complex to the dextran.

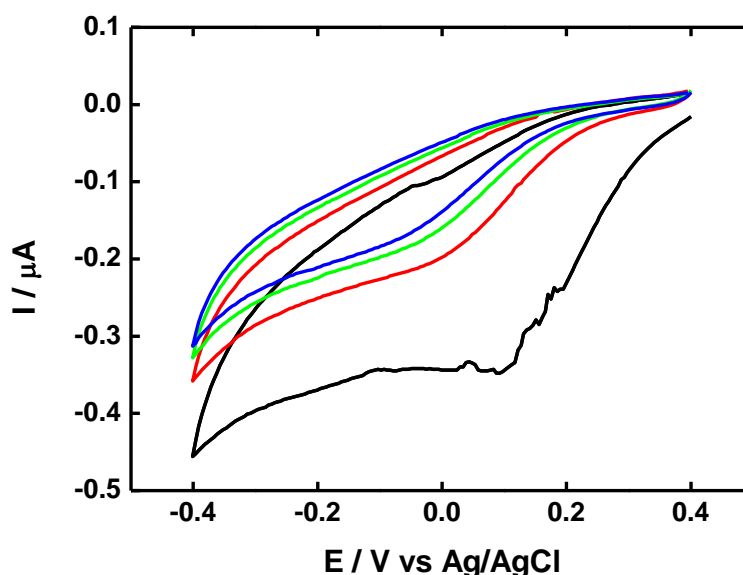


Figure 4.20 Screen-printed electrodes (**Kanichi**) modified with **p-phenylene diamine diazonium salt**. Scans from 1 to 4.

Coupling of the redox complex $[\text{Os}(\text{bipyridine})_2(4\text{-aminomethylpyridine})\text{Cl}]$ was confirmed by cyclic voltammetry, which displayed peaks for redox cycling of the osmium redox centre, **Figure 4.21**.

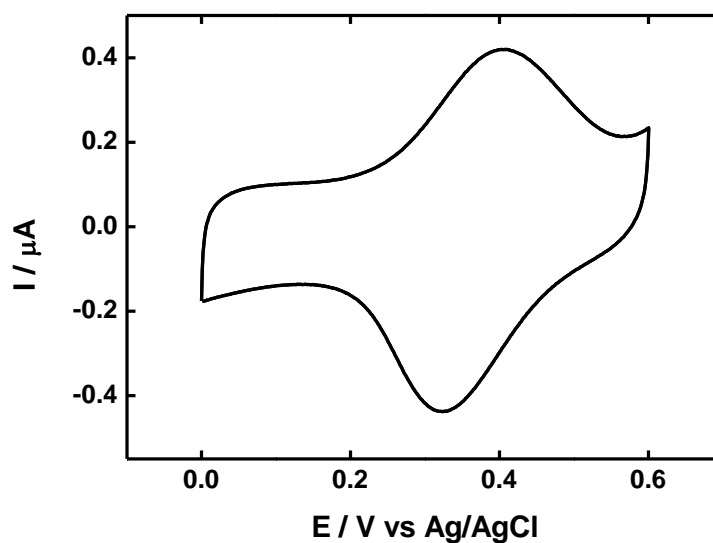


Figure 4.21 Cyclic voltammogram of the redox probe $[\text{Os}(\text{bipyridine})_2(4\text{-aminomethylpyridine})\text{Cl}]^+$ bound within a **CMD** film that is anchored to the **arylamine-derivatised graphite** electrode. 20 mM phosphate buffer, pH 7.4 , scan rate 5 mV/s., **Kanichi** Research screen-printed electrodes, $\varphi = 1$ mm

From the CVs recorded at this electrode as a function of scan rate, the peak currents scale linearly with the square root of the scan rate in the range between 50-400 mV/s, as presented in **Figure 4.22**. Finite-diffusion, “thin-layer”, behaviour can be observed at scan rates under 20 mV/s. (Inset, **Figure 4.22**)

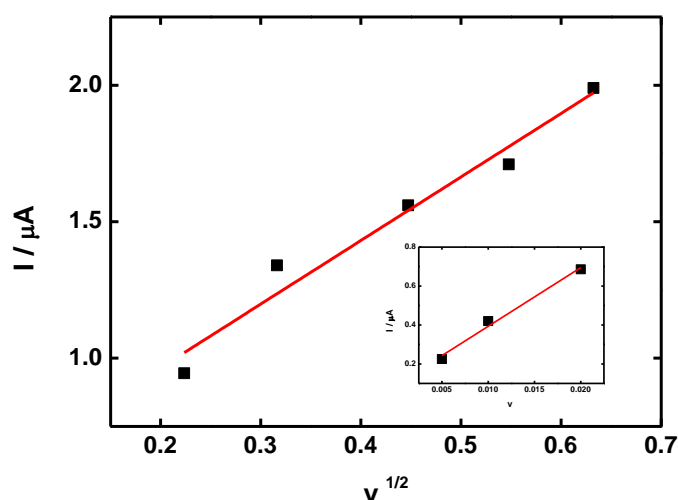


Figure 4.22 Plot of peak currents versus square root of the scan rate and scan rate (inset), redox probe $[\text{Os}(\text{2,2'}$ -bipyridine) $)_2(4\text{-aminomethylpyridine})\text{Cl}]^+$ bound within a **CMD** film on **arylamine-derivatised graphite** electrode. 20 mM phosphate buffer, pH 7.4, **Kanichi** Research screen-printed electrodes, $\phi = 1$ mm

A FWHM value of 174 mV is significantly greater than the $90.6/n$ mV theoretical value for a surface-confined species. (50) The parameters of the redox layer on screen printed electrodes are summarised in **Table 4.3**. An estimate of the surface coverage was calculated from the charge under osmium peak area. The value of 1.6×10^{-8} mol/cm² indicates that the amount of immobilised osmium is roughly 160 times the coverage of the monolayer. Previously, coverage of 4×10^{-9} mol/cm² was reported for the same hydrogel on graphite rod electrodes. (34) OsPVI polymer films yield coverages of active redox sites from 7×10^{-9} to 2×10^{-8} mol/cm² depending on osmium atom loading. (51)

Table 4.3 Electrochemical parameters of $[\text{Os}(\text{2,2'}$ -bipyridine) $)_2(4\text{-aminomethylpyridine})\text{Cl}]^+$ bound to a **CMD** film

	Surface coverage [mol/cm ²]	$D^{1/2}c$	FWHM anode	Redox potential
Average	1.6×10^{-8}	1.8×10^{-9}	0.174	0.35
SD	4×10^{-9}	5×10^{-10}	0.007	0.02
RSD%	22	30	4	6

The currents of the osmium oxidation peak were monitored over time, which provides information on stability of the layer on the surface. Osmium peak currents diminished by approximately 45 % over 30 days. (**Figure 4.24**)

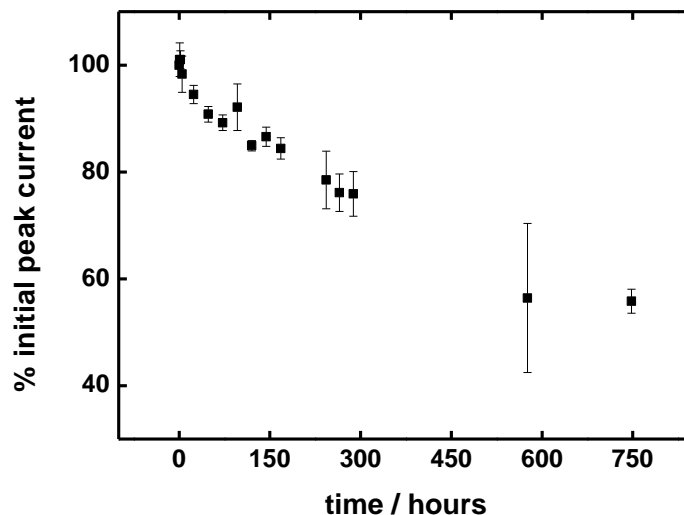


Figure 4.24 The stability of the peak current signal at the modified electrode as a function of time. Peak current extracted from cyclic voltammograms recorded at a scan rate 5 mV /s, at selected time intervals and normalised to the initial peak height. Electrodes stored and analysed in 20 mM phosphate buffer, pH 7.4. Kanichi Research screen-printed electrodes, $\varphi = 1$ mm

As presented previously, it was assumed that the dissolution of surface-bound osmium complex follows pseudo-first order kinetics. A plot of the natural logarithm of percentage of the initial peak versus time represented by **Figure 4.25**, can therefore be used to estimate a rate constant and half-life for the stability of the layer.

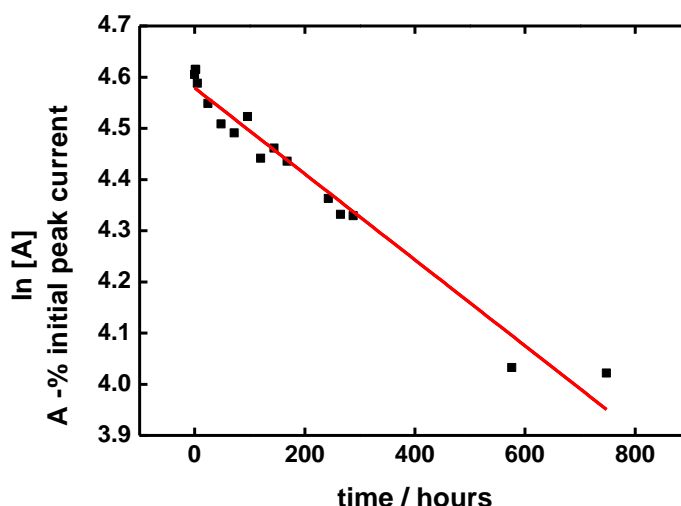


Figure 4.25 A kinetic plot of the natural logarithm of the percentage of the decay versus time for electrode coated with CMD/[Os(2,2'-bipyridine)₂(4-aminomethylpyridine)Cl]

The first order rate constant was extracted from the slope of the linear plot and the value of 0.00084 s^{-1} was obtained. The estimated value of half-life is 835 hours, which indicates a poorer stability compared to the films described in Chapter 2 (4740 h) and 3 (2468 h).

4.3.3. Amperometric detection of DNA hybridization with ssDNA grafted onto CM Dextran with ferrocenemethanol as diffusional mediator on screen-printed electrodes

Following successful coupling of osmium redox probes to screen printed electrodes (Kanichi), these electrodes were modified as before except that attachment of NH₂-terminated ssDNA to the CMD was undertaken, instead of the osmium complex, to provide a sensing platform for DNA hybridisation, analogous to the sensors described in Chapter 3. Screen-printed electrodes modified with CMD and ssDNA were incubated in target DNA solution also containing SDS and milk powder. Hybridisation of biotinylated DNA target followed by reaction with glucose oxidase:avidin conjugate results in bioelectrocatalysis of glucose oxidation in the presence of ferrocenemethanol as the mediator. A glucose oxidation wave can be seen, when biotin-complementary DNA is bound to the surface. (**Figure 4.26**)

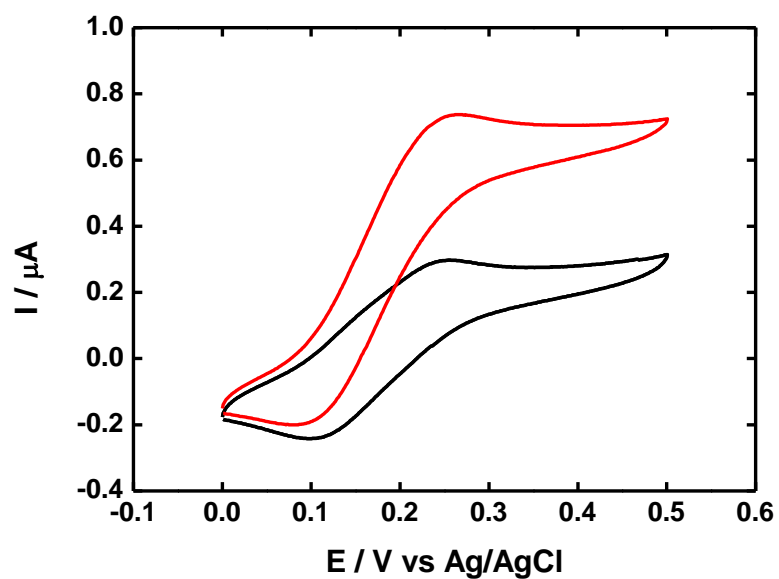


Figure 4.26 Cyclic voltammetry, **biotin-complementary DNA**, 1×10^{-6} M, DNA attached to CMD, no glucose (**black**), with 20 mM glucose (**red**), 0.2 mM ferrocenemethanol, Kanichi Research electrodes, $\varphi = 1$ mm

As observed for the system in Chapter 2 and 3, biocatalytic currents using amperometry, such as in **Figure 4.27** confirms oxidation of glucose in the presence of biotin complementary sequence.

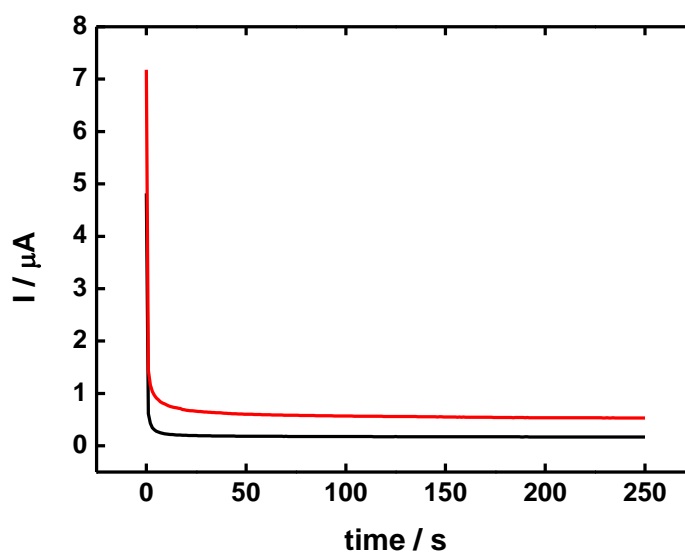


Figure 4.27 Chronoamperometry, **biotin-complementary DNA**, 1×10^{-6} M, DNA attached to CMD, no glucose (**black**), with 20 mM glucose (**red**), 0.2 mM ferrocenemethanol, **Kanichi** Research electrodes, $\varphi = 1$ mm

Amperometric plots of electrodes exposed to solutions containing unmodified complementary DNA and biotin non-complementary DNA, shown in **Figures 4.28** and **4.29**, overlay with the baseline, indicative that non-specific binding of the DNA and enzyme is low. For example, hybridisation to biotin non-complementary DNA results only in 0.5 % of the biotin complementary DNA signal. This is an improvement over the results observed previously, as comparing to the same assay performed on the graphite rod electrodes (Chapter 3) where biotin non-complementary DNA yields 8 % of the signal of biotin-complementary target.

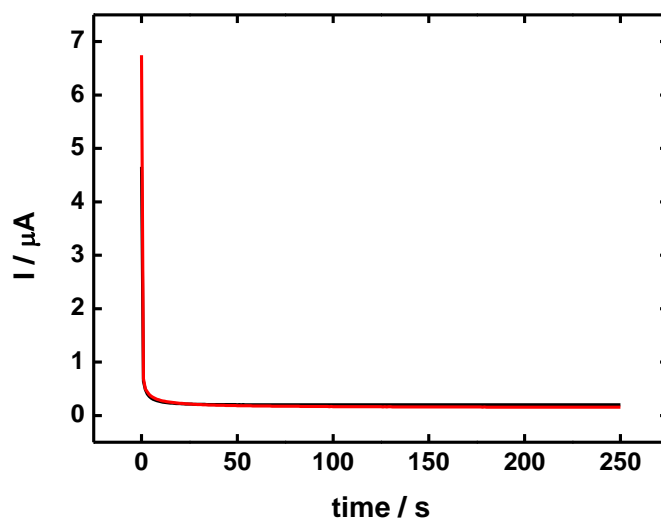


Figure 4.28 Chronoamperometry, **Unmodified-complementary DNA**, 1×10^{-6} M, DNA attached to CMD, no glucose (**black**), with 20 mM glucose (**red**), 0.2 mM ferrocenemethanol, Kanichi Research electrodes, $\phi = 1$ mm

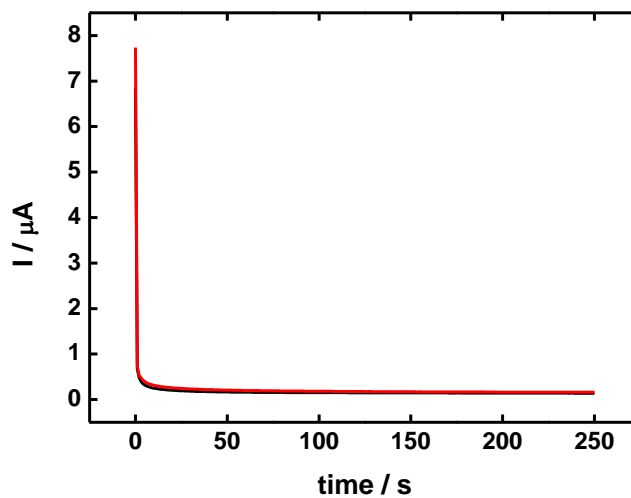


Figure 4.29 Chronoamperometry, **biotin non-complementary DNA**, 1×10^{-6} M, DNA attached to CMD, no glucose (**black**), with 20 mM glucose (**red**), 0.2 mM ferrocenemethanol, Kanichi Research electrodes, $\phi = 1$ mm

The average values of amperometric currents from three consecutive experiments were plotted versus the logarithm of the target DNA concentration. (**Figure 4.30**) A sigmoidal trend similar to the plots obtained Chapter 2 and 3 is clearly visible.

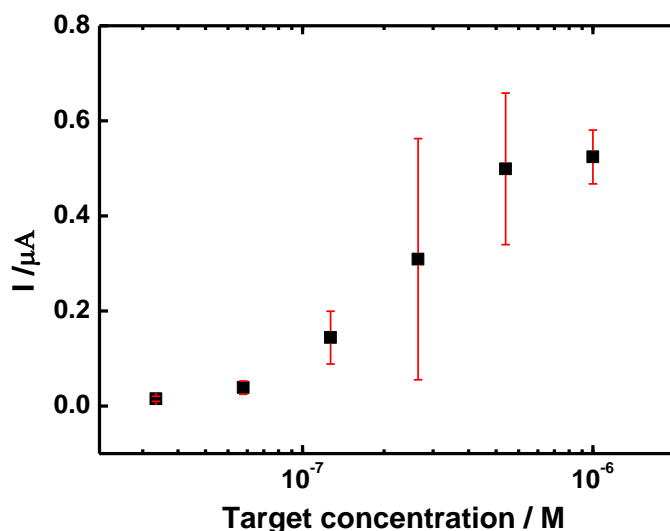


Figure 4.30 Calibration curve (1 μM -0.03 μM), Kanichi SPEs, $\phi = 1$ mm, $n = 3$

The results obtained using screen-printed electrodes are still characterised by imprecision, but improvement is expected as the number of samples is increased. Standard deviation of the bioelectrocatalytic signals is especially high in the linear portion of the sigmoidal curve and for the mid-range concentration it accounts for nearly 81% of the average. The calibration graph, where currents were normalised using electrode areas is presented in **Figure 4.31**. No correlation between the signal and electrode area (estimated using capacitance) was found. Standard deviations of the roughness of the SPEs are $\sim 20\%$ for areas determined using capacitance method and $\sim 11\%$ for areas determined using the redox probe study, so the electrode porosity does not contribute as significantly to the error.

Although use of screen-printed electrodes did not improve reproducibility thus far, non-specific binding of the biotin non-complementary sequence was reduced. A first step to further investigate contributions to variability could be to investigate the effect of blocking on electrode charging currents by using other standard blocking agents, such as pure casein or bovine serum albumin (BSA) instead of milk powder.

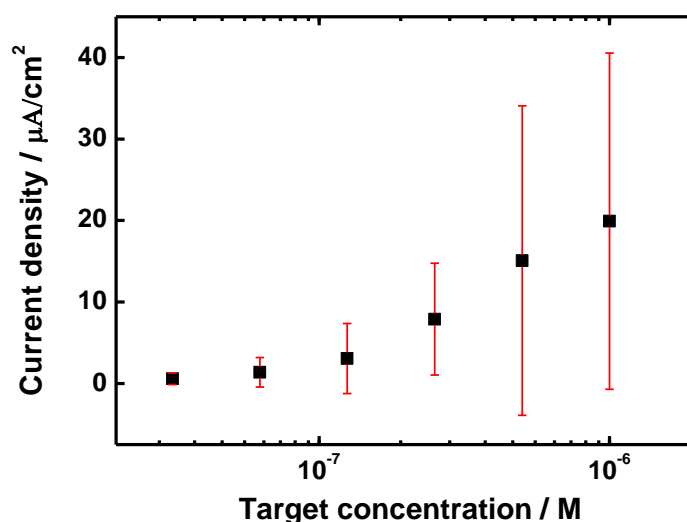


Figure 4.31 Calibration curve (1 μM -0.03 μM), Kanichi SPEs, $\phi = 1$ mm. Current densities plotted versus logarithm of concentration of complementary DNA. Electrode areas were obtained from capacitance.

Future problem solving should also focus on improving the SPE design: difficulty in the proper interfacing of the conducting path of the electrode (printed with carbon only) might be to blame for variability. From a few connection configurations already examined, none was proven satisfactory. Applying a commercial gold plated test clip (3M), neither interfacing of the electrode via edge connector manufactured by Kanichi did not provide a stable contact. The connection was fairly stable, when a crocodile clip was connected directly to the ink. Direct connection of the screen printed conductors to metal is known not to be sufficient to form a reliable and reproducible connection. In the electronic industry the issue of interfacing of printed circuits was solved by binding metal using metal loaded adhesives to form metallurgical type interface. (52) As the contact strip of a screen-printed electrode has to be stable upon multiple connection/disconnection and using metallic coatings over carbon does not eliminate the risk of scratching contact pads. A simple and inexpensive solution is proposed: a layer of the aluminium foil could be easily attached to the contact using a conductive adhesive, such as silver epoxy glue.

4.4. Conclusions

The behaviour of several types of screen-printed electrodes was examined towards benchmark redox couples. It was demonstrated that chemically modified screen-printed graphite electrodes can be used to produce a sensors for qualitative and quantitative analysis of DNA with bioelectrocatalytic amplification of signals. Non-specific binding of biotin non-complementary target and the enzyme was proven to be low. The assay seems to be promising as bioelectrocatalytic signals scale with the increasing concentration of the target DNA. The precision of quantification is still an issue, so further study is required to optimise the protocol and screen-printed electrode design. These properties can be improved by more careful choice of electrode material, varying ink composition and adequate pre-treatment, such as oxidation at high anodic potential (42, 46, 53) and treatment with argon (41) or oxygen (54) plasma.

4.5. References

1. M. Chikae, K. Idegami, K. Kerman, N. Nagatani, M. Ishikawa, Y. Takamura, E. Tamiya, *Electrochem. Commun.* **8**, 1375 (2006).
2. J. Wang, M. Musameh, *Analyst* **129**, 1 (2004).
3. Y. L. de Mattos, L. Gorton, T. Ruzgas, *Biosens. Bioelectron.* **18**, 193 (2003).
4. M. Piano, S. Serban, R. Pittson, G. Drago, J. P. Hart, *Talanta* **82**, 34 (2010).
5. M. Albareda-Sirvent, A. Merkoci, S. Alegret, *Sens. Actuators, B* **69**, 153 (2000).
6. C. Bonnet, S. Andreescu, J.-L. Marty, *Anal. Chim. Acta* **481**, 209 (2003).
7. M. A. Alonso-Lomillo, C. Yardimci, O. Domínguez-Renedo, M. J. Arcos-Martínez, *Anal. Chim. Acta* **633**, 51 (2009).
8. A. Ferancová, E. Korgová, T. Buzinkaiová, W. Kutner, I. Štěpánek, J. Labuda, *Anal. Chim. Acta* **447**, 47 (2001).
9. J. P. Hart, A. K. Abass, *Anal. Chim. Acta* **342**, 199 (1997).
10. G. Silva Nunes, G. Jeanty, J.-L. Marty, *Anal. Chim. Acta* **523**, 107 (2004).
11. A. Vasilescu, S. Andreescu, C. Bala, S.C. Litescu, T. Noguer, J.-L. Marty, *Biosens. Bioelectron.* **18**, 781 (2003).
12. J. D. Newman, A. P. F. Turner, G. Marrazza, *Anal. Chim. Acta* **262**, 13 (1992).
13. A. Cagnini, I. Palchetti, I. Lioni, M. Mascini, A. P. F. Turner, *Sens. Actuators, B* **24-25**, 85 (1995).
14. R. Wedge, R. M. Pemberton, J. P. Hart, R. Luxton, *Analisis* **27**, 570 (1999).
15. M. Piano, S. Serban, N. Biddle, R. Pittson, G.A. Drago, J.P. Hart, *Anal. Biochem.* **396**, 269 (2010).
16. J. P. Hart, S. A. Wring, TrAC, *Trends Anal. Chem.* **16**, 89 (1997).
17. J. Wang, B. Tian, V. B. Nascimento, L. Angnes, *Electrochim. Acta* **43**, 3459 (1998).
18. O. Dominguez Renedo, M. A. Alonso-Lomillo, M. J. Arcos Martinez, *Talanta* **73**, 202 (2007).
19. S. Kroger, S. J. Setford, A. P. F. Turner, *Anal. Chim. Acta* **368**, 219 (1998).
20. F. Ricci, A. Amine, C.S. Tuta, A. Ciucu, F. Lucarelli, G. Palleschi, D. Moscone, *Anal. Chim. Acta* **485**, 111 (2003).
21. S.-H. Lee, H. Y. Fang, W. C. Chen, *Sens. Actuators B* **117**, 236 (2006).
22. J. Wang, X. Zhang, *Anal. Lett.* **32**, 1739 (1999).
23. S. Andreescu, T. Noguer, V. Magearu, J.-L. Marty, *Talanta* **57**, 169 (2002).
24. K. C. Honeychurch, J. P. Hart, D. C. Cowell, D. W. M. Arrigan, *Sens. Actuators, B* **77**, 642 (2001).
25. A. Napier, J.P. Hart, *Electroanalysis* **8**, 1006 (1996).
26. V. Escamilla-Gómez, D. Hernández-Santos, M. B. González-García, J. M. Pingarrón-Carrazón, A. Costa-García, *Biosens. Bioelectron.* **24**, 2678 (2009).
27. G. Marrazza, I. Chianella, M. Mascini, *Anal. Chim. Acta* **387**, 297 (1999).
28. M. Tudorache, C. Bala, *Anal. Bioanal. Chem.* **388**, 565 (2007).
29. G. Marrazza, I. Chianella, M. Mascini, *Biosens. Bioelectron.* **14**, 43 (1999).
30. G. Carpini, F. Lucarelli, G. Marrazza, M. Mascini, *Biosens. Bioelectron.* **20**, 167 (2004).
31. F. Lucarelli, G. Marrazza, M. Mascini, *Biosens. Bioelectron.* **20**, 2001 (2005).

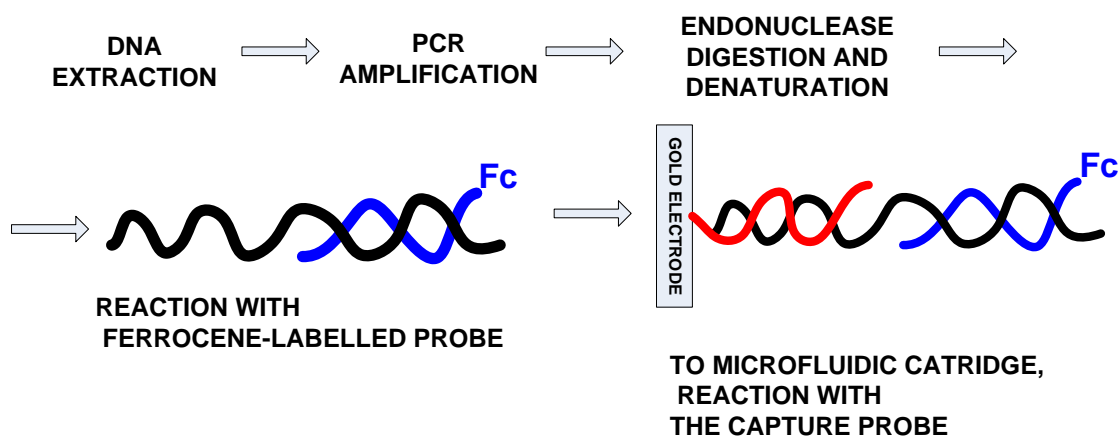
32. S. Laschi, I. Palchetti, G. Marrazza, M. Mascini, *J. Electroanal. Chem.* **593**, 211 (2006).
33. C. A. Marquette, M. F. Lawrence, L. J. Blum, *Anal. Chem.* **78**, 959 (2006).
34. J. Hajdukiewicz, S. Boland, P. Kavanagh, D. Leech, *Biosens. Bioelectron.* **25**, 1037 (2010).
35. S. Boland, F. Barrière, D. Leech, *Langmuir* **24**, 6351 (2008).
36. S. Trasatti, O. A. Petrii, *Pure & Appl. Chem.* **63**, 711 (1991).
37. A. J. Bard, L. R. Faulkner, *Electrochemical methods: fundamentals and applications*. (Wiley, 2001).
38. D. D. Gornall, S. D. Collyer, S. P. J. Higson, *Sens. Actuators, B* **141**, 581 (2009).
39. A. Erlenkotter, M. Kottbus, G.-C. Chemnitz, *J. Electroanal. Chem.* **481**, 82 (2000).
40. A. Morrin, A. J. Killard, M. R. Smyth, *Anal. Lett.* **36**, 2021 (2003).
41. F. Ghamouss, P. Y. Tessier, M. A. Djouadi, M.-P. Besland, M. Boujtita, *Electrochem. Comm.* **9**, 1798 (2007).
42. P. Fanjul-Bolado, D. Hernandez-Santos, P. J. Lamas-Ardisana, A. Martin-Pernia, A. Costa-Garcia, *Electrochim. Acta* **53**, 3635 (2008).
43. R. G. Compton, *Electrode kinetics: reactions*. (Elsevier, 1987).
44. P. M. S. Monk, *Fundamentals of electroanalytical chemistry*. (Wiley, 2001).
45. J.-P. Randin, E. Yeager, *J. Electroanal. Chem.* **58**, 313 (1975).
46. W. J. Blaedel, R. A. Jenkins, *Anal. Chem.* **46**, 1952 (1974).
47. J. Wang, M. Pedrero, H. Sakslund, O. Hammerich, J. Pingarron, *Analyst* **121**, 345 (1996).
48. G. Cui, J. H. Yoo, J. S. Lee, J. Yoo, J. H. Uhm, G.S. Cha, H. Nam, *Analyst* **126**, 1399 (2001).
49. S. C. Wang, K. S. Chang, C. J. Yuan, *Electrochim. Acta* **54**, 4937 (2009).
50. R. W. Murray, in *Electroanalytical Chemistry*, A. J. Bard, Ed. (Marcel Dekker Inc., New York, 1984), vol. 13.
51. R. J. Forster, J. G. Vos, *Langmuir* **10**, 4330 (1994).
52. K. Gilleo, *Polymer thick film*. (Springer, 1996).
53. R. C. Engstrom, *Anal. Chem.* **54**, 2310 (1982).
54. K. S. Prasad, G. Muthuraman, J.-M. Zen, *Electrochem. Commun.* **10**, 559 (2008).

Chapter 5

Conclusions and Future Directions

Electrochemical DNA sensors provide a promising technology for clinical analysis, along with optical, chromatographic and isotopic methods. (1-4) They have some superior qualities, such as the ease of miniaturization and electrical addressing. They also have a potential to be used in remote sensing applications by the means of portable, battery operated devices.

There are however thus far few examples of commercial electrochemical DNA diagnostics systems on the market. One such example is the system developed by GeneMark diagnostics. In their assay format DNA undergoes PCR amplification, followed by endonuclease digestion and denaturation. Then ssDNA is mixed with a ferrocene-labelled probe and hybridized to the capture probe bound to gold electrode as presented in **Scheme 5.1**. Ferrocene oxidation signal indicates DNA binding events. The producer offers exchangeable electrode cartridges and reagents designed for genetic disease screening; reagent kits containing DNA coded for *cystic fibrosis* or *thrombophilia* are available.



Scheme 5.1 Representation of operation of eSensor[®] XT-8 produced by GenMark Diagnostics

Using redox enzymes as tags for detection of nucleic acids offers several advantages, such as possibility of forming conjugates with the DNA, large turnover and high sensitivity. (5) In addition, hybridisation on electrodes with immobilized DNA is superior to solution-phase reaction as the heterogenous hybridization proceeds more efficiently. (6) The output signal of electrochemical sensors is

however sensitive to surface phenomena. Variation of the microscopic and electroactive area as well as interactions of electrode material with ions and other reagents is an obvious cause of discrepancy in the signals corresponding to surface hybridisation. The response of DNA biosensors is dependent on the surface density of the DNA, (7) conformation of DNA strands (8) and presence of pinholes in the immobilized molecular layers. (9) Many researchers addressed the issue of non-specific binding (NSB) of the DNA (10) and the label molecule (11) to electrodes. Diercks et al. recommended including surface blocking agents in order to reduce the NSB. (12) The authors report reduction of background signal of the DNA assay on gold electrodes can be achieved by immersion in bovine serum albumin prior to hybridization. They observed that the currents corresponding to specific interactions have also diminished upon blocking.

This thesis is concerned with development of a sensing platform for detection of the short DNA sequences, with a view to detect the presence of pathogenic bacteria in environmental samples. Films containing immobilized single-stranded DNA on electrodes were used to perform hybridization of a biotin-labelled complementary DNA. Development of an amplified signal is provided by interaction of the biotin with glucose oxidase:avidin conjugate to produce a catalytically active surface capable of oxidizing glucose in solution and transferring electron to the surface, producing a current.

In the first part of the thesis an enzyme-amplified amperometric sensor, where DNA is cross-linked to an osmium-based hydrogel on gold microelectrodes was described. The hybridization of a complementary strand coded for *Listeria Monocytogenes* results in the oxidation of glucose catalyzed by the enzyme label. The assay was improved upon miniaturization in comparison with a previous study published by Kavanagh and Leech (13) as the detection limit was lowered by 1000 fold when using a gold microelectrode instead of macroelectrode. Excellent stability of redox hydrogels on microelectrodes was also observed. (14)

Because of complexity of the microelectrode-based assay, with difficulty in polishing of microelectrodes and depositing reproducible droplets, an alternative approach for electrode modification was proposed. Instead of a drop-coating/drying method, the electrode was functionalized with a covalently attached polymer, and the

mediator and the DNA coupled to this polymer by sequential introduction of the reagents in the solution phase.

A model study was conducted to estimate the coupling efficiency of the redox probe $[\text{Os}(2,2',2''\text{-bipyridine})_2(4\text{-aminomethylpyridine})\text{Cl}]\text{PF}_6$ and polymeric supports on gold and carbon electrodes, by monitoring the electrochemical redox response of the Os(II)/(III) couple upon coupling. From this study it was concluded that coupling of the carboxymethylated dextran on smooth gold and glassy carbon electrodes did not produce a sufficient number of binding sites for the complex within the surface-attached polymer. The only exception to this was for reactions undertaken using graphite, which allowed binding of the equivalent of 40 monomolecular layers of the osmium complex. It was therefore postulated that graphite could provide a high density of binding sites for DNA in an assay format based on coupling within CMD attached to surfaces because of their relatively high microscopic roughness, compared to the smoother gold and glassy carbon surfaces.

Coupling of the ssDNA to the carboxymethylated dextran and reaction with the biotin complementary target and glucose oxidase: avidin generates bioelectrocatalytic current in the presence of glucose and ferrocenemethanol, a solution-phase electron transfer mediator. Use of the blocking agents was investigated in this approach. When milk powder and sodium dodecyl sulphate were added to the hybridisation solution non-specific binding of the DNA and the enzyme was significantly reduced. A sigmoidal plot of currents versus logarithm of concentration was obtained, when taking the average of five DNA samples. A sigmoidal trend can be seen for all assays described here and it is commonly obtained for enzyme electrodes. (15) Despite the well-defined trend, the standard deviation of the signals was found to be high. An attempt was made to identify the source of the error, by normalizing the currents versus a surface area. No obvious correlation between the roughness of the surface and the hybridization signal was found. Overall, the assay holds a promise for qualitative and quantitative determination of DNA sequences. The solution-phase immobilisation protocol allows developing a technique, where a probe molecules and DNA target and enzyme can be coupled sequentially in the flow system, similar to commercial Surface Plasmon Resonance devices. (16) Replacing an optical method with electrochemical detection would allow multiple addressing of the sensing chips and

it should improve sensitivity. It is proposed, that in order to reduce variability, electrodes that are smoother and thus present more reproducible surface areas and reactivity have to be sought.

In an effort to simplify, for the user, the assay protocol, preliminary studies were conducted on co-immobilisation of osmium redox complex and DNA on carboxymethylated dextran, in order to remove the requirement to add solution-phase mediator. A bioelectrocatalytic response, which is binding dependent, was observed, but reproducibility was less comparing to solution-phase mediator.

Further research focused on DNA sensing using disposable, graphite electrodes. Using cheap, commercially available electrodes solves the problem of analyzing large number of samples within short time scale, also reducing greatly the sample contamination; a new electrode can be used for each sample. A practical DNA screening system must be able to perform multiple hybridizations in parallel. Construction of electrode arrays can bring a solution to this issue. Screen-printed electrodes offer flexibility of cell design, such as integrating of the electrodes into the flow system.

The electrochemical behavior of screen-printed electrodes obtained from commercial and academic sources was examined towards their performance with benchmark redox complexes. Few of examined electrodes displayed a clear redox couple for cyclic voltammetry of potassium ferricyanide. Although peak separation indicated irreversible electrochemical reaction, they were considered suitable for further processing. The coupling of diazonium salt of a p-phenylene diamine, carboxymethylated dextran and osmium complex to electrodes manufactured by Kanichi Research was studied and the electrode films have been shown to display a sufficient number of functional groups available for biomolecule coupling. In addition, the osmium complex film was found to withstand a long immersion in fluids. In further studies the immobilisation of carboxymethylated dextran and the DNA was demonstrated. Subsequent to DNA layer formation on dextran, hybridization of the biotin complementary target and addition of the GOx:avidin was performed, resulting in bioelectrocatalysis of glucose in the presence of ferrocenemethanol. The behaviour of the screen-printed electrodes was similar to that observed with graphite disc electrodes. The currents scale with increasing DNA

concentration yielding a sigmoidal plot of signals versus logarithm of concentration. The assay on such electrodes was successful in distinguishing between complementary and non-complementary DNA. However difficulties with precision of response were still encountered. An improvement in conductivity of the carbon inks, reproducibility of the electrode areas and reactivity and appropriate interfacing of the electrode is required for future studies.

There are multiple areas for improvement of the protocols. For example, increasing the concentration and improving the mass transport of glucose, helping to minimize errors associated with glucose mass transport variations, by measurements in a flow cell should be considered. In addition, high precision cannot be achieved without using well-defined, reproducible electrode surface areas and with reproducible electrochemistry and reactivity. No direct link between an electroactive area estimate and the hybridization signal was found, illustrating that the precision does not solely depend on the electrode area. Assay variables, such as surface concentration of probe DNA, concentration of the enzyme, blocking agents, glucose and ferrocenemethanol concentrations should be optimised. Direct electrical heating of the electrode surface might also improve the performance of the DNA sensor. (17) Following simple statistical rules (with the help of electrode arrays and signal multiplexing), such as increasing the number of samples and reducing time intervals between the measurements can also reduce the error. From the data presented in Chapters 3 and 4, it is clear that performing replicate analysis allows identification of the trend between the signal and the concentration of the DNA, even if the error is often away from being statistically acceptable.

An initial study has been conducted to optimize the concentration of glucose substrate. Assuming that glucose oxidation mediated by ferrocenemethanol fulfills Michaelis-Menten model and that the current is proportional to the reaction rate, it is possible to use an expression for the velocity of the enzyme-catalysed reaction:

$$V = \frac{V_m [S]}{K_m + [S]} \quad (5.1)$$

Where:

K_m – Michaelis-Menten constant corresponding to $[S] = 0.5 V_m$

V_m – maximum rate of reaction

[S]- substrate concentration

When determining the concentration of the enzyme, and this is the case of the enzyme-amplified DNA assays, it is advised that the substrate concentration should be significantly greater than K_m . (15) The opposite is the case for procedures that seek to determine glucose concentration; the maximum performance is achieved at glucose concentrations lower than K_m in amperometric glucose-sensing devices. A Michaelis-Menten plot (**Figure 5.1**) was obtained by varying the concentration of glucose for the measurement on electrodes with high coverage of the enzyme. This was achieved by reaction with high target DNA concentrations: 5×10^{-6} M.

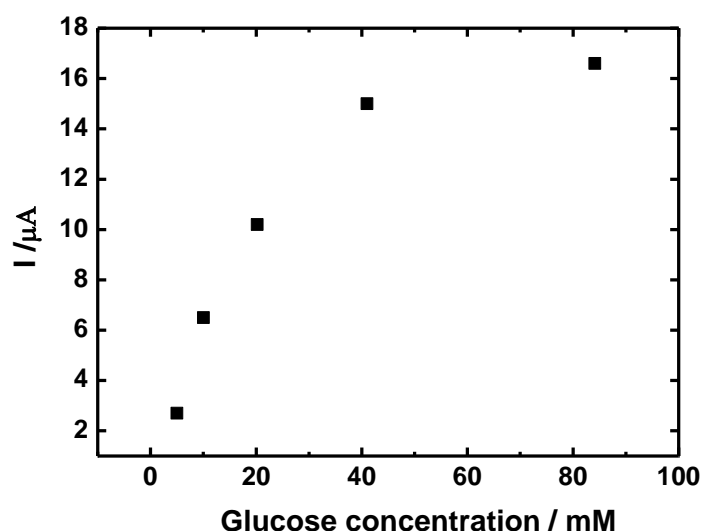


Figure 5.1 Michaelis-Menten plot for glucose oxidation at carboxymethylated dextran – based DNA sensing film reported in Chapter 3, which reacted with **biotin complementary target** and glucose oxidase:avidin, DNA concentration – 5×10^{-6} M. 0.2 mM ferrocenemethanol, 20 mM phosphate buffer, pH 7.4

Fitting of the hyperbola function allowed estimation of a value of K_m of 22 mM. This value is close to glucose concentration of 20 mM used in the studies detailed in chapter 2-4 in this thesis. An improvement of precision might be gained when operating the sensors at glucose concentrations of 100 mM and higher, due to the higher currents observed, and the presumed decrease in variability.

In conclusion, extension of this research is necessary to be able to perform analysis of real DNA samples: a platform device such as that proposed needs to

demonstrate much higher precision for the model samples of DNA used, prior to any attempt at translation to real sample measurements

5.1. References

1. S. Cosnier, P. Mailley, *Analyst* **133**, 984 (2008).
2. E. Hvastkovs, D. A. Buttry, *Analyst* **135**, 1817 (2010).
3. E. Palecek, *Electroanalysis* **21**, 239 (2009).
4. A. Sassolas, B. Leca-Bouvier, L. Blum, *Chem. Rev.* **108**, 109 (2008).
5. I. Willner, B. Shlyahovsky, B. Willner, M. Zayats, in *Functional Nucleic Acids for Analytical Applications.*, Y. Li, Y. Lu, Eds. (Springer, 2009).
6. V. Chan, D. J. Graves, S. E. McKenzie, *Biophys J.* **69**, 2243 (1995).
7. A. W. Peterson, R. J. Heaton, R. M. Georgiadis, *Nucleic Acids Res.* **29**, 5163 (2001).
8. M. Gębala, W. Schuhmann, *Chem. Phys. Chem.* **11**, 2887 (2010).
9. V. Dharuman, J. H. Hahn, *Sens. Actuators, B* **127**, 536 (2007).
10. M. I. Pividori, A. Merkoçi, S. Alegret, *Biosens. Bioelectron.* **15**, 291 (2000).
11. L. Zhang, D. Li, W. Meng, Q. Huang, Y. Su, L. Wang, S. Song, C. Fan, *Biosens. Bioelectron.* **25**, 368 (2009).
12. S. Diercks, K. Metfies, L. K. Medlin, *Biosens. Bioelectron.* **23**, 1527 (2008).
13. P. Kavanagh, D. Leech, *Anal. Chem.* **78**, 2710 (2006).
14. J. Hajdukiewicz, S. Boland, P. Kavanagh, A. Nowicka, Z. Stojek, D. Leech, *Electroanalysis* **21**, 342 (2009).
15. J. Wang, *Analytical electrochemistry.* (Wiley-VCH, 2006).
16. S. Sjoelander, C. Urbaniczky, *Anal. Chem.* **63**, 2338 (1991).
17. G.-U. Flechsig, J. Peter, G. Hartwich, J. Wang, P. Gründler, *Langmuir* **21**, 7848 (2005).

A – adenine

4-AMP – 4-aminomethylpyridine

AP – alkaline phosphatase

bpy – 2,2'-bipyridine

C – cytosine

CMD – carboxymethylated dextran

CME – chemically modified electrode

CV – cyclic voltammetry

DMSO - dimethyl sulfoxide

DNA – deoxyribonucleic acid

dsDNA – double strand DNA

DTSP – dithiobis(succinimidyl) propionate

EDC - 1-ethyl-3-(3-dimethylaminopropyl) carbodiimide

E_{FWHM} – full width at half peak maximum

EtOH - ethanol

FAD - flavin adenine dinucleotide

FADH₂ – reduced (hydroquinone) form of FAD

FWHM – full width at half peak maximum

G – guanine

GC – glassy carbon

GL - glucose

GOx – glucose oxidase

HEPES - (4-(2-hydroxyethyl)-1-piperazineethanesulfonic acid)

HOPG – highly oriented pyrolytic graphite

HRP – horseradish peroxidase

HSsDNA – single strand DNA with a thiol modification to the phosphate backbone

IgG – Immunoglobulin G

IUPAC - The International Union of Pure and Applied Chemistry

MAX – maximum

MeOH - methanol

MIN - minimum

NHS - N-Hydroxysuccinimide

NSB – non-specific binding

Os-PAA-PVI - osmium complex bound to a polyallylamine-polyvinylimidazole copolymer

OsPVI - $[\text{Os}(2,2'\text{-bipyridine})_2(\text{polyvinylimidazole})_{10}\text{Cl}]^{+2+}$

PAA – polyallylamine

PDDA - poly(diallyldimethylammonium chloride)

PEGDGE - poly-(ethylene glycol)bisglycidyl ether

PVI – polyvinylimidazole

R_f – roughness coefficient

RNA- ribonucleic acid

RSD – relative standard deviation

SAM – self-assembled monolayer

SBP – soybean peroxidase

SDS – sodium dodecyl sulphate

SD – standard deviation

SPE – screen-printed electrode

ssDNA – single strand DNA

TIRF - Total Internal Reflection Fluorescence

T- thymine

UCC – University College Cork

Publications:

- J. Hajdukiewicz et al. *Enzyme-Amplified Amperometric Detection of DNA Using Redox Mediating Films on Gold Microelectrodes*. *Electroanalysis* (2009) **21**, No. 3-5, 342 – 350
- J. Hajdukiewicz et al. *An enzyme-amplified amperometric DNA hybridisation assay using DNA immobilised in a carboxymethylated dextran film anchored to a graphite surface*. *Biosensors and Bioelectronics* (2010) **25**, 1037–1042

Oral presentations:

- “*Enzyme-Amplified Amperometric DNA Hybridization Assay Based on Bioelectrocatalysis Using Redox-Polymer Modified Electrodes*”, Electrochem08, Liverpool, September 2008
- “*Enzyme-Amplified Amperometric DNA Hybridization Assay Based on Bioelectrocatalysis Using Redox-Polymer Modified Electrodes*”, SMCBS 2009 workshop, Krakow, Poland, November 2009
- “*Electroreduction of CO₂. Catalysis by macrocyclic complexes of copper*” - ELCAT Training School on “Structural and electronic effects in electrocatalysis” Leiden, Netherlands, August 2010
- “*Electroreduction of CO₂. Catalysis by macrocyclic complexes of copper*” - ELCAT Workshop: “Nanoparticles and nanostructures for electrocatalytic reactions” - Liblice (near Prague): January 2011
- “*Equipment development for high pressure electrochemistry of CO₂*” - ELCAT Training course on theoretical electrochemistry and DFT modeling, Gothenburg, August 2011

Poster presentations:

- “*Redox polymer mediation of enzymes for amplified amperometric detection of DNA hybridization*” International Society for Electrochemistry Spring Meeting, Dublin, May 2007
- “*Enzyme-amplified amperometric DNA hybridisation sensor for detection of environmental pathogens*”, Chemistry Colloquium, Dublin, May 2007
- “*Enzyme-amplified amperometric DNA hybridisation sensor for detection of environmental pathogens*”, Analytical Research Forum, Glasgow, July 2007
- “*Enzyme-amplified amperometric DNA hybridization sensor for detection of environmental pathogens*”, EPA Strive seminar, Dublin, November 2007
- “*Enzyme-amplified amperometric DNA hybridization assay based on bioelectrocatalysis using polymer modified electrodes*”, ECI Research Day, Galway, June 2008
- “*Enzyme-amplified amperometric DNA hybridization assay based on bioelectrocatalysis using redox hydrogel-modified electrodes*” - Chemistry 60th Colloquium, Cork, June 2008
- “*Enzyme-amplified amperometric DNA hybridization assay based on bioelectrocatalysis using redox polymer-modified electrodes*”, Electrochemistry of Nucleic Acids and Proteins, Brno, June 2008
- “*Enzyme-amplified amperometric DNA hybridization assay based on bioelectrocatalysis using redox-polymer modified electrodes*” – Environ 2009, Waterford, February 2009
- “*An amperometric detection platform based upon bioelectrocatalysis for recognition of DNA hybridization*” – 42nd IUPAC congress, Glasgow, August 2009

- “*Functionalized carbon surfaces for DNA biosensor technology*” – International Symposium on Functional Nanomaterials, Dublin, September 2009
- “*Enzyme-amplified amperometric DNA hybridization assay based on bioelectrocatalysis using redox-polymer modified electrodes*” – EPA doctoral seminar, Dublin, November 2011

Awards:

RSC conference bursary, 2007

Messel bursary awarded by Society of Chemical Industry, 2008

RSC conference bursary, 2009

RSC, Analytical Division Ireland travel award, 2009

BOC Gases Ireland, Chemistry Prize, 2008/2009